The rate of energy loss of high energy muons

N. S. Palmer

THE RATE OF ENERGY LOSS OF HIGH ENERGY MUONS.

by

N.S.Palmer, B.Sc.

Thesis submitted for the degree of M.Sc. in the University of Durham.

Abstract.

A survey is made of experimental measurements of the underground cosmic ray muon intensity, appropriate corrections being made where necessary to provide a reliable estimate of the variation of intensity with depth.

An experiment has been carried out using the Durham spectrograph to obtain the effect of bias, due to accompanied particles, which was present in the published sea level spectrum of muons. These, and other experimental data, are used to derive a sea level spectrum up to 10,000 GeV.

The effect of fluctuations in energy loss on the underground intensities is considered and shown to be important at depths greater than 1,000 metres water equivalent.

The rate of energy loss of muons is then derived and is found to be well represented by the equation

$$-\frac{dE}{dx} = 1.88 + 0.0766 \ln \frac{Em'}{mc^2} + bE \quad \text{MeV g}^{-1}\text{ cm}^2$$

where b takes a value $(3.15 \pm 0.3) \times 10^{-6}$ g^{-1} cm^2. The theoretical value of b is derived and found to be 4.0×10^{-6} g^{-1} cm^2. The disagreement is thought to be due to an underestimate of the muon intensity at high energies, where the possible effect of kaons has been neglected.

Finally, a revised version of the sea level spectrum of muons is derived covering the range 10 - 10,000 GeV.

Preface.

This thesis describes work carried out by the author in the Physics Department of the (then) Durham Colleges in the University of Durham under the supervision of Dr. A. W. Wolfendale.

The author was responsible for the solution of the fluctuation problem and the analysis leading to the conclusions regarding the energy loss of the muon and the sea level spectrum. The apparatus necessary for the experimental work was prepared in conjunction with his colleagues, but the collection of data for the bias experiment was carried out solely by the author.

Part of the work has been published in papers to the Physical Society and the Royal Society:

Hayman, P.J., Palmer, N.S. and Wolfendale, A.W., 1962, Proc. Phys. Soc., 80, 800.

Hayman, P.J., Palmer, N.S. and Wolfendale, A.W., 1963, Proc. Roy. Soc., 275, 391.

Contents.

Chapter 1. Introduction.

The primary cosmic radiation of high energy incident upon the upper layers of the earth's atmosphere consists mainly (~88%) of protons, the remainder being made up of α-particles and heavier nuclei. The α-particles and heavy nuclei are rapidly removed by fragmentation, while the main removal process for the protons is that of nuclear interaction. By this process about 75% of the protons interact in the first 100 g cm^{-2} of the atmosphere, mainly producing charged and uncharged pions with smaller numbers of heavier particles. The neutral pions decay into gamma rays which in turn initiate electron - gamma ray cascades. If sufficient energy is available the cascades and their products may reach sea level where they are generally known as extensive air showers. The charged pions either interact with air nuclei, producing further pions, or decay into muons which, having a relatively small interaction with matter, may reach sea level and penetrate underground.

At sea level the flux of particles is made up of about 70% muons and about 30% electrons, the proton component having diminished to about 1%. The present work is concerned mainly with the muon component at sea level and underground, and in particular with the energy loss of these particles.

Due to the very small interaction rate of the muon, direct measurements of its energy loss is difficult and indirect methods

have to be used. The usual procedure is to correlate measurements of the underground intensity with the energy spectrum at sea level. Such treatments have been carried out by a number of workers, notably Barrett et al. (1952), George (1952), Pine et al. (1959), Ashton (1961) and Ozaki (1962). The method has, however, given varying results due to the inaccuracy in the sea level and underground intensity measurements, together with the lack of information about the effect of fluctuations on the energy loss of the muon. An analysis has been carried out in the present work using more recent experimental data and an attempt has been made to reduce some of the errors present in such an analysis.

The most recent measurements of sea level muon intensities have been carried out by Hayman and Wolfendale (1962) and Duthie et al. (1962), together covering the range 0.4-10,000 GeV. In the lower energy region a bias is present due to the rejection of accompanied particles and an experiment has been carried out to obtain an estimate of the effect.

The work of Miyake et al. (1962) has recently extended the depth-intensity curve to a depth of 8,000 m.w.e. and their results, together with previous data, have been used to derive a best estimate of this relation.

The effect of fluctuations in energy loss has been investigated by Bollinger (1951), Zatsepin and Kuzmin (1962), Mando and Sona (1953) and Ramanamurthy (1962), giving varying results. The problem has been attempted in the present work

and it is found that the effect is significant.

Finally, in the light of the various corrections necessary, an analysis of the experimental data is carried out, and a value of the energy loss parameter is derived. This is then compared with the theoretical value and an explanation of the discrepancy is advanced.

Chapter 2. Underground Intensities.

2.1 General Considerations.

Many workers have made measurements of the cosmic ray intensity underground but the considerable spread in the measured values has led to a variety of depth-intensity relations being proposed. One of the purposes of the present work is to make a reliable estimate of this relation. It is first necessary to consider the errors likely to occur in the measurements. The main sources of error are as follows:

(i) Normalisation.

In order to make an absolute measurement of intensity both the angular acceptance of the apparatus and the zenith angle dependance of the intensity have to be found. In order to avoid the errors which may arise in the determination of these quantities relative measurements of intensities may be carried out. This is done by measuring the counting rate of a detector at a series of depths including a measurement at some fairly shallow depth (in the region 10-100 m.w.e.). The normalisation factor necessary to give agreement between this measurement and the intensity predicted on the basis of a known sea level spectrum and some assumed energy loss is found. This factor is then applied to the measurements at deeper locations. The energy loss corresponding to this depth is known quite accurately but some workers have used different sea level spectra and systematic differences in the resulting intensities have occured.

(ii) Local radio-activity.

Unless special precautions are taken, measurements can be invalidated by the contribution to the counting rate by local radio-active materials.

(iii) Knock-on electrons.

A significant increase in the counting rate of an underground detector can arise due to muons producing secondary electrons by the knock-on process. In general the electrons produced are of low energy and the majority can be filtered out by the introduction of a small thickness of lead above the counting apparatus.

(iv) Geometrical effects.

As stated previously, an absolute measurement of intensity requires a knowledge of the angular distribution of particles. The accuracy with which this distribution and its variation with depth underground are known is a limiting factor in such a measurement.

An attempt has been made to select data which are relatively free from the errors described above, appropriate corrections being made where they were considered necessary.

2.2. Summary of the data used.

Clay and van Gemert (1939).

A measurement of the variation of cosmic ray intensity underwater down to a depth of 440 m. was made by Clay, van Gemert and Clay (1939). The same apparatus was subsequently operated by Clay and van Gemert underground to a depth of 620 m. The apparatus consisted of a threefold coincidence Geiger counter array, operated with various thicknesses of lead shielding. It was noticed by these workers that absorption of cosmic rays in various substances is not proportional to their densities, as they had expected. Table 2.1 gives the depth in metres water equivalent (m.w.e.) of rock and the corresponding depth in water at which the same counting rate was obtained.

Table 2.1.

Depth (m.)	h_s	h_e	h_s/h_e	$h_s/1.19$
0	10	10		
43	101	85	1.19	85
102	260	204	1.27	219
143	370	287	1.29	311
195	510	427	1.19	427
255	672			563
375	992			835
495	1320			1107
615	1644			1380

Key: h_s -equivalent depth according to density (m.w.e.)

h_e -corresponding depth in m.w.e. water.

The best value of the ratio of these corresponding depths was taken to be 1.19 and this factor had been applied to all values of the depths in m.w.e. of rock to convert to m.w.e. of water. It has been necessary therefore, to convert the published figures of these workers back to m.w.e. of rock by multiplying by the factor 1.19.

Results have been given as obtained using 0, 5, and 10 cm. thickness of lead shielding. The data selected as being the most reliable is that for 10 cm. of lead, and is presented in table 2.2.

Table 2.2

depth in m.w.e. water from top of atmosphere	depth in m.w.e. rock from top of atmosphere	depth in m.w.e. rock from sea level	vertical rate (counts/min)	normalised intensity ($cm^{-2}sec^{-1}st^{-1}$)
10	10	0	$1.61 \times 10^{2} \pm 1.6\%$	
85	101	91	$7.11 \pm 1.1\%$	2.55×10^{-4}
219	260	250	$1.14 \pm 1.1\%$	4.08×10^{-5}
311	370	360	$4.93 \times 10^{-1} \pm 4.0\%$	1.77×10^{-5}
427	510	500	$1.97 \times 10^{-1} \pm 2.5\%$	7.06×10^{-6}
563	672	662	$8.02 \times 10^{-2} \pm 4.7\%$	2.88×10^{-6}
1107	1320	1310	$1.32 \times 10^{-2} \pm 3.0\%$	4.72×10^{-7}

The errors shown are published errors. The data have been normalised at 91 m.w.e. of rock to 2.55×10^{-4} sec^{-1} cm^{-2} st^{-1}. This intensity has been arrived at using the spectrum derived in chapter 4, and a range-energy relation of the type described later.

The range-energy relation down to this depth is well established and the process is thus considered valid.

Ehmert (1937)

The experiment by Ehmert was to measure the variation of intensity with depth underwater and was carried out using a three-fold geiger telescope with a 5 cm. thickness of lead absorber. The results obtained are quoted in table 2.3.

Table 2.3

Depth in m.w.e. water from top of atmosphere	Depth in m.w.e. rock from top of atmosphere	Depth in m.w.e. rock from sea level	Relative vertical intensity	Normalised intensity ($sec^{-1}cm^{-2}st^{-1}$)
84.9	101	91	0.546	2.55×10^{-4}
82.9	98.5	88.5	0.561	
113.0	134.5	124.5	0.324	1.51×10^{-4}
141.6	168.0	158	0.206	9.61×10^{-5}
184.0	219	209	0.126	5.88×10^{-5}
223.8	266	256	0.0876	4.09×10^{-6}
245.0	291	281	0.0739	3.45×10^{-6}
242.9	289	279	0.0746	3.48×10^{-6}

The depths have been published in units of m.w.e. of water and have been converted to m.w.e. of rock by the factor 1.19 obtained by Clay and van Gemert. The measurements have been normalised as before to 2.55×10^{-4} sec^{-1} $cm^{-2}st^{-1}$ at 91 m.w.e.

Randall and Hazen (1951).

This experiment was carried out at a depth of 850 m.w.e. of rock using coincidences between two trays of geiger counters. It is not clear from the paper whether the depth stated refers to depth from the top of the atmosphere or from sea level, and it is assumed to be the latter. The thickness of lead absorber used was 15 cm. The zenith angle distribution near the vertical was obtained by measuring the counting rate of the apparatus for six different tray separations. The result is thus an absolute measurement. The figures given are:

$$I = (2.17 \pm 0.02) \times 10^{-6} \quad \text{sec}^{-1}\,\text{cm}^{-2}\,\text{st}^{-1}$$

$$n = 2.8 \pm 0.1$$

Where n is the exponent of the angular distribution, assuming it takes the form $I(\theta)=I_v \cos^n\theta$. The data obtained has since been reanalysed by the same authors (1958) and the latest figures are

$$I = (2.10 \pm 0.5) \times 10^{-6}\,\text{sec}^{-1}\,\text{cm}^{-2}\,\text{st}^{-1}$$

$$n = 2.3 \pm 0.3$$

Bollinger (1951).

This worker has made absolute measurements at depths of 1500 m.w.e. and 1840 m.w.e. using a four-fold geiger system. The values obtained are given in table 2.4.

Table 2.4

	Depth in m.w.e. rock below sea level	Intensity (sec^{-1} cm^{-2} st^{-1})
Location II	1500	3.9×10^{-7}
Location I	1840	1.91×10^{-7}

By examining the zenith angle distribution obtained at the two locations, the intensities at greater depths were inferred. These figures have been corrected by Hayman (1962) who divided the data into two categories. Firstly, the data at effective depths less than 3000 m.w.e. were divided by the factor

$$F = \frac{B+E}{B+E\cos\theta}$$

where B = 89.26 GeV. The corrected data are given in table 2.5.

Table 2.5 Location I

Intensity (sec^{-1} cm^{-2} st^{-1})	Counts	Zenith angle (deg.)	Effective depth (m.w.e.)	Energy (Gev)	Correction factor, F	Corrected intensity ($sec^{-1}cm^{-2}st^{-1}$)
1.52×10^{-7}	217	$16\frac{3}{4}$	1920	780	1.02	1.48×10^{-7}
1.23×10^{-7}	176	26	2046	850	1.10	1.12×10^{-7}
1.14×10^{-7}	162	$31\frac{3}{4}$	2162	930	1.17	9.80×10^{-8}
8.60×10^{-8}	122	$37\frac{3}{4}$	2322	1060	1.25	6.90×10^{-8}
6.88×10^{-8}	97.5	$42\frac{7}{8}$	2507	1200	1.33	5.18×10^{-8}
5.56×10^{-8}	79	$48\frac{1}{2}$	2773	1500	1.46	3.82×10^{-8}

(continued

Table 2.5		Location II				
Intensity ($sec^{-1}cm^{-2}st^{-1}$)	Counts	Zenith angle (deg.)	Effective depth (m.w.e.)	Energy (Gev)	Correction factor F	Corrected intensity
2.61×10^{-7}	210	20	1597	580	1.06	2.47×10^{-7}
2.11×10^{-7}	169	$32\frac{3}{4}$	1784	680	1.17	1.80×10^{-7}
1.57×10^{-7}	127	$39\frac{1}{2}$	1945	780	1.28	1.22×10^{-7}
1.11×10^{-7}	89	45	2119	900	1.36	8.10×10^{-8}
7.45×10^{-8}	60	$50\frac{3}{4}$	2369	1100	1.52	4.87×10^{-8}
4.84×10^{-8}	39	$55\frac{7}{8}$	2668	1300	1.71	2.84×10^{-8}

The data at larger effective depths were corrected by Hayman for two effects. The first correction was to account for the enhancement of the high energy part of the spectrum at large zenith angles and the second for the effect of scattering in the rock above the apparatus. The results are reproduced in Table 2.6.

Table 2.6		Location I				
Intensity ($sec^{-1}cm^{-2}st^{-1}$)	Counts	Zenith angle (deg.)	Effective depth (m.w.e.)	Correction factor	Scattering correction %	Corrected intensity ($sec^{-1}cm^{-2}st^{-1}$)
3.10×10^{-8}	44	$53\frac{1}{2}$	3094	1.40	-1.0	2.20×10^{-8}
1.44×10^{-8}	20.5	$59\frac{1}{8}$	3580	1.72	-1.4	8.25×10^{-9}
7.39×10^{-9}	10.5	$65\frac{1}{8}$	4370	2.35	-1.7	3.09×10^{-9}
3.52×10^{-9}	5	$70\frac{3}{4}$	5560	2.90	-3.0	1.19×10^{-9}
7.04×10^{-10}	1	$77\frac{1}{4}$	8330	5.05	-6.4	1.28×10^{-10}

(Continued

Table 2.6 Location II

Intensity ($sec^{-1}cm^{-2}st^{-1}$)	Counts	Zenith angle (deg.)	Effective depth (m.w.e.)	Correction factor	Scattering correction %	Corrected intensity ($sec^{-1}cm^{-2}st^{-1}$)
3.10×10^{-8}	25	$60\frac{1}{4}$	3020	1.75	-1.4	1.75×10^{-8}
1.73×10^{-8}	14	$66\frac{1}{2}$	3760	2.3	-2.0	7.35×10^{-8}
8.67×10^{-9}	7	$71\frac{1}{2}$	4730	2.9	-3.3	2.90×10^{-9}
1.24×10^{-9}	1	$76\frac{3}{8}$	6350	4.15	-5.8	2.83×10^{-10}
3.52×10^{-10}	0.5	$81\frac{3}{8}$	12300	9.10	-12.1	-

Barrett et al. (1952)

These workers used an array of five layers of geiger counters with alternate trays crossed. The apparatus was operated under fivefold coincidence with 12" of lead and 1.5" of iron as absorber. Each counter was hodoscoped and the resulting minimum resolution of the angle of the particles was 7^{o}. An absolute determination of the underground intensity and the angular distribution at a depth of 1574 m.w.e. was made and the results given are:

$$I = (3.25 \pm 0.05) \times 10^{-7} \text{ sec}^{-1} \text{ cm}^{-2} \text{ st}^{-1}$$

$$n = 3.06 \pm 0.10$$

A correction of 2% has been applied to these figures to account for errors due to secondary electrons produced inside the apparatus.

Avan and Avan (1955).

These workers exposed nuclear emulsions at three locations underground, and calculated the exponent of the zenith angle distribution and the vertical intensity. The results are:

Table 2.7

Depth (m.w.e.)	I (sec^{-1} cm^{-2} st^{-1})	n
300	$(3.80 \pm 0.17) \times 10^{-5}$	1.73 ± 0.10
580	$(7.30 \pm 0.40) \times 10^{-6}$	2.09 ± 0.12
1280	$(8.0 \pm 0.6) \times 10^{-7}$	2.63 ± 0.22

It seems likely that neglecting to use any screening material has caused some inaccuracies in the above figures. The results for the vertical intensity are probably over--estimated due to the contribution from electron secondaries, while the values for the exponent n are probably too low due to the more isotropic distribution of the electrons.

Sreekantan et al. (1952, 1956).

The apparatus used by these workers was a four-fold geiger counter telescope arrangement, using 10 cm. of lead as absorber. The apparatus was operated at five locations giving the following results:

Table 2.8

Depth in m.w.e. rock from sea level	Intensity (1952) ($sec^{-1}cm^{-2}st^{-1}$)	Intensity (1956) ($sec^{-1}cm^{-2}st^{-1}$)	Normalised intensity ($sec^{-1}cm^{-2}st^{-1}$)
90	-	3.42×10^{-4}	2.60×10^{-4}
371	$1.76 \times 10^{-5} \pm 13.6\%$	-	1.34×10^{-5}
465	$1.24 \times 10^{-5} \pm 10.5\%$	-	9.42×10^{-6}
674	$5.55 \times 10^{-6} \pm 12.6\%$	-	4.22×10^{-6}
875	$2.37 \times 10^{-6} \pm 11.4\%$	-	1.80×10^{-6}

The values were normalised at 90 m.w.e. to a value of 2.60×10^{-4} sec^{-1} cm^{-2} st^{-1} as given by the sea level spectrum and an assumed energy loss.

The values of the depths of the four deeper locations had been quoted in error in the 1952 paper and have been corrected in the 1956 paper.

Barton (1961).

This worker used two trays of geiger counters in coincidence, between which was situated a plastic scintillation counter. A hodoscope record of the triggered geiger counters

and the pulse height from the scintillation counter was made using magnetic tape. The experiment was carried out in two parts. In the first part the apparatus was operated at 3280 m.w.e. with the scintillation counter under differing discrimination requirements. The angular distributions for the two cases were found to be basically different and it was reported that one of these was consistent with an isotropic distribution. These events were identified as being due to gamma radiation from the surrounding rock. The results for the intensity measurement, therefore, are relatively free from spurious events. The results are given in table 2.9.

Table 2.9.

Depth. (m.w.e.)	Adjusted depth (m.w.e.)	Normalised rate	Intensity ($cm^{-2}sec^{-1}st^{-1}$)
0		1	7.54×10^{-3}
1660	1690	$(2.95 \pm 0.4) \times 10^{-5}$	2.22×10^{-7}
3280	3370	$(1.0 \pm 0.3) \times 10^{-6}$	7.54×10^{-9}
5050	5180	$< 2.2 \times 10^{-7}$	$< 1.65 \times 10^{-9}$

At the lowest depth no events were observed in the running time of 21 days and the figures are an upper limit to the intensity at this depth.

If depth intensity measurements are correlated with the sea level spectrum to obtain information about the energy loss of muons, it is obviously most convenient to refer all

measurements to a material having the same values of Z and A (see chapter 5). The energy loss processes of bremsstrahlung and pair-production are both proportional to the factor Z^2/A. The value of Z^2/A for the case of Barton's experiment was 5.85, and since most of the other data correspond to a value 5.50, the results of Barton have been adjusted to this figure. The choice of whether to correct the values of the depths or the intensities is quite arbitrary; in the present work it was decided to correct the depths.

Miyake et al. (1962).

Measurements at the deepest locations so far have been carried out by these workers. The apparatus used consisted of two plastic scintillators each of area 1.62 m^2 and each viewed by two photomultipliers. In between the scintillators was a tray of geiger counters and a layer of lead 5 cm. thick. The selection criterion was a five-fold coincidence between the geigers and each of the four photomultipliers. The effect of this was to virtually eliminate chance coincidences due to noise in the photomultipliers, which may be significant at deep locations where the rate of genuine events is very low. At the two deepest locations, 6380 and 8400 m.w.e., two virtually identical units were operated. At shallower depths, where the four-fold chance coincidence rate is negligible in comparison with the genuine rate, a single unit was operated under four-fold coincidence requirements.

The value of n, the exponent of the angular distribution, was calculated using an iterative process assuming a relation $n = m - 1$, where m is the slope of the logarithmic plot of intensity against depth i.e.

$$m = -\frac{\delta \log I}{\delta \log d}$$

The counting rate as a function of depth was plotted and the slope, m, was found. The resulting value of n was used to correct the intensities and the process was repeated until sufficient accuracy was obtained. The resulting intensities are thus absolute and do not require normalisation.

The value of Z^2/A for the rock above the apparatus was 6.33, and the depths have been adjusted, in the same manner as described previously, to correspond to a value of 5.50. The results of Sreekantan et al., which were given earlier, were obtained at the same location as those of Miyake et al. These however, have not been adjusted since the correction for depths less than 1,000 m.w.e. is negligible. The final results are given in the table.

Table 2.10

Depth in m.w.e. rock from sea level	Adjusted depth (m.w.e.)	n	Intensity ($sec^{-1}\ cm^{-2}\ st^{-1}$)
806	830	2.3	$(2.51 \pm 0.15) \times 10^{-6}$
1802	1870	3.1	$(1.77 \pm 0.07) \times 10^{-7}$
3400	3600	4.5	$(1.42 \pm 0.14) \times 10^{-8}$
4270	4530	5.2	$(3.24 \pm 0.35) \times 10^{-9}$
6370	6840	6.6	$(1.92 \pm 0.47) \times 10^{-10}$
8390	-	-	$< 10^{-11}$ (no counts recorded)

2.3. The Best Estimate of the Depth-intensity Relation.

The various measurements of underground intensity have been plotted as a function of depth in figures 2.1 and 2.2. The adopted depth-intensity relation has been found by weighting each of the intensities shown in the figures according to an estimate of its reliability and taking a weighted mean curve. This is the curve shown in the figures. The numerical values are given in table 2.11. Finally, confidence limits have been derived outside of which it is considered unlikely (probability $\lesssim 10\%$) that the true relation should lie; these limits are shown in figure 7.1.

Table 2.11.

Depth in m.w.e. rock below sea level.	Vertical intensity ($sec^{-1}\ cm^{-2}\ st^{-1}$)
100	2.18×10^{-4}
150	1.10×10^{-4}
200	6.20×10^{-5}
300	2.70×10^{-5}
500	7.95×10^{-6}
700	3.18×10^{-6}
1000	1.10×10^{-6}
1500	3.13×10^{-7}
2000	1.16×10^{-7}
3000	2.32×10^{-8}
4000	6.20×10^{-9}
5000	1.87×10^{-9}
6000	5.45×10^{-10}
7000	1.55×10^{-10}

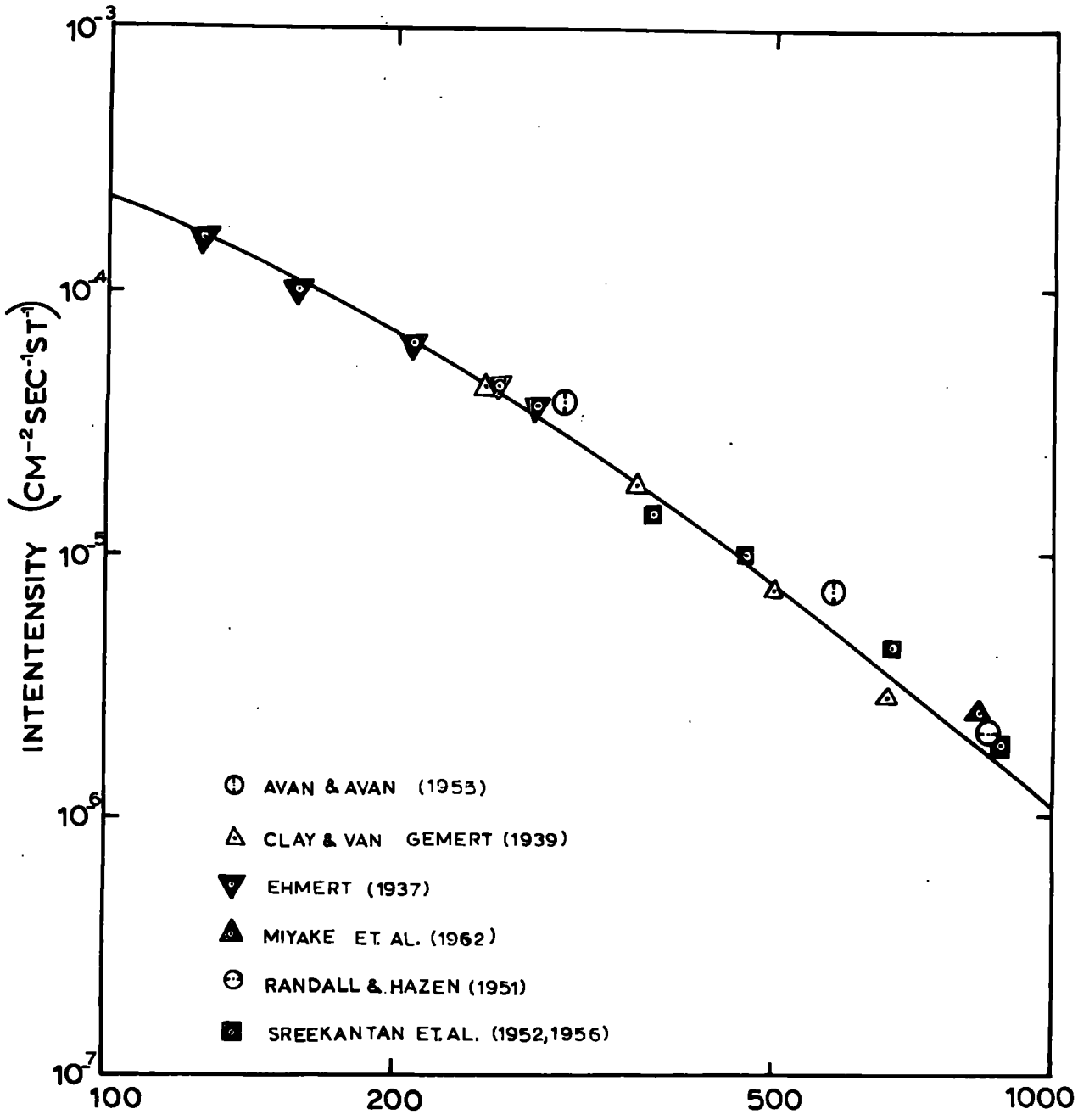
10^{-3}
10^{-4}
10^{-5}
10^{-6}
10^{-7}
INTENSITY $(CM^{-2}SEC^{-1}ST^{-1})$
100
200
500
1000
DEPTH M.W.E. ROCK
AVAN & AVAN (1953)
CLAY & VAN GEMERT (1939)
EHMERT (1937)
MIYAKE ET AL. (1962)
RANDALL & HAZEN (1951)
SREEKANTAN ET AL. (1952,1956)

FIGURE 2·1

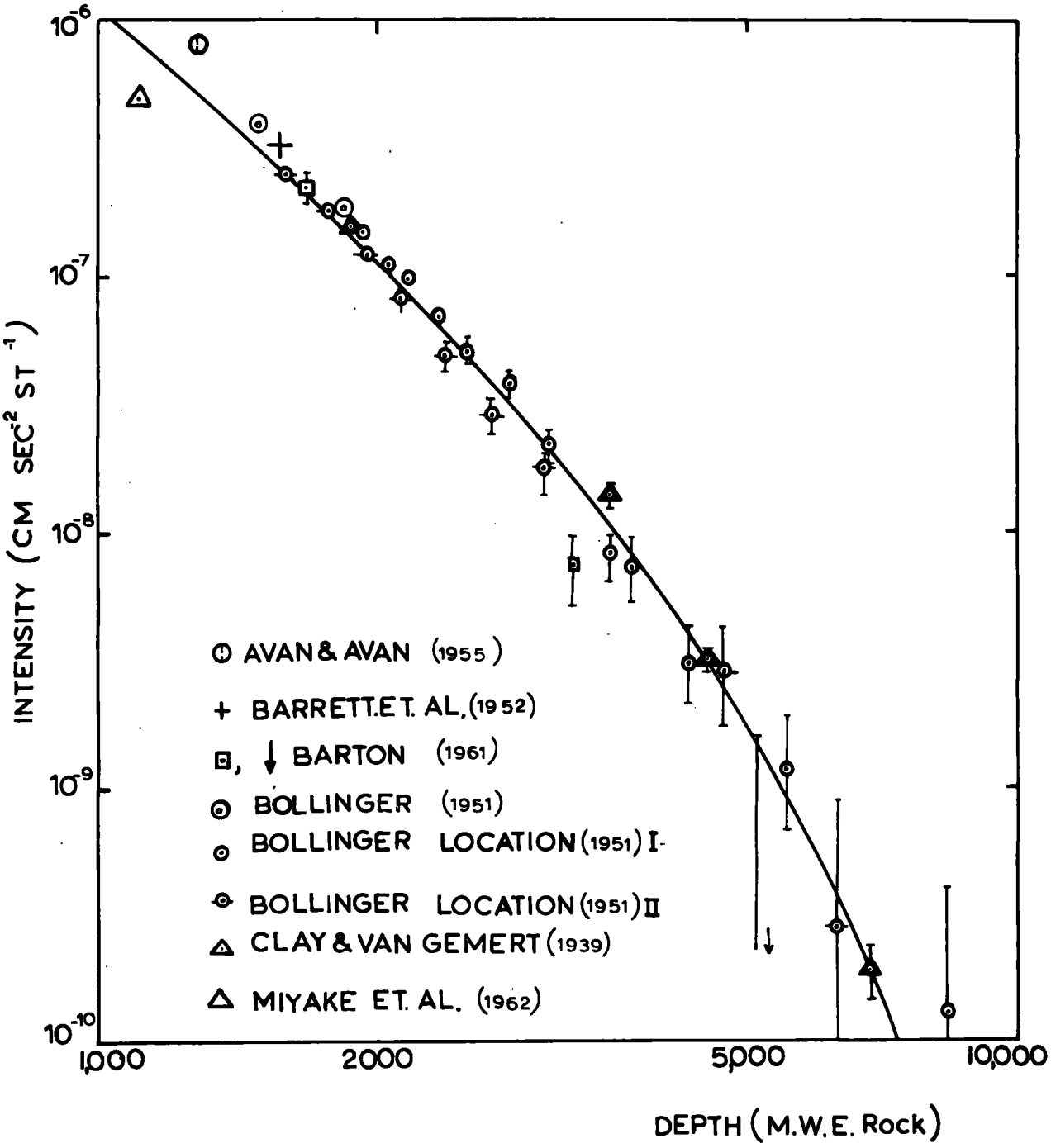
INTENSITY (CM SEC^{-2} ST^{-1})
10^{-6}
10^{-7}
10^{-8}
10^{-9}
10^{-10}
1,000
2000
5,000
10,000
DEPTH (M.W.E. Rock)
AVAN & AVAN (1955)
BARRETT.ET. AL.,(1952)
BARTON (1961)
BOLLINGER (1951)
BOLLINGER LOCATION (1951) I
BOLLINGER LOCATION (1951) II
CLAY & VAN GEMERT (1939)
MIYAKE ET. AL. (1962)

FIGURE 2·2

Chapter 3. The Sea Level Muon Spectrum.

3.1. The measured spectra.

3.1.1. The Durham Spectrum.

The most recent direct measurement of the sea level spectrum is that due to Hayman and Wolfendale, 1962, (the "Durham spectrum") and covers the range 0.4-1,000 GeV. These data, which are shown in figure 3.1, refer essentially to single particles, i.e. those which traversed the cosmic ray spectrograph unaccompanied by secondaries. Since it is the total spectrum of muons that is required, irrespective of whether the muons are accompanied or not, an estimate of the selection bias is required.

An experiment has since been carried out in an attempt to obtain an estimate of this bias using a slightly modified version of the Durham spectrograph. This experiment is described in detail in Chapter 4.

3.1.2. The Bristol Spectrum.

There have been no direct measurements of the muon spectrum much above 1,000 GeV. Instead, indirect determinations must be made, either from the interaction rates of the sea level component, or from measurements made on other cosmic ray components. The interaction studies are typified by the measurement of the frequency of electromagnetic bursts at sea level (Krasilnikov, 1962) using ionisation chambers. However, since in this type of method assumptions have to be made about the correctness of the theoretical expressions for

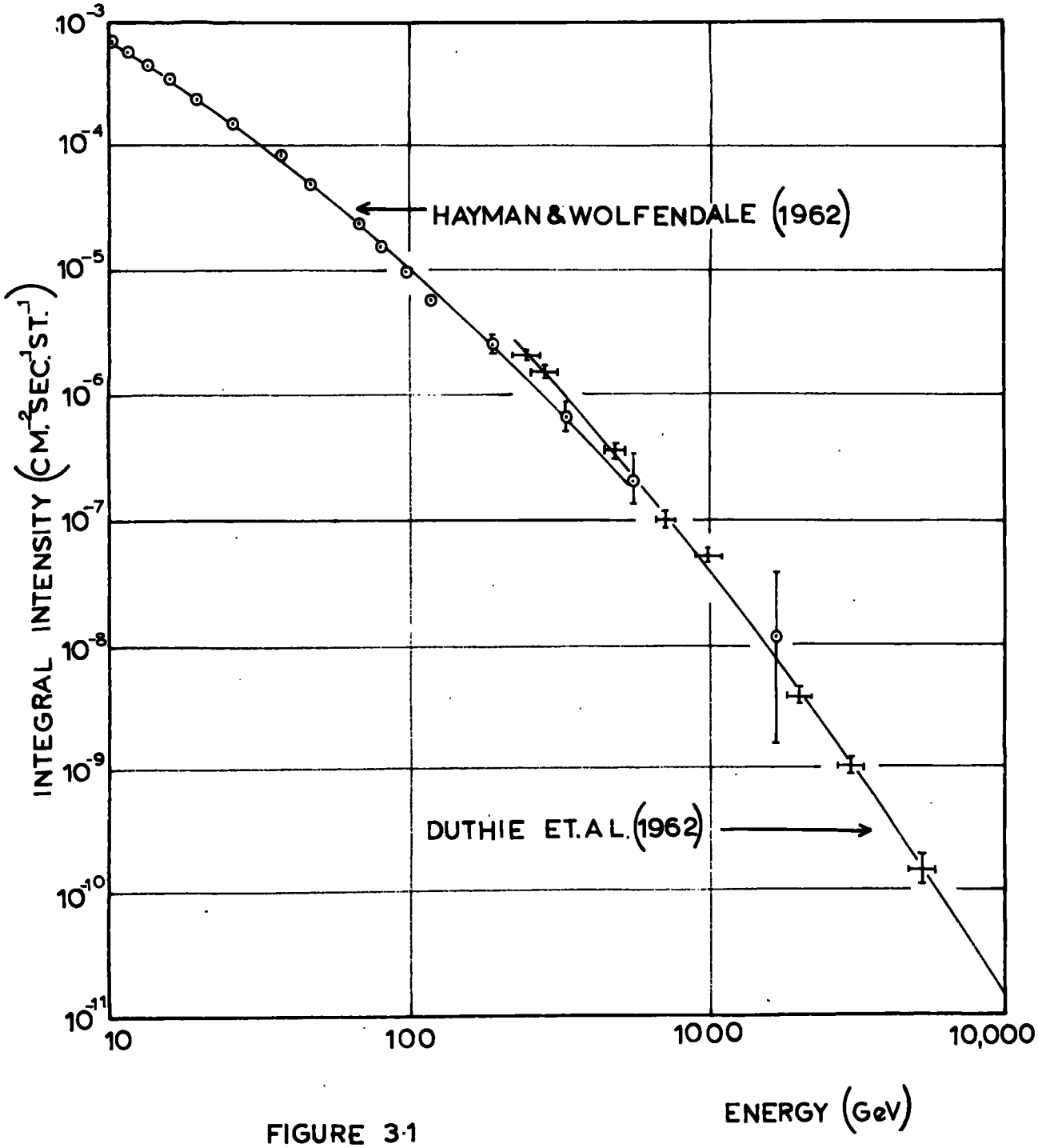
INTEGRAL INTENSITY (CM.$^{-2}$SEC.$^{-1}$ST.$^{-1}$)
10^{-3}
10^{-4}
10^{-5}
10^{-6}
10^{-7}
10^{-8}
10^{-9}
10^{-10}
10^{-11}
HAYMAN & WOLFENDALE (1962)
DUTHIE ET. A L. (1962)
10
100
1000
10,000
ENERGY (GeV)

FIGURE 3·1

the energy loss of muons (mainly bremsstrahung), they cannot be used for the present purpose.

An accurate measurement of the spectrum of γ- rays at high altitudes has been made by Duthie et al. (1962), using stacks of nuclear emulsion flown by balloon and aircraft. By assuming a model for the propagation of cosmic rays through the atmosphere and in particular that pions alone are the source of muons these workers have calculated the expected spectrum of muons arriving at sea level. The predicted intensities found in this way are also shown in figure 3.1 (the "Bristol spectrum").

3.2. Derivation of a Composite Spectrum.

It is apparent that in the overlap region (200-1,000 GeV) between the Durham and Bristol spectra a small systematic difference exists. This difference is thought to consist of the bias due to the rejection of accompanied particles in the Durham measurement, together with errors likely to arise through the indirect nature of the Bristol work. In the following chapter an estimate of the bias is made and in section 4.9 the corrected Durham data are combined with the Bristol results to give the composite spectrum adopted for the purpose of examining the rate of energy loss.

Chapter 4. Bias Effects on the Spectrum.

4.1. Sources of Bias.

As mentioned in the previous chapter, the main source of bias in the Durham measurement of the sea level spectrum was due to the rejection of "accompanied" events.

The electronic selection system used in the spectrograph rejected events in which two or more geiger counters were discharged in any one layer. The three main types of event which were lost due to this selection criterion are thus

(i) Events in which an incoming muon generated a knock-on electron, either in the lead shielding above the spectrograph, or in the flash-tube trays themselves.

(ii) Events in which a muon, forming part of an extensive air shower, penetrated the spectrograph but was rejected because of the presence of accompanying electrons. The removal of these electrons due to absorption in the atmosphere is less marked as the energy increases, and so this bias is expected to increase with energy.

(iii) The rather more infrequent event where two muons were sufficiently close together to pass through either part or the whole of the spectrograph at the same time.

It has unfortunately not been possible to carry out a bias experiment with the apparatus used by Hayman and Wolfendale under identical conditions, but a suitable correction has been applied to account for the modifications to the spectrograph and it is considered that the application

of the results obtained to the Hayman and Wolfendale spectrum is accompanied by little error. The main modification to the spectrograph, namely, the introduction of a solid iron plug into the air gap of the magnet, is discussed in the subsequent section.

4.2. The Experimental Arrangement.

4.2.1. The Magnet.

In principle, the spectrograph consists of a magnetic field to cause a deflection of incoming charged particles and suitably placed detecting elements for the purpose of measuring the deflection. In the original spectrograph, as used in the experiment of Hayman and Wolfendale, the magnetic field was produced by an air-gap magnet which produced a field volume of 6.025×10^5 gauss cm. at an excitation current of 58 amps.

Due to the extremely weakly-interacting nature of muons it is possible to use solid magnetized iron for the purposes of deflection (Bennett and Nash, 1960, O'Connor and Wolfendale, 1960). The main advantage of this method is that by its use it is possible to obtain a much larger volume of uniform high intensity field than in the air-gap case. For this purpose the Durham spectrograph has been modified by the insertion of a solid iron block of dimensions 45 x 45 x 40 cm., the resultant field volume obtained being 7.2×10^5 gauss cm. at an excitation current of 60 amps. The particle collection rate of this arrangement is higher than in the previous case by a factor of approximately four.

4.2.2. The Detecting Elements.

In order to define the trajectories of particles passing through the spectrograph, detecting elements are arranged at four levels. Two of these levels, denoted A and B, are located above the magnet and two, C and D, below. (figure 4.1). The arrangement is essentially that described by Brooke et al. (1962).

The detectors at each level are of two kinds. The initial detection of particles is carried out by means of geiger counters, 25 in each of layers A and D, and 9 in each of B and C. The dimensions of the counters are given in table 4.1.

Table 4.1.

Tray	Counter length (cm.)	
A	60	External diameter 3.6 cm.
B	25	Internal diameter 3.4 cm.
C	25	
D	60	

The counters in each tray are arranged to be perpendicular to the particle deflection plane with a lateral separation of 3.8 cm. between each. If the geiger counters alone are used to define the particle trajectory, the maximum detectable momentum (m.d.m.) obtained under these conditions is 32.0 GeV/c at a magnet current of 60 amps.

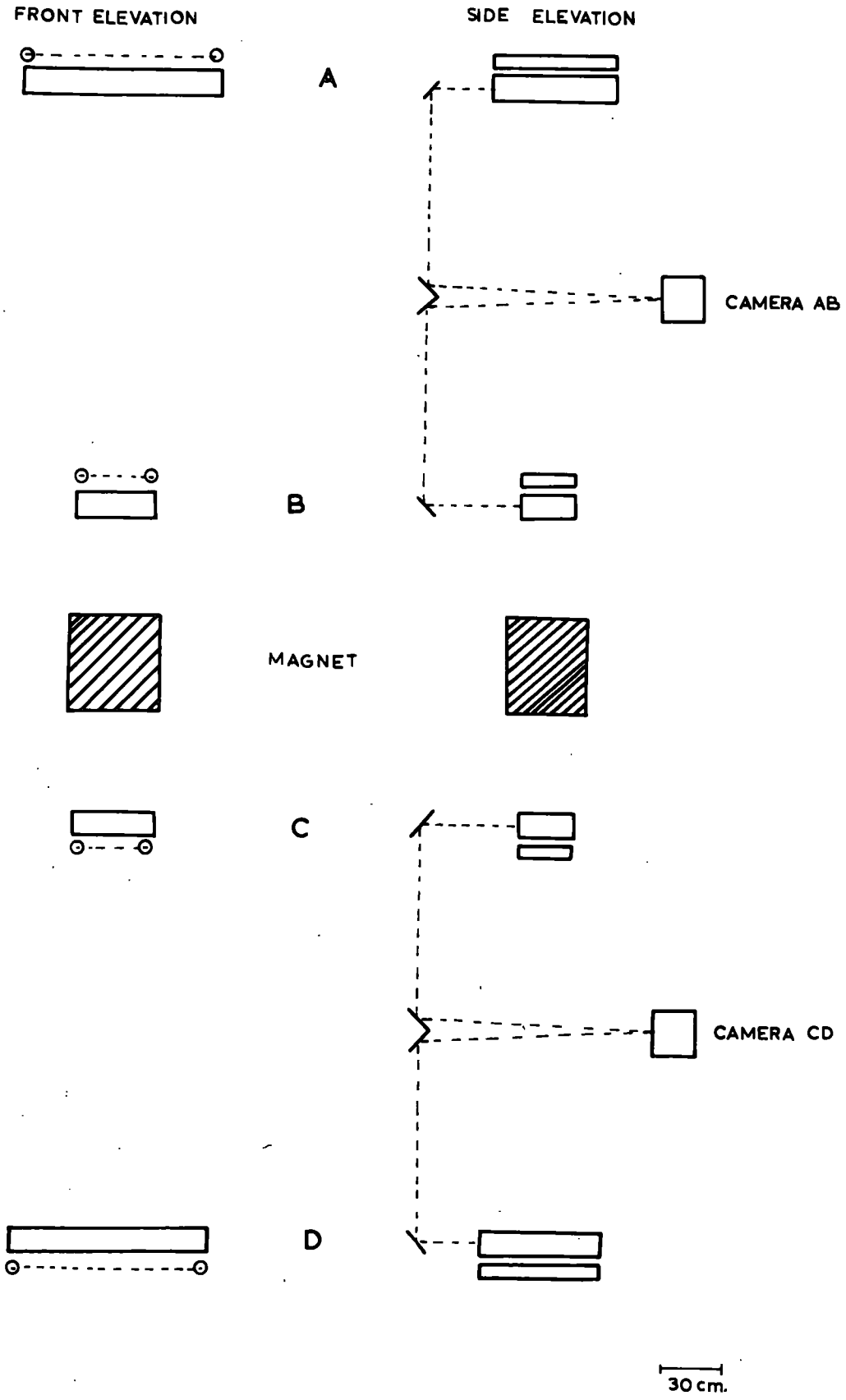
FRONT ELEVATION
SIDE ELEVATION
A
CAMERA AB
B
MAGNET
C
CAMERA CD
D
30 cm.

FIGURE 4·1

In order to increase the accuracy with which the position of the trajectory at each level could be found, further detectors capable of higher spatial resolution were necessary. This was achieved in the form of trays of neon flash tubes as described by Hayman and Wolfendale (1962). The flash tube is essentially a narrow glass tube containing neon at high pressure, and has the property of emitting a visible flash of light if it is subjected to the application of a high voltage pulse within a few micro--seconds of the passage of a charged particle through the gas. If the tubes are stacked in close arrays, they can be photographed and the particle position determined accurately. In the Durham spectrograph eight layers of tubes are used at each level with the layers staggered with respect to one another in order to achieve uniform accuracy over the acceptance of the instrument ($\pm$ 13^{o} from the vertical in the deflection plane and $\pm$ 6.5^{o} in the perpendicular plane.). The details of the flash tubes are reproduced in table 4.2.

Table 4.2.

Internal diameter 0.59 cm.
External diameter 0.72 cm.
Horizontal separation in a layer 0.80 cm.
Vertical separation of the layers 1.15 cm.
Length, levels A and D 67 cm.
Length, levels B and C 42 cm.
Gas pressure 2.3 atmospheres
Gas content 98% Ne, 2% He, 10^{-4}% air
Glass soda (GEC, X8)

4.2.3. The Electronic Circuits.

The basic requirement is that the passage of a particle through all four geiger counter trays (a four-fold coincidence) should cause a high voltage pulse to be applied to the flash tube trays as quickly as possible. It is also necessary for this event to cause illumination of reference bulbs and clocks, winding on of cameras and so on. These aims are achieved by means of subsidiary electronic equipment, the majority of which have been described by Brooke et al. (1962), Jones et al. (1962) and Hayman and Wolfendale (1962).

The geiger counter trays are connected to a conventional Rossi unit, which selects four-fold coincidences of trays A, B, C and D. The master pulse which is generated by the Rossi unit on the occurrence of these events is used to trigger both the flash tube pulsing unit and the cycling system.

The pulsing unit, shown in figure 4.2, delivers 5.4 kV to a system of thin aluminium electrodes which are situated between the rows of flash tubes. The resulting field across the tubes is approximately 4.7 kV/cm.

The cycling system, figure 4.3, comprises a system of relays and relaxation circuits which, on receipt of a triggering pulse, carries out the following sequence of operations:

(i) Causes one channel of the Rossi unit to be earthed so preventing the acceptance of particles during cycling.

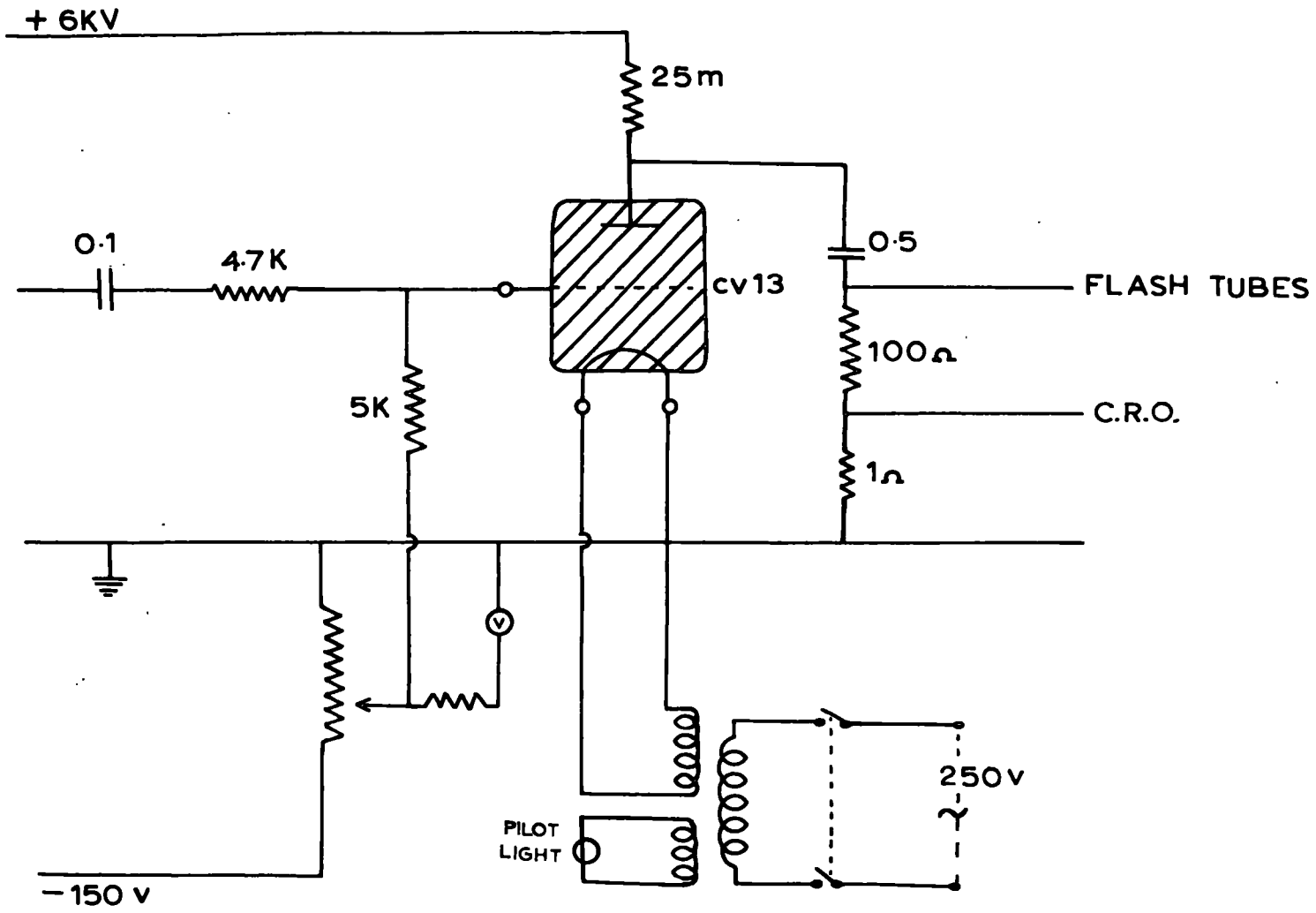
+ 6KV
25m
0·1
4·7K
CV13
0·5
FLASH TUBES
100Ω
C.R.O.
5K
1Ω
250V
PILOT
LIGHT
−150 V

FIGURE 4·2

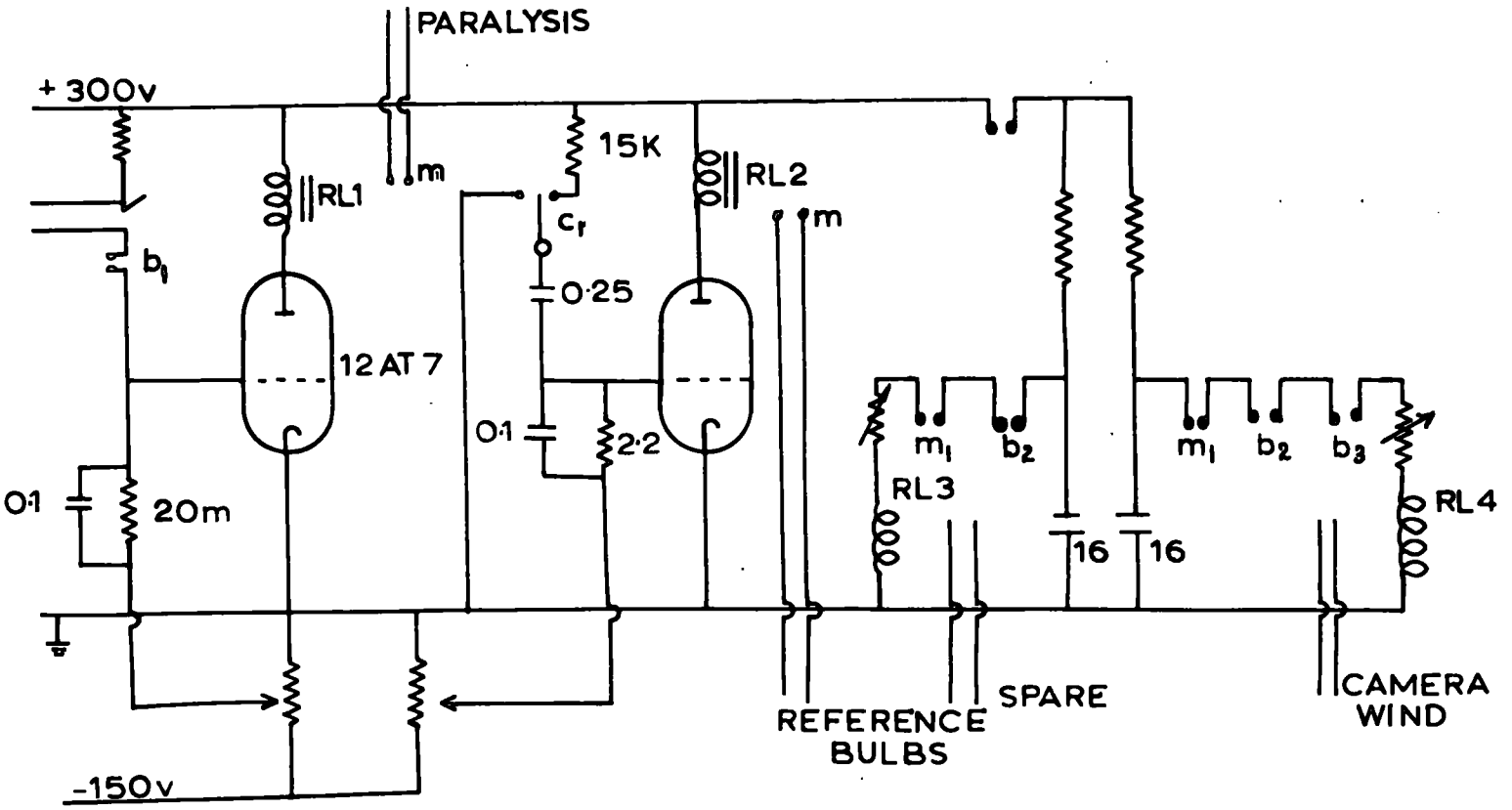
PARALYSIS
+300v
m
15K
RL1
RL2
c_r
m
b_1
0·25
12 AT 7
0·1
2·2
0·1
20m
m_1
b_2
m_1
b_2
b_3
RL3
RL4
16
16
-150v
REFERENCE BULBS
SPARE
CAMERA WIND

FIGURE 4·3

(ii) Illuminates reference bulbs on the face of each flash tube array, and illuminates the two clocks, which allow the records from each of the two cameras to be correlated.

(iii) Winds on the film in the cameras.

(iv) Removes the "paralysis".

The spectrograph is then prepared to detect the next event. The whole operation takes only about two seconds, and it is found that this "dead" time with the counting rate obtained, results in only about 2% of the events being undetected.

4.3. Experimental Procedure.

4.3.1. Preliminary Measurements.

In order to define the trajectory of a particle, the coordinates of the intersection of the particle with each measuring level are found. These are termed a, b, c and d. The displacement of the particle is then given by $\Delta = (a + a_o) - (b + b_o) - (c + c_o) + (d + d_o)$ where the quantities a_o, b_o, c_o and d_o are the distances from a vertical axis to the zero of the measuring scale on each array. The factor 0.972 which appeared in the equation given by Hayman and Wolfendale has been removed since the flash tube arrays have been adjusted so that the distances between trays A and B, and C and D are now equal.

The constants of the equation can be collected together so that $\Delta_o = a_o - b_o - c_o + d_o$ and the displacement is thus $\Delta = a - b - c + d - \Delta_o$.

A convenient unit in which to measure these quantities is the "tube spacing" or "t.s." which is the distance between adjacent tubes in a layer. This unit is equal to 0.8 cm.

To measure the displacement, Δ , of the particle accurately, it is obviously necessary not only to obtain accurate values of the co-ordinates a, b, c and d, but also an accurate value for the constant Δ_o . Two methods are available for the determination of Δ_o , the first by direct measurement of the quantities a_o, b_o, c_o and d_o, and the second by operation of the spectrograph at zero magnetic field. A measurement of the second type was carried out in which 172 events were measured and a frequency distribution of the quantity (a - b - c + d) plotted. This is shown in figure 4.4. The spread of the distribution is indicative of the large amount of scattering which occurs in the iron. This is a limiting factor in the accuracy to which Δ_o is obtained by this method. The mean of the distribution gives a value of Δ_o . The result obtained by this method is

$$\Delta_o = 61.40 \pm 0.63 \text{ t.s.}$$

while direct measurement gave a value

$$\Delta_o = 60.83 \pm 0.05 \text{ t.s.}$$

The consistency of these results is evident. Since the latter value is more accurate, it has been used in the analysis of the data.

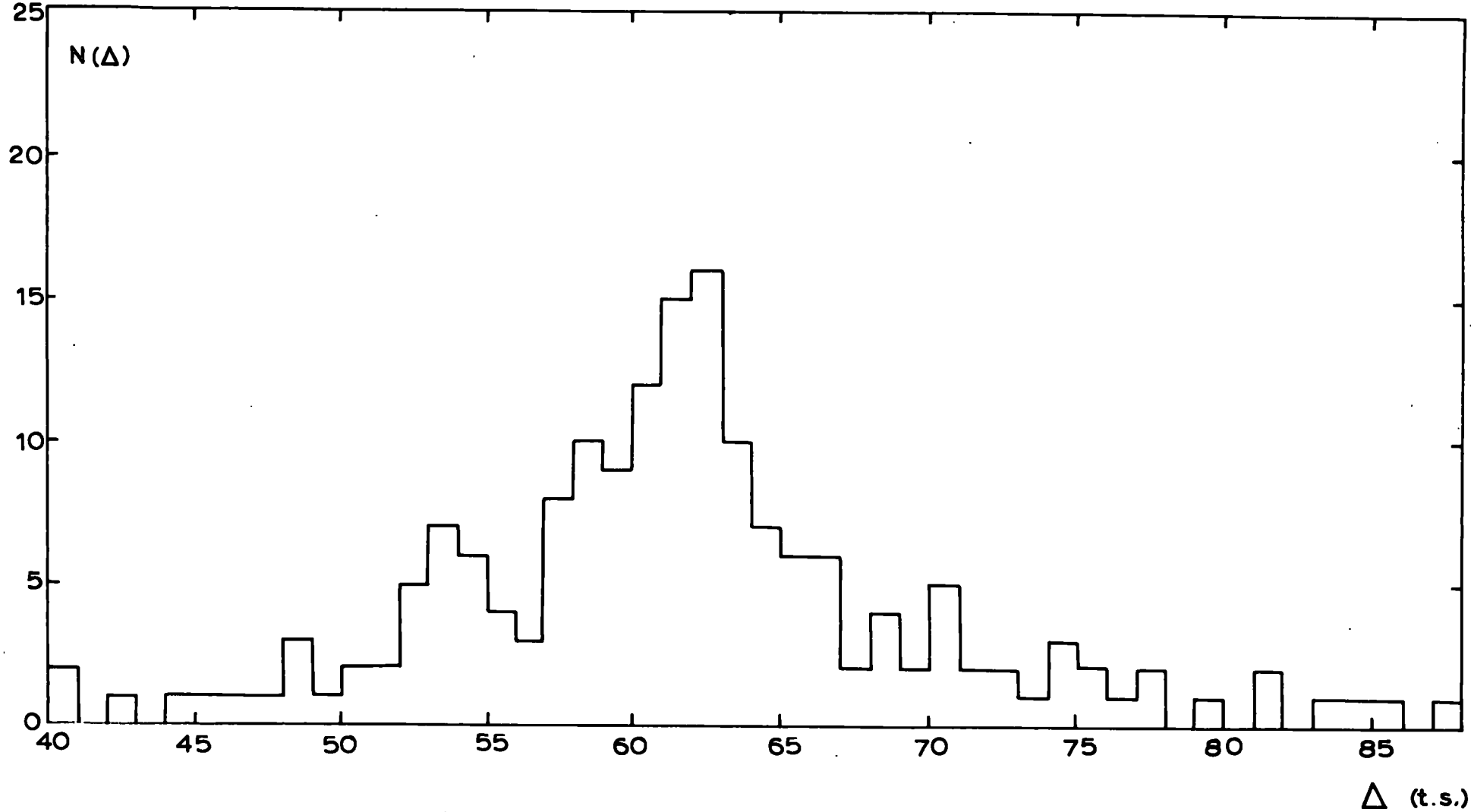

FIGURE 4·4

4.3.2. The Collection of Data.

The collection of data was accomplished during August 1963 when some 4000 useful events were obtained. Some typical events are shown in figures 4.5 to 4.10. Following the standard practice, frequent reversals of field were carried out. The excitation current used was 60 amps giving a value for the line integral of the magnetic field of $\int Hdz = 7.2 \times 10^5$ gauss cm. The momentum of a particle can be calculated from the relation $p = k/\Delta$, where $k = 300\ (AB)\int Hdz$ and AB is the distance between measuring levels A and B (Brooke et al (1962)).

Inserting the appropriate values, the result for k is

$$k = 51.20 \quad \text{GeV/c} \quad \text{t.s.}$$

$$= 40.96 \quad \text{GeV/c} \quad \text{cm.}$$

4.4. Classes of Events.

The data obtained were allocated to two main categories. The majority of events consisted of a single particle passing through the spectrograph unaccompanied by secondaries. These were classified as "single" events. Apart from unusable events i.e. those due to chance coincidences or technical failure (representing a small percentage of the total) the remaining events consisted of cases where two or more particles were detected in at least one detecting array. These were classified as "accompanied" events; a detailed description is given in section 4.1. To these events the criterion was applied of whether or not two geiger counters in one layer would have been

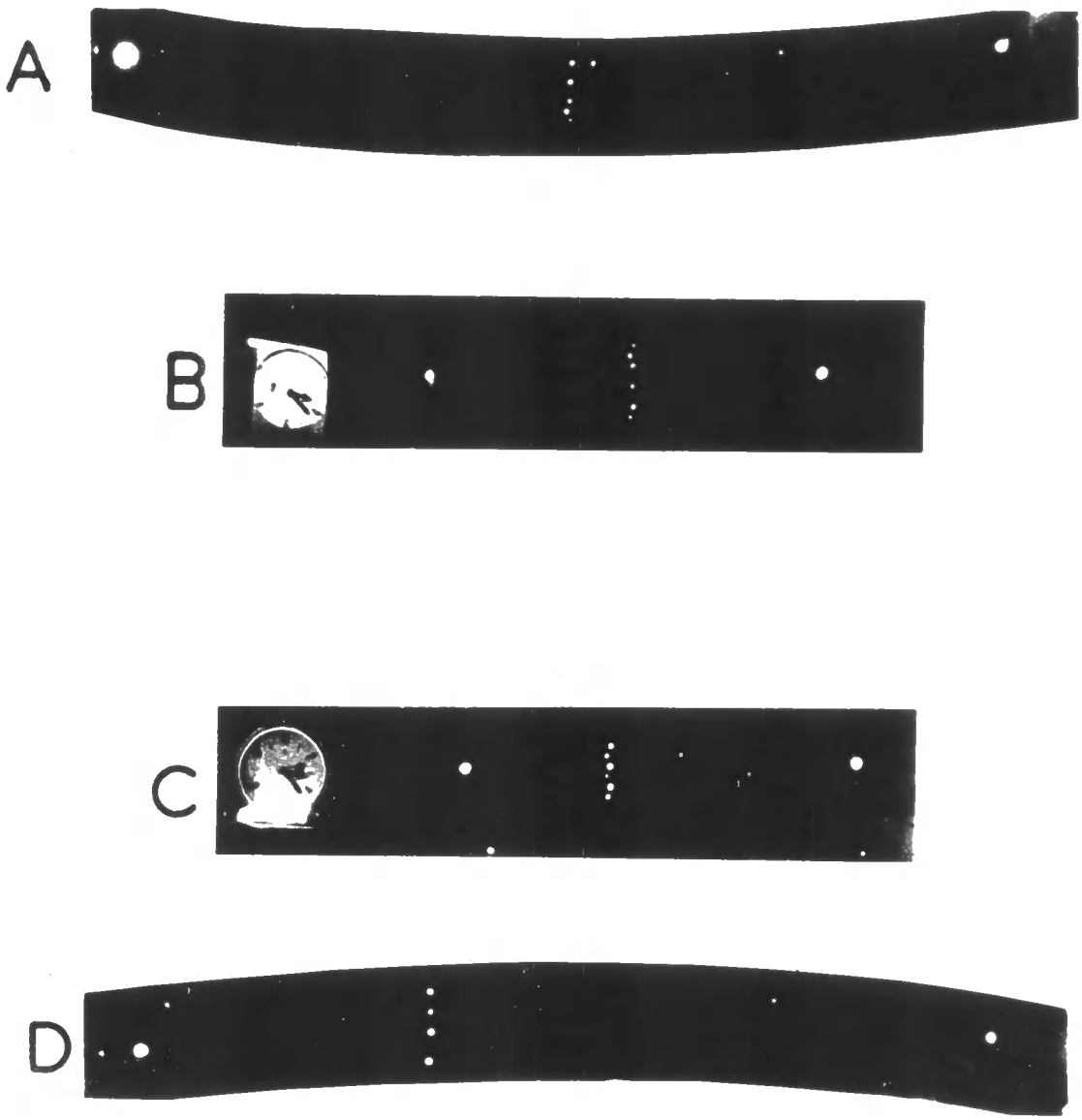

FIGURE 4·5

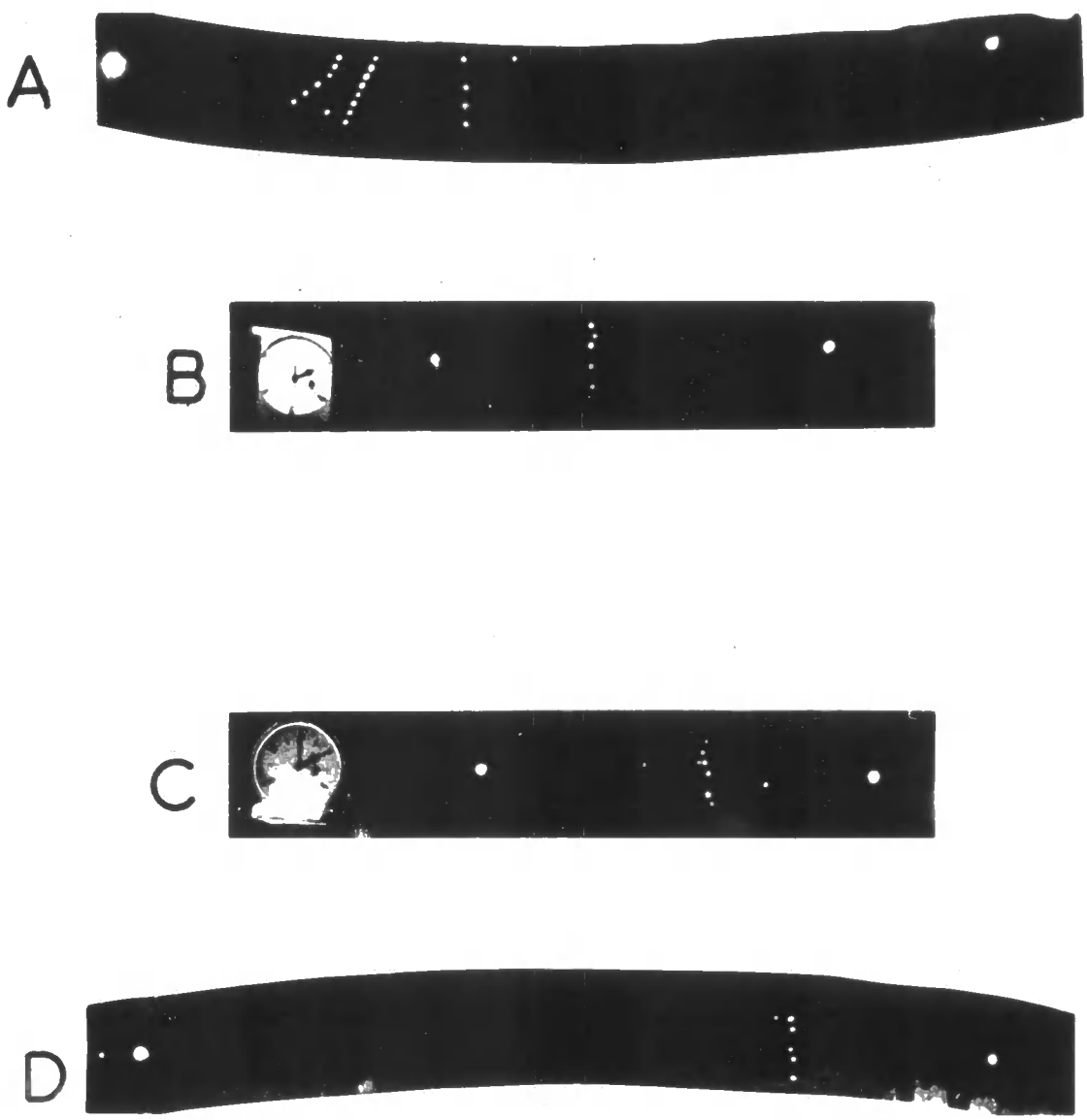

FIGURE 4·6

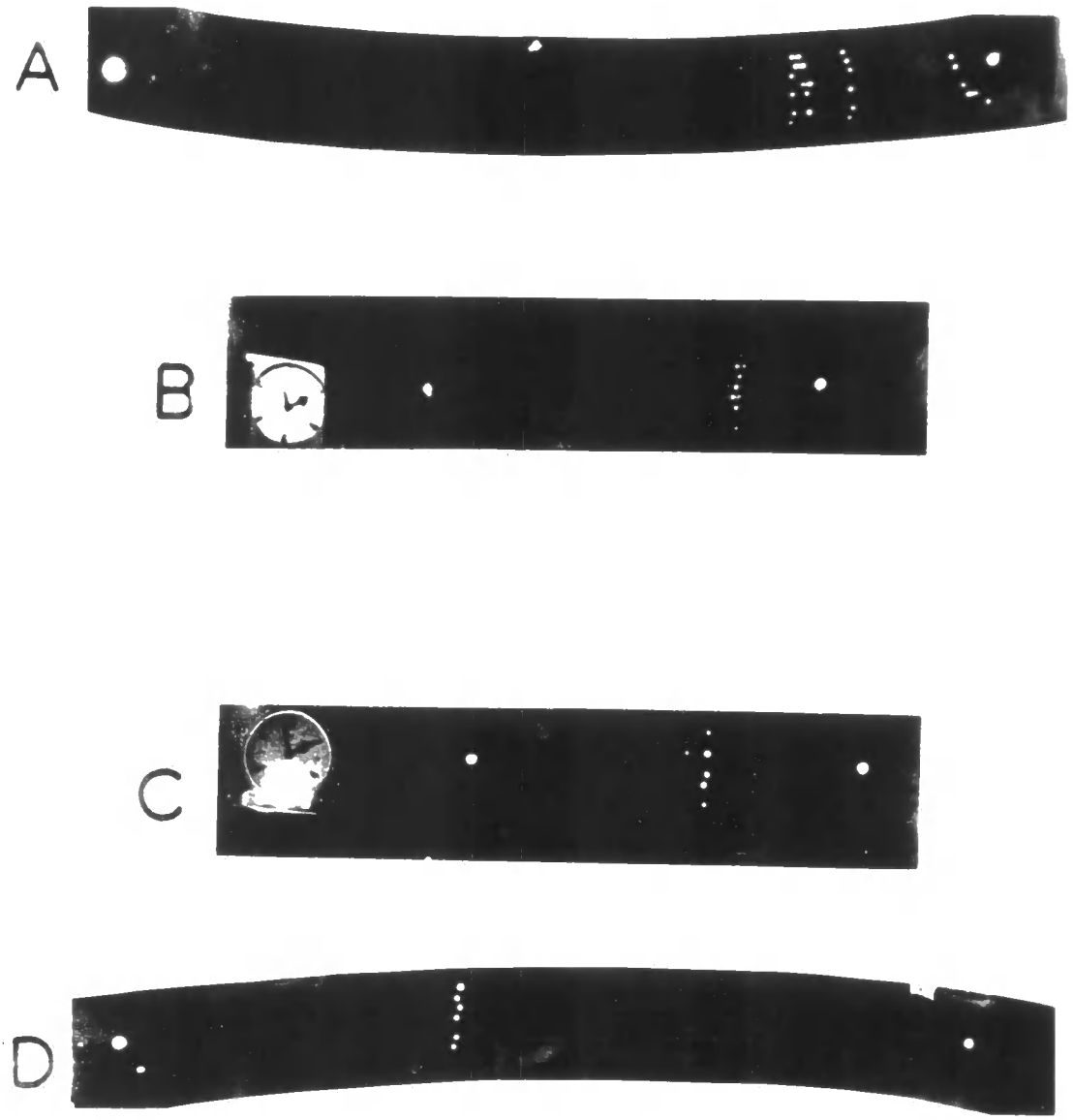

FIGURE 4.7

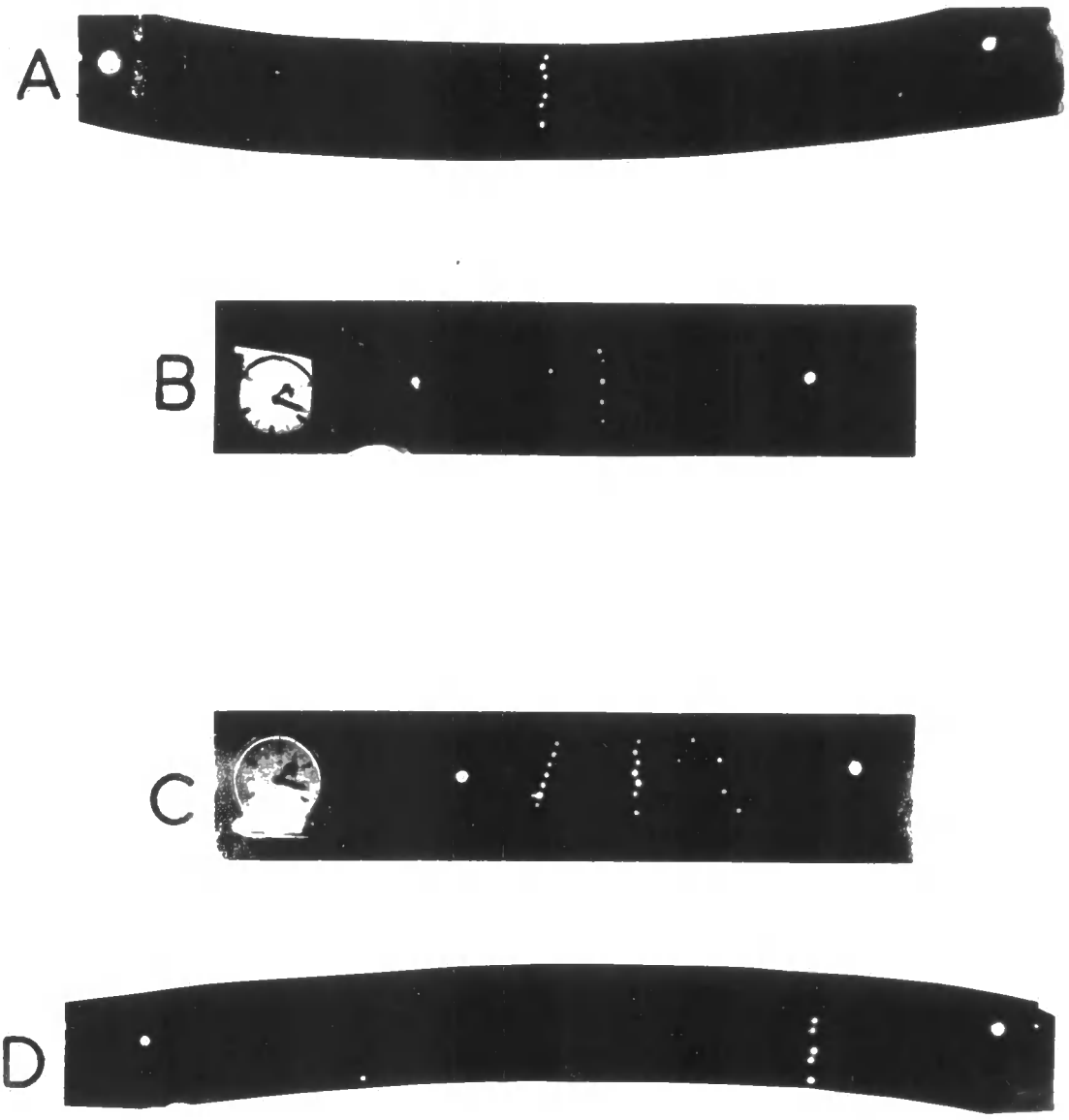

FIGURE 4·8

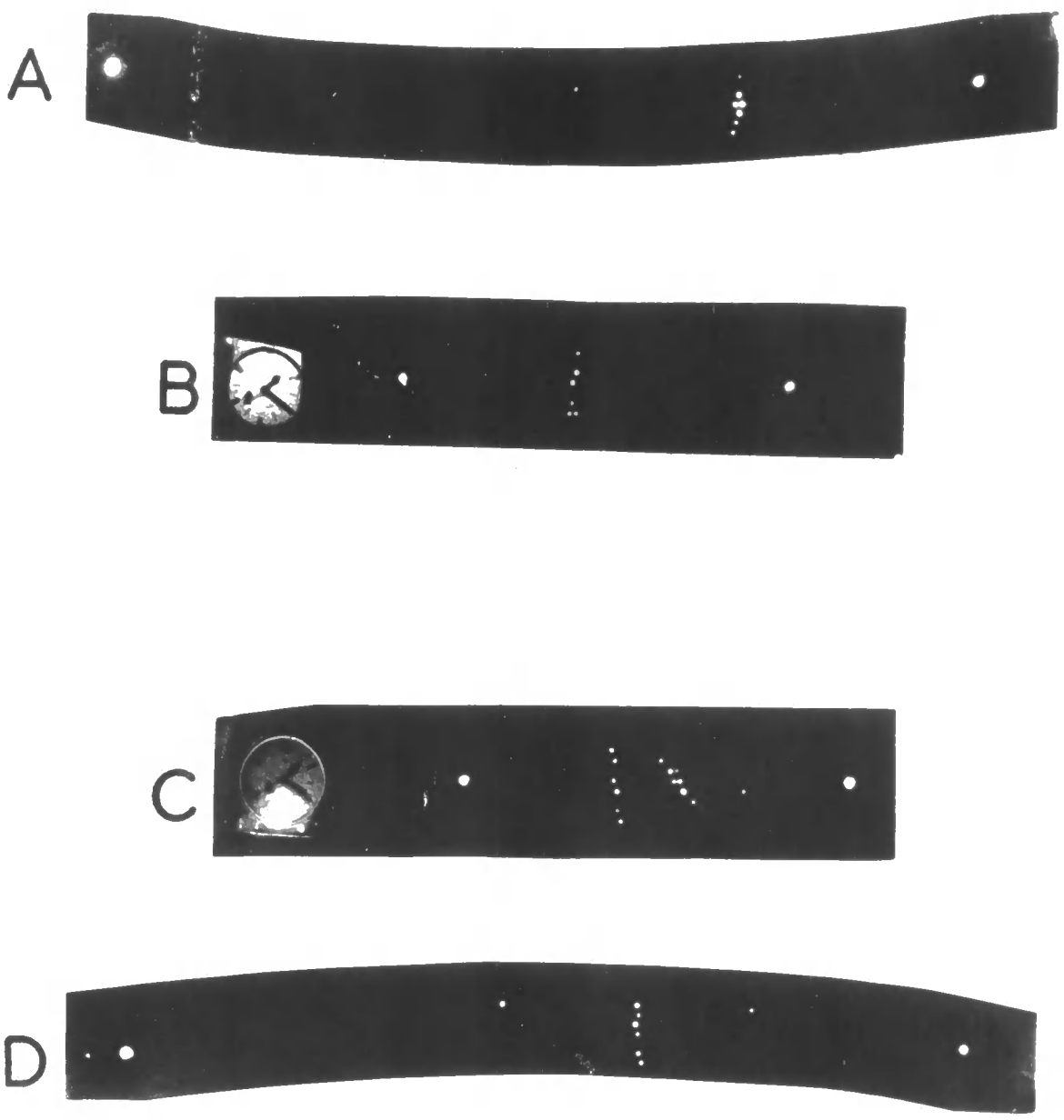

FIGURE 4.9

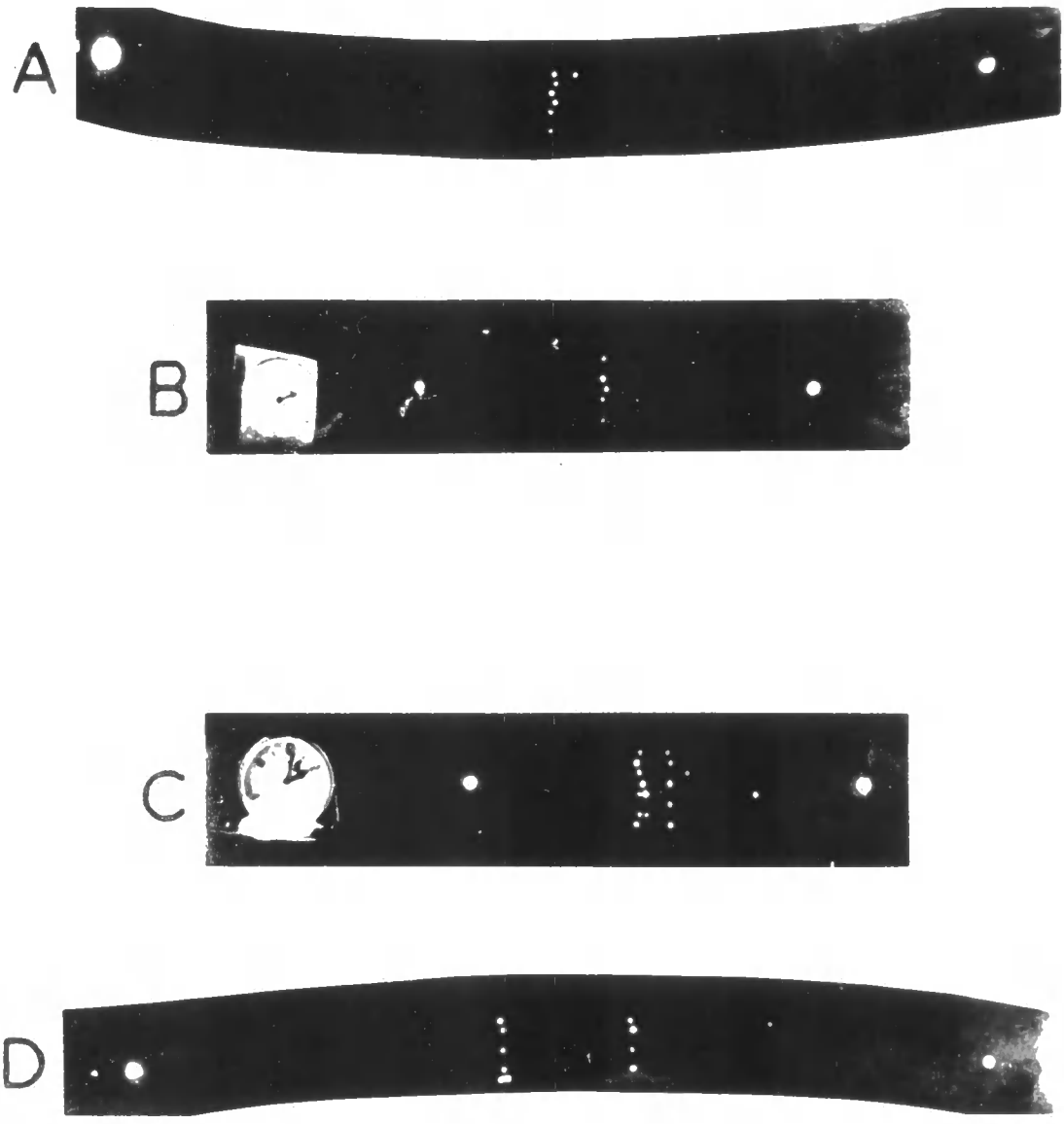

FIGURE 4.10

triggered i.e. those events automatically rejected in the experiment of Hayman and Wolfendale. No fixed rule could be applied to such a selection since it depended not only on the proximity of the two particles in the tray, but also the angle. If it was considered that only one counter would have been triggered, the particle was included in the single category; if two or more counters, it was included in the accompanied category.

Since in the experiment of Hayman and Wolfendale, the particles were deflected in an air gap magnet, and in the present case in a solid iron magnet, those accompanied events in which a knock-on electron was created in the magnet were rejected in the first instance, in order that the bias effect on the Hayman and Wolfendale spectrum could be calculated. For the sake of completeness these events have been included in a separate calculation, giving the effect of bias on the present Durham spectrograph.

4.5. The Measuring Techniques.

4.5.1. The Projector Method.

The data were analysed in the first instance by projecting the films via a system of mirrors on to an approximately full--size chart on which the flash tube trays had been drawn. A scale on each diagram enabled the co-ordinates a, b, c and d to be found using a small cursor to select the trajectory through each tray. In this way the single events were analysed and the

accompanied events selected. The analysis of these latter was aided by the use of scale diagrams of the spectrograph on which the various trajectories could be drawn, thus enabling in most cases, the single particle to be found.

From the values of a, b, c, d and Δ_o, the displacement was calculated in each case. For values of $\Delta \leqslant 3$ t.s. the "error at the centre", x, was calculated. This is the apparent discrepancy at the centre line of the magnet and is given by the relation

$$x = 0.40 + 1.324\ b + 0.318\ d - 1.318\ c - 0.324\ a$$

The frequency distribution in x is given in figure 4.11. The spread of the distribution is due partly to the effect of scattering and partly to errors in measurement at each level. If it is assumed that the scattering of such high momentum particles is small, this distribution can be used to find the error in Δ due to measuring errors. The standard deviation, δx, is found to be 0.268 ± 0.020 t.s. Using the appropriate equations, the relation between δx and the standard deviation of the distribution in Δ is

$$\delta\Delta = 1.040\ \delta x = 0.279 \pm 0.020 \text{ t.s.}$$

The maximum detectable momentum (m.d.m.) is defined as the momentum corresponding to a deflection equal to the median error in the displacement. This is calculated to be 0.188 ± 0.014 t.s., corresponding to an m.d.m. of 273 ± 20 GeV.

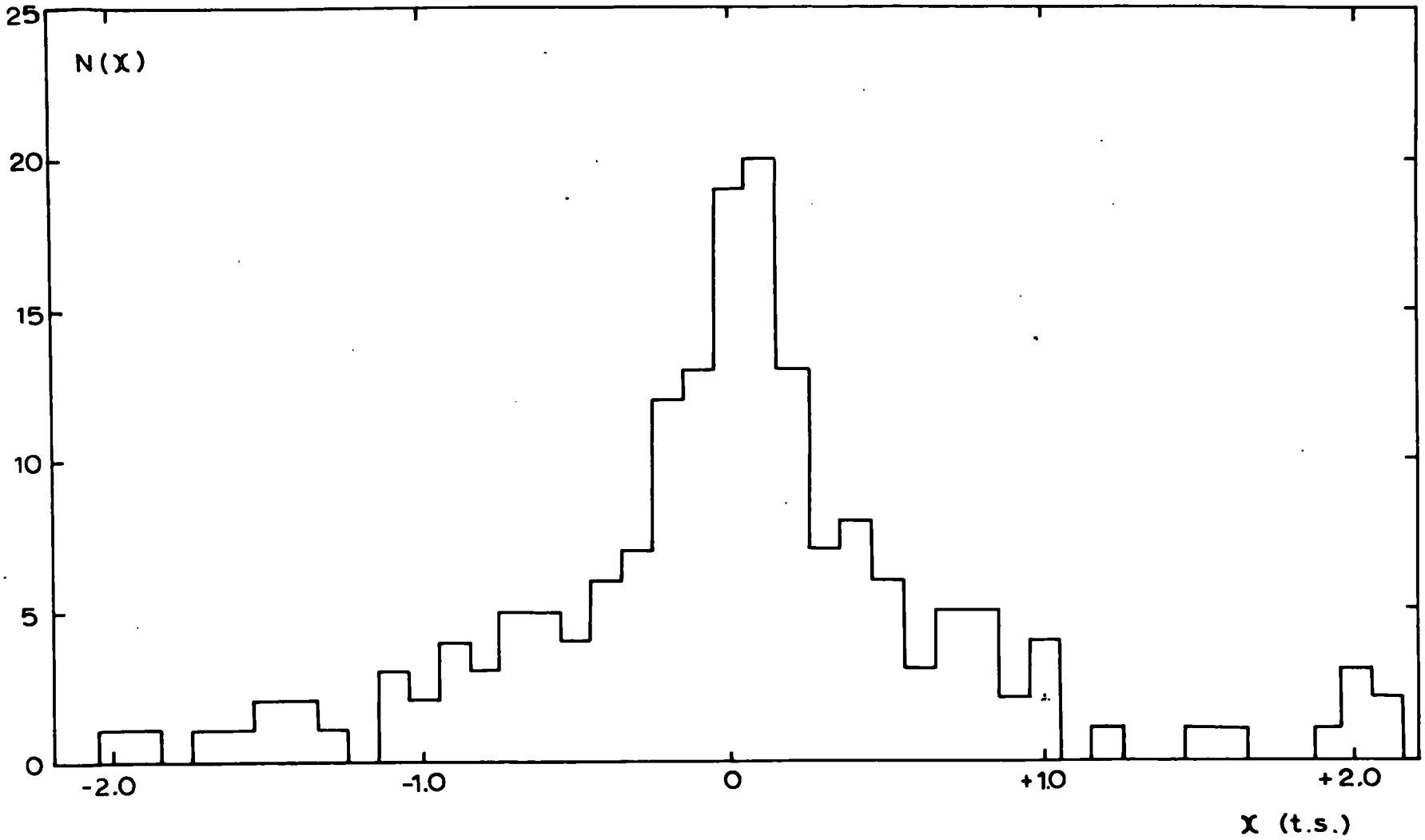

FIGURE 4.11

4.5.2. The Track Simulator Method.

For particles having a displacement $\leqslant 1$ t.s. the tracks were re-analysed using a "track Simulator". This is essentially as described by Hayman and Wolfendale. It consists of a model of a flash tube array in which the horizontal dimensions are enlarged by a factor of ten and the vertical dimensions by a factor of three. Each flash tube is thus represented as a slot which can be illuminated to represent a tube which has flashed. A cursor on the surface of the device can be set to the angle of the particle trajectory, which is known accurately from the projector values of a, b, c and d. The pattern of flashes is set up on the track simulator and the cursor is set to give a fit with the pattern according to certain established criteria. The position of the intersection of the particle trajectory with the upper surface of each flash tube array is thus found, and a more accurate value of Δ is obtained.

The error at the centre, x, for these events is found and the frequency distribution plotted as before. This is shown in figure 4.12. The m.d.m. for the track simulator method was calculated in a similar manner to the previous section and was found to be 403 ± 73 GeV.

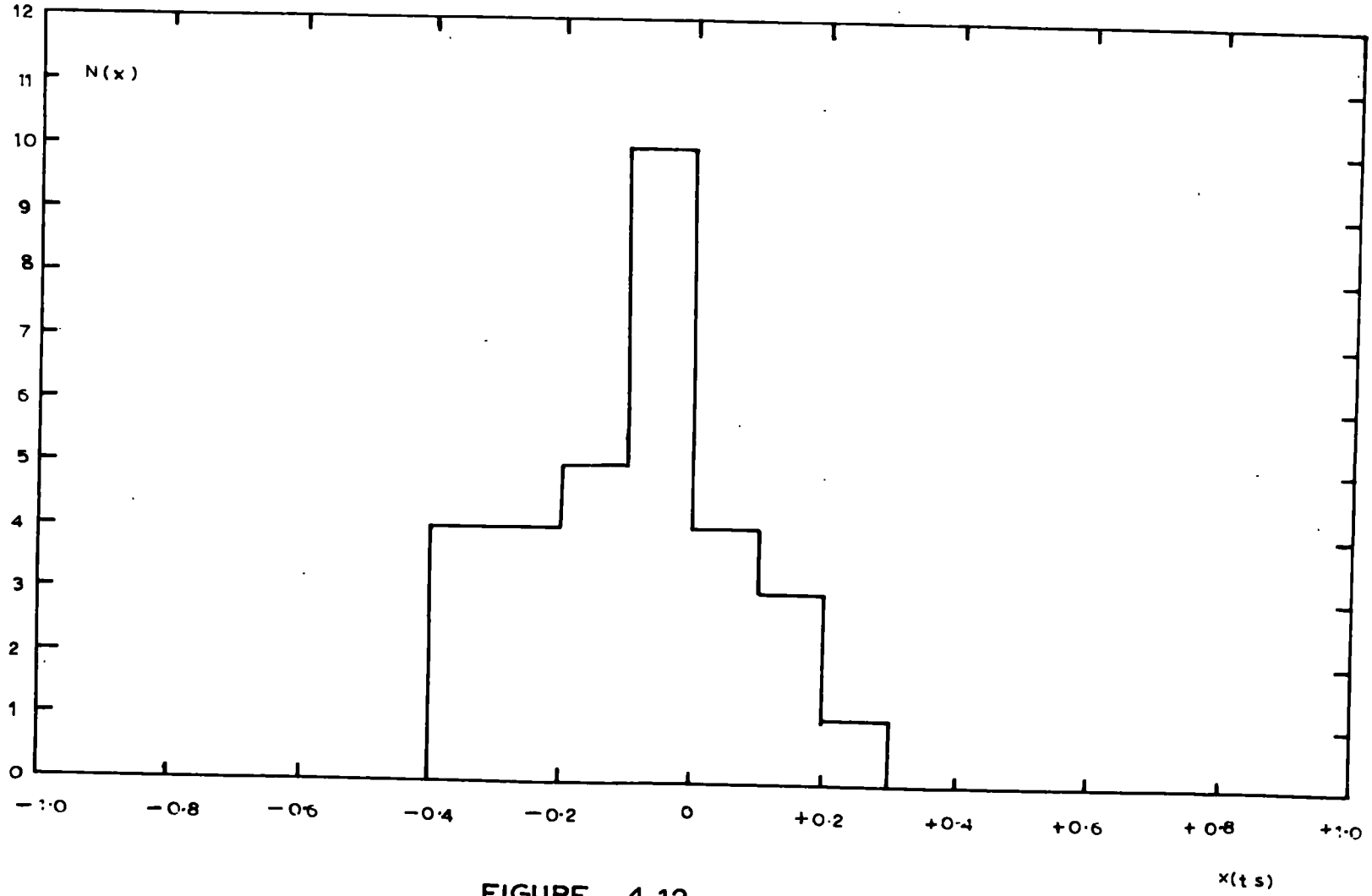

FIGURE 4·12

4.6. The Single Particle Spectrum.

From the analysis of the particles of the single category, the frequency distribution $N(\Delta)$ was obtained. The momentum spectrum for this type of event was then calculated from the expression

$$N(p) = \frac{N(\Delta)}{\delta(\Delta)} \bar{\Delta}^2$$

where $\delta(\Delta)$ is the cell size in units of Δ and $\bar{\Delta}$ is the mean displacement of the cell. The mean momentum for each cell was calculated from the relation

$$\bar{p} = \frac{(\gamma-1)}{(\gamma-2)} \left[\frac{P_1^{(2-\gamma)} - P_2^{(2-\gamma)}}{P_1^{(1-\gamma)} - P_2^{(1-\gamma)}} \right]$$

where p_1 and p_2 are the cell limits and γ is the slope of the differential momentum spectrum over that particular range. The results were normalised by a factor 3.537×10^{-8} at 15.3 GeV/c to a value 4.35×10^{-5} as given by the results of Hayman and Wolfendale. The figures are given in table 4.3. A comparison of the results with those of Hayman and Wolfendale is shown in figure 4.13. The solid line is that of Hayman and Wolfendale and the experimental points are those of the present work. The agreement between these results is clear.

4.7. The Accompanied Particle Spectrum.

In an identical manner to that described in the previous section the spectrum of the accompanied particles was calculated. The results are given in table 4.4. and in figure 4.14.

The integral ratio of accompanied particles to single particles as a function of momentum has been calculated, in the first place, as applicable to the results of Hayman and Wolfendale i.e. neglecting accompanied events originating in the solid iron magnet of the present experiment. The results are given in table 4.5 and figure 4.15.

Finally, the ratio of accompanied to single events as a function of momentum including the events in the magnet is presented. The results are shown in table 4.6 and figure 4.16.

Table 4.3.

Displacement cell (t.s.)	Mean momentum (GeV/c)	Events.	Relative Intensity	Normalised Intensity ($cm^{-2}sec^{-1}st^{-1}(GeV/c)^{-1}$)	Error (%)
50-100	0.76	314	3.53×10^{4}	1.25×10^{-3}	5.65
20-50	1.69	1029	4.22×10^{4}	1.49×10^{-3}	2.75
10-20	3.62	727	1.64×10^{4}	5.80×10^{-4}	3.7
5-10	7.06	486	5.45×10^{3}	1.93×10^{-4}	4.55
2-5	15.3	300	1.23×10^{3}	4.35×10^{-5}	5.8
1-2	34.6	57	1.28×10^{2}	4.53×10^{-6}	13.2
0.5-1	68.4	11	1.24×10	4.39×10^{-7}	$^{+39}_{-30}$
0.2-0.5	131	10	4.10	1.45×10^{-7}	$^{+42}_{-31}$
0-0.2	431	1	5.00×10^{-2}	1.77×10^{-9}	$^{+230}_{-83}$

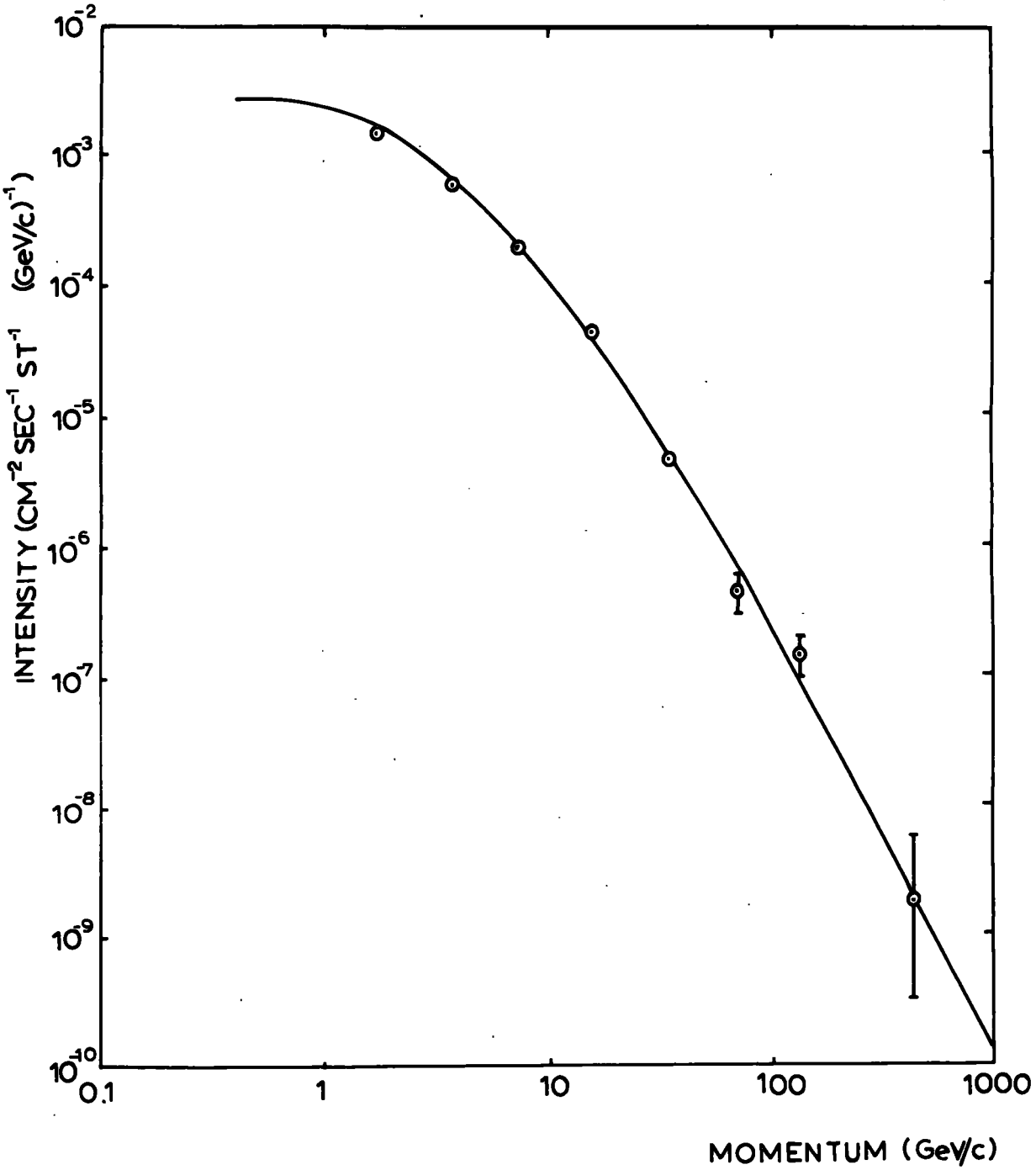
INTENSITY (CM^{-2} SEC^{-1} ST^{-1} (GeV/c)$^{-1}$)
10^{-2}
10^{-3}
10^{-4}
10^{-5}
10^{-6}
10^{-7}
10^{-8}
10^{-9}
10^{-10}
0.1
1
10
100
1000
MOMENTUM (GeV/c)

FIGURE 4·13

Table 4.4. The Accompanied Particle Spectrum.

Displacement cell (t.s.)	Mean momentum (GeV/c)	Events	Relative intensity	Normalised intensity ($cm^{-2}sec^{-1}st^{-1}$ $(GeV/c)^{-1}$)	Error (%)
50-100	0.76	17	1.91×10^{3}	6.76×10^{-5}	+30 -24
20-50	1.69	109	4.47×10^{3}	1.58×10^{-4}	9.6
10-20	3.62	104	2.34×10^{3}	8.28×10^{-5}	9.8
5-10	7.06	77	8.62×10^{2}	3.05×10^{-5}	11.4
2-5	15.3	47	1.93×10^{2}	6.83×10^{-6}	14.6
1-2	34.6	8	1.80×10	6.37×10^{-7}	+48 -35
0.5-1	68.4	4	4.50	1.59×10^{-7}	+78 -48
0.2-0.5	131	2	8.20×10^{-1}	2.90×10^{-8}	+132 -64.6
0-0.2	431	0	-	-	-

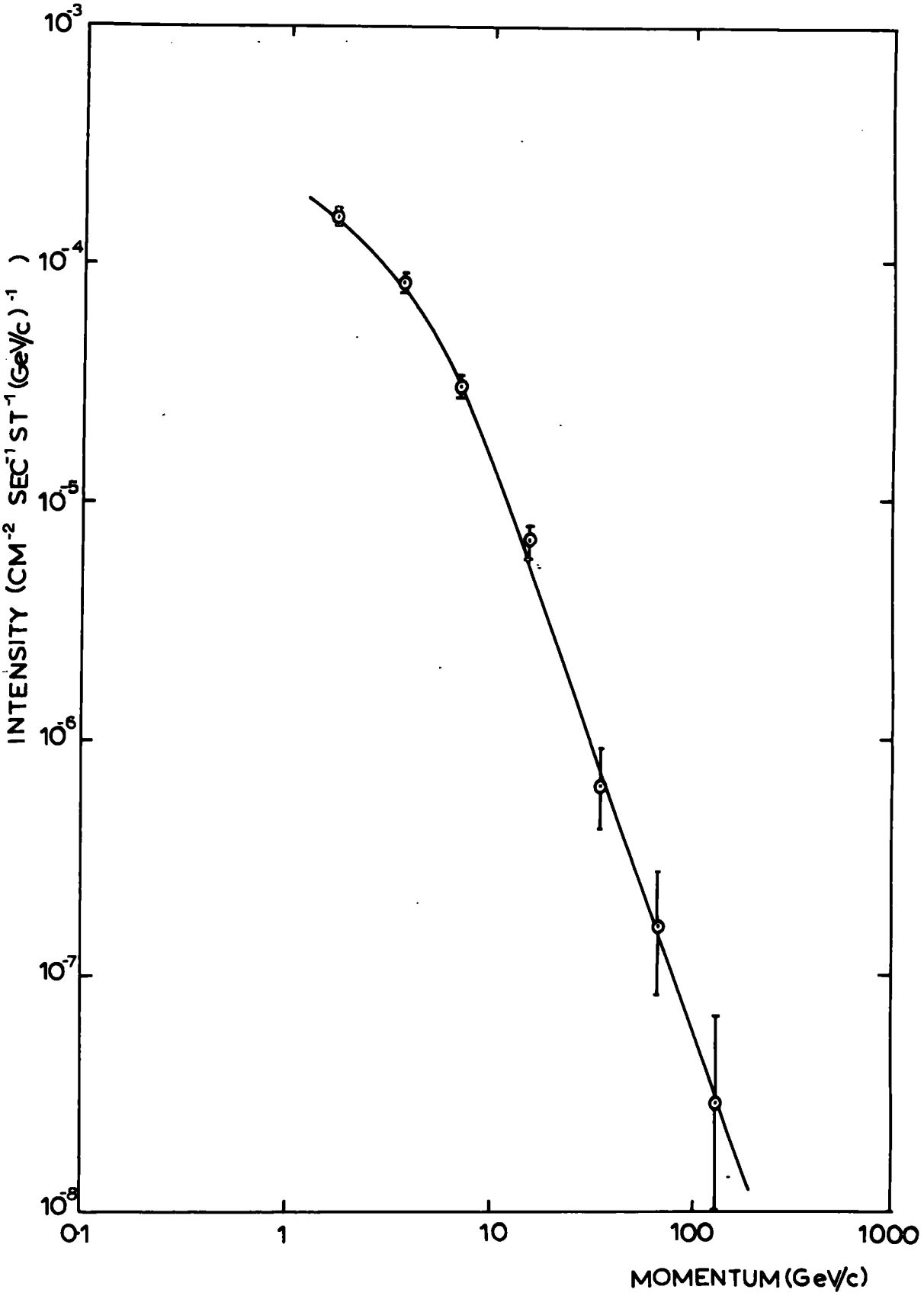
10^{-3}
10^{-4}
10^{-5}
10^{-6}
10^{-7}
10^{-8}
INTENSITY (CM^{-2} SEC^{-1} ST^{-1} $(GeV/c)^{-1}$)
0·1
1
10
100
1000
MOMENTUM (GeV/c)

FIGURE 4·14

Table 4.5. Ratio of Accompanied to Single Events.

Maximum Displacement (t.s.)	Minimum momentum (GeV/c)	Ratio (%)	Error (%)
100	0.51	9.30	± 0.59
50	1.02	9.96	± 0.65
20	2.56	10.99	± 0.88
10	5.12	11.10	± 1.19
5	10.2	11.87	± 1.87
2	25.6	12.65	+ 5.50 - 4.17
1	51.2	13.64	+13.41 - 8.30
0.5	102.4	-	-

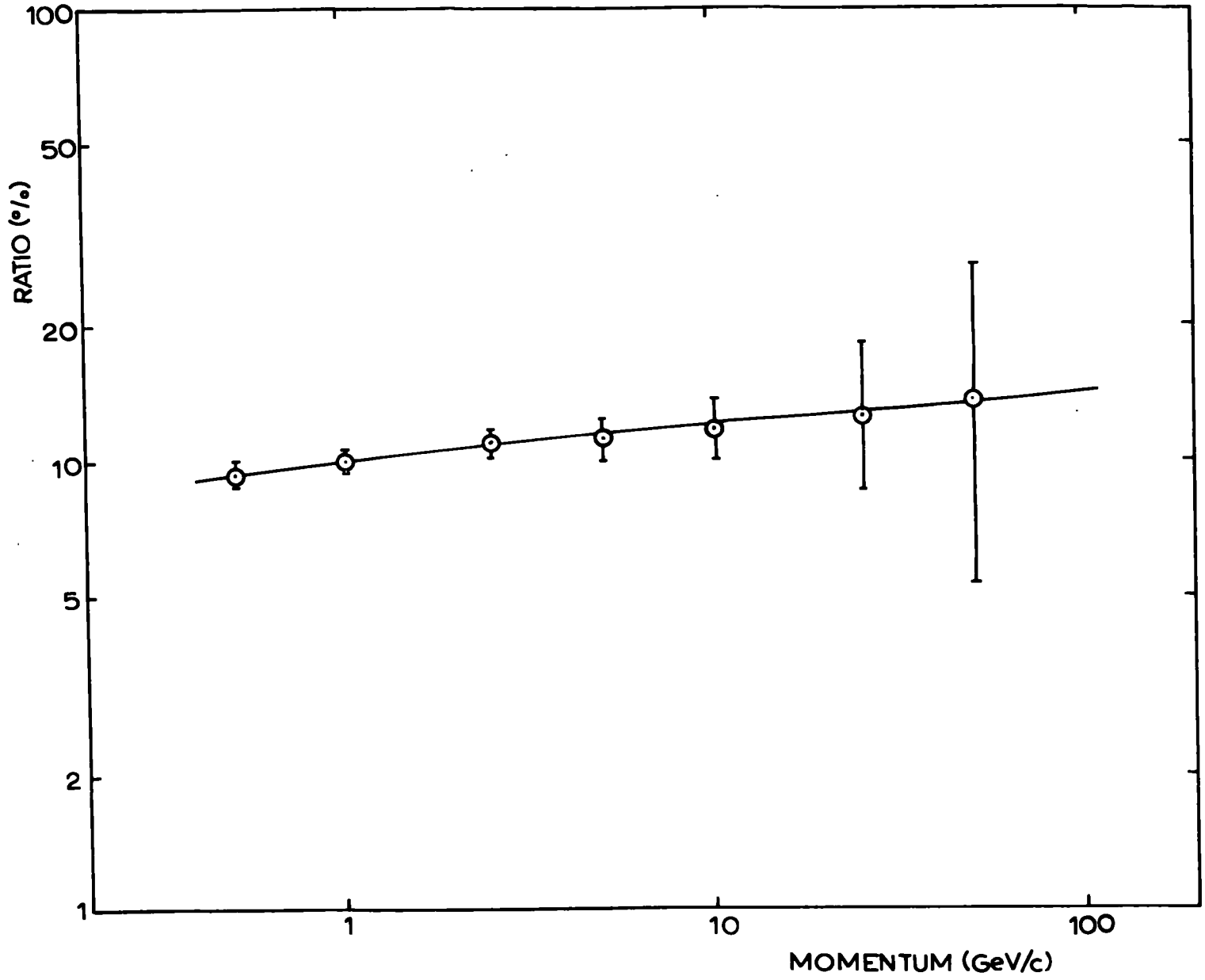

FIGURE 4·15

Table 4.6. Ratio of Accompanied to Single Events including Events originating in the Solid Iron Plug.

Maximum Displacement (t.s.)	Minimum momentum (GeV/c)	Ratio (%)	Error (%)
100	0.51	12.54	± 0.69
50	1.02	13.39	± 0.76
20	2.56	15.20	± 1.05
10	5.12	15.95	± 1.46
5	10.2	16.09	± 2.22
2	25.6	17.72	+ 6.18 - 5.18
1	51.2	27.3	+17.1 -13.1
0.5	102.4	18.2	+24.6 -13.7

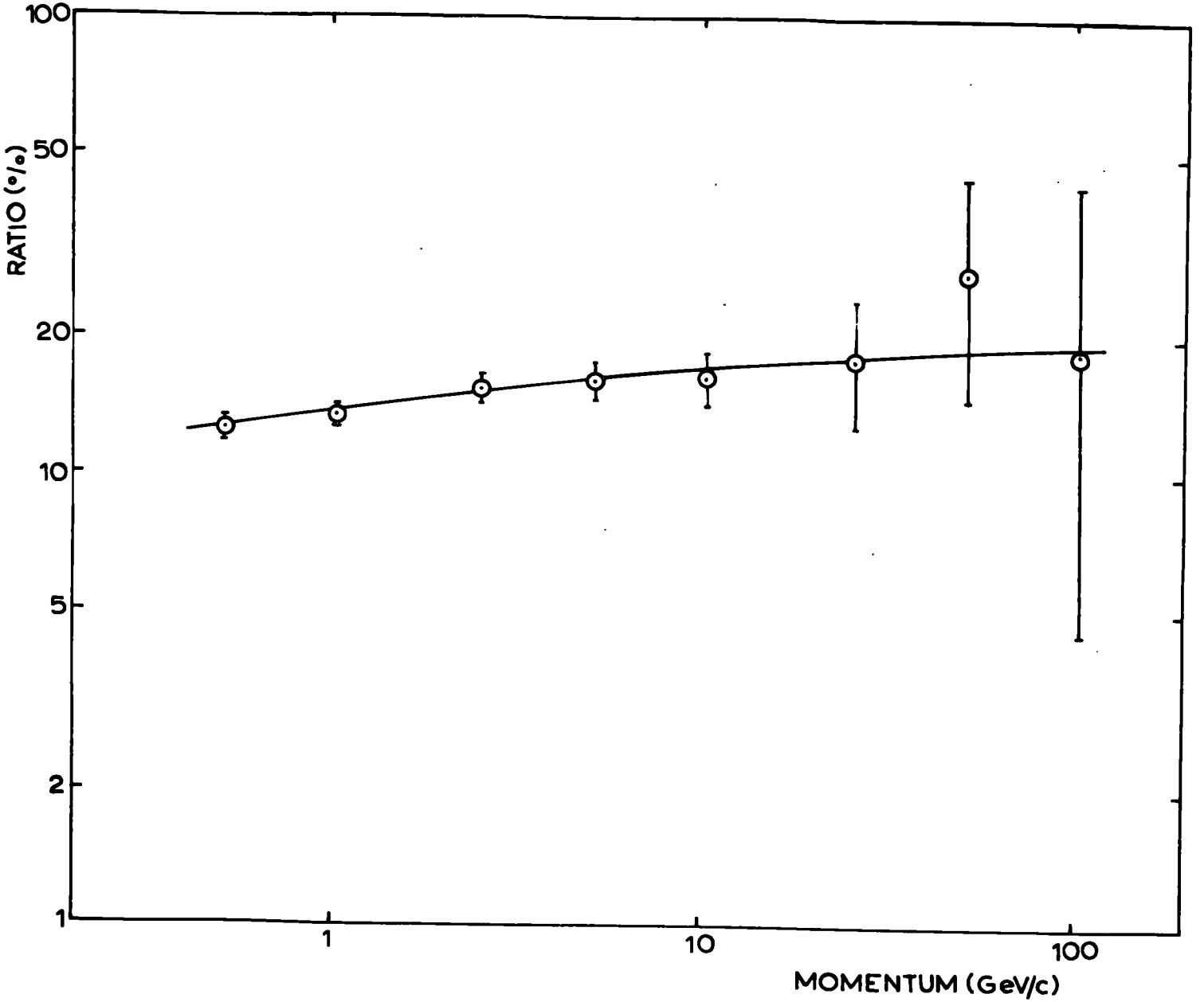

FIGURE 4.16

4.8. Derivation of an unbiassed muon spectrum.

Chapter 3 describes the two most recent measurements of the sea level spectrum in the range 1-10,000 GeV. In order to obtain a reliable spectrum from the data it is necessary to correct the data of Hayman and Wolfendale for the effect of accompanied particles bias. Figure 4.15 gives the effect of this bias. However, the correction to be applied is smaller than that given in figure 4.15 since the Durham data have been normalised at 1 GeV/c to Rossi's differential value of 2.45×10^{-3} cm^{-2} sec^{-1} st^{-1} $(GeV/c)^{-1}$ which refers to all particles. Little error is introduced if this is considered to be equivalent to an integral normalisation at 1 GeV/c to 5.70×10^{-3} cm^{-2} sec^{-1} st^{-1}. This step is necessary since the value given by Rossi is based on an absolute measurement of the integral intensity of all particles by Greisen (1942, 1943). The corrected integral spectrum therefore is found by applying the ratio given in figure 4.15 to the results of Hayman and Wolfendale and then renormalising at 1 GeV/c. The resulting increase in the spectrum can be seen in figure 4.17.

4.9. The Composite Sea Level Spectrum.

A composite sea level spectrum has been derived by Hayman et al. (1963) from the data of Hayman and Wolfendale and Duthie et al. (1962). The resulting spectrum is made up of the Durham line below 30 GeV, the Bristol line above 1,000 GeV and a smooth curve joining up these lines in the intermediate region.

If the Durham data is corrected for bias as described in the preceding section, the resulting composite spectrum will be increased in the low energy region. Figure 4.17 shows the ratios of the corrected and uncorrected Durham integral spectra to the composite spectrum as given by Hayman et al. It will be noticed that the effect of bias is not sufficient to explain the difference in the two sets of data in the region of 300 GeV.

The final version of the sea level spectrum has been derived from the corrected Durham data below 30 GeV, the best line of Hayman et al. above 100 GeV and a smooth curve joining up the lines in between. The values of the resulting sea level spectrum are given in table 4.7.

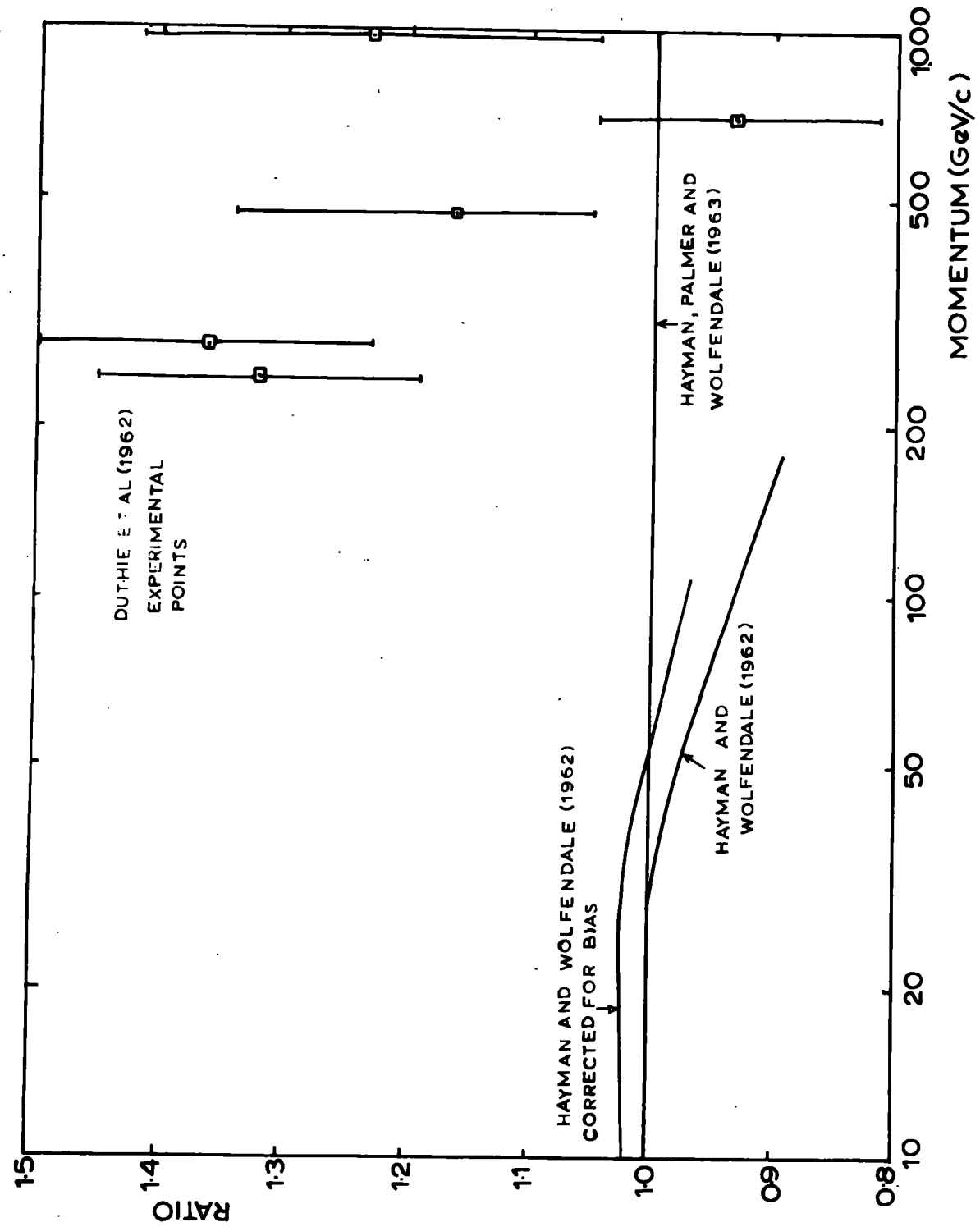
RATIO
1·5
1·4
1·3
1·2
1·1
1·0
0·9
0·8
10
20
50
100
200
500
1000
MOMENTUM (GeV/c)
DUTHIE ET AL (1962)
EXPERIMENTAL
POINTS
HAYMAN, PALMER AND
WOLFENDALE (1963)
HAYMAN AND
WOLFENDALE (1962)
HAYMAN AND WOLFENDALE (1962)
CORRECTED FOR BIAS

FIGURE 4·17

Table 4.7.

Energy (GeV)	Intensity ($cm^{-2}\ sec^{-1}\ st^{-1}$)
10	7.13×10^{-4}
15	3.91×10^{-4}
20	2.45×10^{-4}
30	1.21×10^{-4}
50	4.54×10^{-5}
70	2.31×10^{-5}
100	1.08×10^{-5}
150	4.50×10^{-6}
200	2.40×10^{-6}
300	9.50×10^{-7}
500	2.70×10^{-7}
700	1.05×10^{-7}
1000	3.80×10^{-8}
1500	1.08×10^{-8}
2000	4.10×10^{-9}
3000	1.02×10^{-9}
5000	1.70×10^{-10}
7000	5.00×10^{-11}
10000	1.43×10^{-11}

Chapter 5. Muon Energy Loss.

5.1. The Theoretical Energy Loss Relations.

The main processes by which muons lose energy in passing through matter are as follows:

(i) ionization and excitation

(ii) direct pair-production

(iii) bremsstrahlung

(iv) nuclear interaction

These processes have been subjected to a number of theoretical treatments and analyses, notably by Barrett et al. (1952), Campbell et al. (1962), Cousins (1960), Cousins and Nash (1962), George (1952), Hayman (1962), Hayman et al. (1963), Mando and Ronchi (1952), Rozental and Streltsov (1959) and Zatsepin and Kuzmin (1961). Following these workers, a similar analysis has been carried out in the following sections, where each process is considered in turn in an attempt to arrive at the most appropriate theoretical energy loss relation. The values of the constants for rock used in the calculations are $Z = 11$, $A = 22$ and $\rho = 2.65$ g cm^{-3}.

5.1.1. Collision.

In passing through an absorber, a muon can lose energy to the atomic electrons of the medium due to the coupling of their electric fields. The electron may be raised to an excited state, or, if given sufficient energy, may be completely removed from the atom. The method of calculation of the average

rate of energy loss for this process is to treat the distant collisions and close collisions separately. A distant collision is defined as that which takes place when an amount of energy less than some value η is transferred to the electron; a close collision when the transfer is greater than η. The treatment is different for these two categories because a distant collision is essentially an interaction between the muon and the atom as a whole, while for a close collision the relative effect of the remaining part of the atom on the struck electron is so small that the interaction can be looked on as that between a muon and a free electron. The value taken for η to satisfy the above requirements is in the region of 10^4 to 10^5 eV.

The differential cross-section for the case of close collisions has been evaluated by Bhabha (1938) and Massey and Corben (1939) who arrive at identical expressions. They give the probability per g cm^{-2} for muons of mass m and energy E to produce an electron with energy between E' and E' + dE' as

$$\phi\,(E,E')\,dE' = \frac{2\pi NZ}{A\beta^2}\; r_e^2\; m_e c^2\; \frac{dE'}{E'^2}\left[1 - \beta^2\frac{E}{E_m'} + \frac{1}{2}\left(\frac{E'}{E+mc^2}\right)^2\right] \qquad 5.1.$$

where r_e is the classical electron radius, m_e the mass of the electron, N is Avogadro's number and E_m' is the maximum energy transferrable to the electron. The value of E_m' is

given by Bhabha (1938) as

$$E_m' = \frac{E^2 - mc^2}{mc^2\left[\frac{m}{2m_e} + \frac{m_e}{2m} + \frac{E}{mc^2}\right]} \qquad 5.2$$

which reduces to

$$E_m' = E^2\left(E + \frac{m^2c^4}{2m_e c^2}\right)^{-1} -$$

$$= E^2\left(E + 1.093 \times 10^4\right)^{-1} \quad \text{MeV} \qquad 5.3$$

for $E \gtrsim 10$ GeV.

The average rate of energy loss is found by integration over the appropriate range of E', i.e.

$$-\left(\frac{dE}{dx}\right)_{>\eta} = \int_{\eta}^{E_m'} E' \,\phi\,(E,E')\, dE'$$

$$= 0.0766\left[\ln\frac{E_m'}{\eta} - 1 + \frac{1}{4}\cdot\left(\frac{E'}{E+mc^2}\right)^2\right] \qquad 5.4$$

The approximation of taking $\beta^2 = 1$ is valid for $E > 1$ GeV. The final term approaches the value 0.25 at high energies. At 100 GeV its value is 0.20 and since this is the region where collision loss is most important, little error is introduced in taking this value. The final result is thus:

$$-\left(\frac{dE}{dx}\right)_{>\eta} = 0.0766\left[\ln\frac{E_m'}{\eta} - 0.8\right] \quad \text{MeV g}^{-1}\,\text{cm}^2 \qquad 5.5$$

For the case of distant collisions, the minimum energy transfer is taken to be the minimum excitation of ionisation potential of the atom. This has been determined experimentally and the approximate value usually taken is

$$I(Z) = 13.5Z \text{ eV}$$

The average rate of energy loss in this category has been derived by Bethe (1930, 1932) to be

$$-\left(\frac{dE}{dx}\right)_{<\eta} = \frac{2\pi NZ}{A\beta^2} r_e^2 m_e c^2 \left[\ln \frac{2 m_e c^2 \beta^2 \eta}{(1-\beta^2) I^2(z)} - \beta^2\right] \quad 5.6$$

A correction (the density correction) has to be applied to this result since it includes impact parameters of the same order as the distance between the atoms of the medium. The incoming muon causes polarisation of the surrounding atoms which act in turn to decrease the effective field of the meson. The reduction in the rate of energy loss was first calculated by Fermi (1939) and later by Wick (1941, 1943), Halpern and Hall (1940, 1948) and Sternheimer (1952, 1953, 1956). The reduction is

$$\Delta = \frac{2\pi NZ}{A\beta^2} r_e^2 m_e c^2 \left[\ln\left\{\frac{ZN\rho e^2 h^2 c^2}{A\pi(1-\beta^2) m_e c^2 I^2(z)}\right\} - 1\right] \quad 5.7$$

The effective rate of energy loss due to distant collisions is thus

$$-\left(\frac{dE}{dx}\right)_{<\eta} - \Delta = 0.0766 \ln\left[\frac{2m_e^2 c^4 \eta A\pi}{ZN\rho h^2 c^2}\right]$$

$$= 1.94 + 0.0766 \ln \frac{\eta}{mc^2} \quad \text{MeV g}^{-1}\text{cm}^2 \quad 5.8$$

The total rate of energy loss due to collision is obtained from the addition of equations 5.5 and 5.8. The result is

$$-\left(\frac{dE}{dx}\right)_c = 1.88 + 0.0766 \ln \frac{E_m'}{mc^2} \quad \text{MeV g}^{-1}\text{ cm}^2 \quad 5.9$$

This equation, which is valid for $E > 10$ GeV is the equation used by Barrett et al. (1952) and Ozaki (1962); similar forms have been used by many other workers and its validity below

about 100 GeV is not in doubt. Above 100 GeV, the contribution to the energy loss by other processes becomes of greater importance.

It has been shown by Fermi (1940) and, with more detail, by Schönberg (1951) that the energy loss due to Cerenkov radiation is implicitly included in the above expression for collision loss and so need not be considered further.

5.1.2. Direct Pair-Production.

This is the process whereby a high energy muon loses energy by the direct creation of an electron-positron pair in the nuclear coulomb field.i.e. with no intermediate γ-ray. The cross-sections have been derived by a number of workers but no general agreement has been reached. The cross-sections usually considered are those due to Bhabha (1935) and Racah (1937). The cross-sections of Racah have been integrated by Mando and Ronchi (1952), giving the result

$$-\left(\frac{dE}{dx}\right)_p = \frac{N}{A} \cdot \frac{m_e}{m} \cdot \left(\frac{\alpha Z r_e}{\pi}\right)^2 \cdot E \left[19.3 \ln \frac{E}{mc^2} - 53.7\right] \text{ MeV g}^{-1}\text{cm}^2 \qquad 5.10$$

This equation has been derived neglecting the screening effect of the atomic electrons. Screening becomes important at high energies where pairs can be created at impact parameters of the same order as the atomic radius; the effect is to cause a reduction in the rate of energy loss.

The cross-sections have been derived by Bhabha for both the screened and unscreened cases. They have been derived in separate

non-overlapping regions of transferred energy. These cross-sections have been integrated by Hayakawa and Tomonaga (1949) using an approximate treatment based on the extrapolation of Bhabha's formulae. In the case neglecting screening, they obtain

$$-\left(\frac{dE}{dx}\right) = \frac{8}{\pi}(\alpha Z r_e)^2 \frac{N}{A} \cdot \frac{m_e}{m}\left\{E\left[\frac{16}{9}\ln\frac{E}{mc^2} - \frac{m_e}{m}\ln\frac{E}{mc^2} - \right.\right.$$

$$\left. - \frac{14}{9} + \ln 2 - \frac{m_e}{m}\ln 2\right] + \frac{14}{9}mc^2\left[\ln\frac{E}{mc^2}(1 - \ln 2) + \right.$$

$$\left.\left. + (2 - 2\ln 2 + \ln^2 2)\right]\right\} \qquad 5.11$$

When screening is taken into account, the result is

$$-\left(\frac{dE}{dx}\right) = \frac{8}{\pi}(\alpha Z r_e)^2 \frac{N}{A} \cdot \frac{m_e}{m}\left\{E\left[\frac{16}{9}\ln a + 1 - \frac{m_e}{m}\ln\frac{2E}{mc^2}\right]-\right.$$

$$- \frac{14}{9}mc^2\left[a(1-\ln 2)\ln\frac{E}{amc^2} + a\left(\frac{65}{28} - 2\ln 2 + \ln 2\right)-\right.$$

$$\left.\left. - (1 - \ln 2)\ln\frac{E}{mc^2} - (2 - 2\ln 2 + \ln^2 2)\right]\right\} \qquad 5.12$$

where $a \approx \alpha Z^{-1/3}$

While this method is inaccurate, it is important since it can be used to obtain an estimate of the screening effect, which in turn can be used to correct the equation of Mando and Ronchi (equation 5.10). The ratio of equations 5.11 and 5.12 can be approximated to

$$f = \frac{\text{screening}}{\text{no screening}} = \left[\frac{16}{9}\ln a + 1\right]\left[\frac{16}{9}\ln\frac{E}{mc} - \frac{14}{9} + \ln 2\right]^{-1} \qquad 5.13$$

These equations are the ones quoted by Mando and Ronchi.

The resulting energy loss relation including the effect of screening is obtained from the product of equations 5.10 and 5.13 for $E > 30$ GeV and equation 5.10 alone for $E < 30$ GeV.

The disagreement between the cross sections of Bhabha and Racah is such that the resulting energy loss derived from Bhabha's cross section is approximately a factor two larger than that of Racah. The work of Block et al. (1954) showed that Bhabha's cross sections could be modified to give agreement with those of Racah. These workers also carried out experiments in which they investigated tridents in nuclear emulsions. Their results were consistent with Racah's cross section.

A later derivation of the pair-production cross section has been carried out by Murota et al (1954), again giving results about a factor two greater than Racah's result.

More recent experimental work has been carried out by Roe and Ozaki (1959), Gaebler et al (1961) and Stoker et al (1961). All agree in showing the Murota et al. cross section to be too large by a factor of approximately two.

Above an energy of about 500 GeV, where the contribution from pair-production is significant, the rate of energy loss can be represented quite accurately up to an energy of about 10,000 GeV by the approximate expression

$$-\left(\frac{dE}{dx}\right)_p = 1.6 \times 10^{-6} \; E \quad \text{MeV g}^{-1}\,\text{cm}^2 \qquad 5.14$$

5.1.3. Bremsstrahlung.

Bremsstrahlung is the radiation emitted when the muon is accelerated in the coulomb field of the nucleus. An estimate of the cross section for this process by electrons was made by Bethe and Heitler (1934), both with and without the effect of the screening of atomic electrons. The calculation for the unscreened case was repeated more rigorously by Christy and Kusaka (1941) who obtained

$$\phi(E,v)\,dv = \frac{16}{3} \cdot \frac{N}{A} \cdot \alpha Z\, r_e^2 \left(\frac{m_e}{m}\right)^2 \left(\frac{3v}{4} - \frac{1-v}{v}\right) \times \left[\ln\left(\frac{12}{5} \cdot \frac{1-v}{v} \cdot \frac{E}{mc^2 Z^{1/3}}\right) - \frac{1}{2}\right] dv \qquad 5.15$$

This relation has been used universally at low muon energies.

It has been shown by Rossi (1952) that screening is important for energies above E_o, where

$$E_o = \frac{2\pi}{\alpha Z^{1/3}} \frac{(mc^2)^2}{m_e c^2} \cdot v \qquad 5.16$$

For the important region of energy transfer, $E_o \sim 4{,}000$ Gev. For energies below E_o, equation 5.15 is used resulting in a rate of energy loss given by

$$-\left(\frac{dE}{dx}\right) = 1.80 \times 10^{-7} E \left[\ln \frac{E}{mc^2} - 0.257\right] \text{ MeV g}^{-1}\text{ cm}^2 \qquad 5.17$$

For energies greater than E_o, Rozental and Streltsov (1959) and Bethe and Heitler (1934) give

$$\phi(E,v)\,dv = 4\alpha \frac{N}{A} Z^2 r_e^2 \left(\frac{m_e}{m}\right)^2 \left[\left\{1 + (1-v)^2 - \frac{2}{3}(1-v)\right\} \cdot \ln\left(\frac{m}{m}\, 183 Z^{-1/3}\right) + \frac{1}{9}(1-v)\right] \frac{dv}{v} \qquad 5.18$$

which gives a rate of energy loss

$$-\left(\frac{dE}{dx}\right) = 4\alpha\frac{N}{A}Z^2 r_e^2 \left(\frac{m_e}{m}\right)^2 E\left[\ln\left(\frac{m}{m_e}183Z^{-1/3}\right) + \frac{1}{18}\right] \qquad 5.19$$

$$= 1.76 \times 10^{-6} E \qquad \text{MeV g}^{-1}\text{ cm}^2 \qquad 5.20$$

Over the energy range 500-10,000 GeV the rate of energy loss can be represented by the approximate expression

$$-\left(\frac{dE}{dx}\right)_B = 1.70 \times 10^{-6} E \qquad \text{MeV g}^{-1}\text{cm}^2 \qquad 5.21$$

5.1.4. Nuclear Interaction.

The work of George and Evans (1950), was the first to indicate that the muon could lose energy by virtue of its interaction with the nucleus. These workers observed stars in nuclear emulsions which had been exposed for 6 to 12 months at depths up to 60 m.w.e. underground. It has been suggested by several workers that the interaction can be interpreted as that between the nucleus and a virtual photon associated with the charge of the muon. The cross section for the interaction can then be derived from a knowledge of the virtual photon flux of the muon and the interaction cross section for real photons. Unfortunately, neither of these factors is known with any degree of certainty and so until sufficient experimental results become available an accurate estimate of the muon cross section is not possible.

The original derivation of the virtual photon flux is due

to Williams-Weizsacker (W.W.), and was used in the analyses of George and Evans, and Marshak (1952). The relation is

$$N\ (E,v)\ dv = \frac{2\alpha}{\pi}\ \frac{1}{v}\ \ln\ \frac{1}{v}\ dv \qquad 5.22$$

where vE is the photon energy.

If it is now assumed that the photo-nuclear cross section, σ_v, is independent of energy, the average rate of energy loss is

$$-\left(\frac{dE}{dx}\right) = 2\,\frac{N\alpha}{\pi}\,\sigma_v\,E$$

$$= 2.80 \times 10^{21}\,\sigma_v \qquad \text{MeV g}^{-1}\text{ cm}^2 \qquad 5.23$$

Experimental measurements using real photons have been made only up to an energy of 1 GeV, where the cross section is found to be of the order of 10^{-26} cm^2/nucleon. Designating $\sigma_v = n.10^{-26}$ cm^2/nucleon, the rate of energy loss is

$$-\left(\frac{dE}{dx}\right) = 2.80\ .\ n\ .\ 10^{-7}\ E \qquad \text{MeV g}^{-1}\text{cm}^2 \qquad 5.24$$

This expression has been used by a number of workers, with values of n between one and two. For example, Ozaki (1962) has taken n = 2 with the corresponding result $-dE/dx \sim 5.10^{-7}$ MeV g^{-1} cm^2.

It has been suggested by Kessler and Kessler (1957) that a more accurate relation for the virtual photon flux of the muon is

$$N\ (E,v)\ dv = \frac{2\alpha}{\pi}\ \frac{dv}{v}\left[\left(1 - v + \frac{v^2}{2}\right)\ \ln\ \frac{E}{mc^2}\ (1 - v) - \frac{1 - v}{2}\right] \qquad 5.25$$

Under the same assumptions concerning as before, the resulting rate of energy loss is

$$-\left(\frac{dE}{dx}\right) = \frac{2N \propto \sigma_\nu}{\pi} \cdot E \left[\frac{2}{3} \ln \frac{E}{mc^2} - \frac{29}{36}\right] \qquad 5.26$$

$$= 1.87\ n \times 10^{-7}\ E \left[\ln \frac{E}{mc^2} - 1.21\right] \text{ MeV g}^{-1} \text{ cm}^2 \qquad 5.27$$

Although the choice between the Kessler - Kessler and Williams-Weizsacker treatments is not clear, recent evidence from Dalitz and Yennie (1957) and Higashi et al.(1962) seems to indicate the latter. The experiment of Higashi et al. yields a value of $(2.6 \pm 0.3) \times 10^{-28} \text{cm}^2$/ nucleon for the photo-nuclear cross section at photon energies above 5 GeV. Assuming that σ_ν is independent of energy, the rate of energy loss can be obtained by substituting the above value in equation 5.24. This gives

$$-\left(\frac{dE}{dx}\right)_N = 7.3 \times 10^{-7}\ E \quad \text{MeV g}^{-1}\text{cm}^2 \qquad 5.28$$

5.1.5. The Total Theoretical Rate of Energy Loss.

The energy loss relations given in the preceding equations can be combined to give the total theoretical rate of energy loss. In table 5.1 the values of dE/dx for the various processes as calculated by various workers are given for the purposes of comparison. It can be seen that for low muon energies the dominant processes are ionization and excitation but above 1,000 GeV other processes become predominant. The

figures given under "present work" are those calculated from the accurate expressions quoted in the previous sections; the approximate expressions have been used in the calculations described in chapters 6 and 7.

The relation for the total rate of energy loss can be written as

$$-\left(\frac{dE}{dx}\right) = 1.88 + 0.0766 \ln \frac{E_m'}{mc} + b E \quad \text{MeV g}^{-1}\text{cm}^2 \qquad 5.29$$

where the first two terms represent the contribution from ionization and excitation, which, as pointed out earlier, are not in doubt, and the final term contains the contribution from the other three processes. In fact, b varies slightly with energy, as can be seen from table 5.1, but over the range of greatest importance (500-10,000 GeV) in the present analysis, the value of b for this energy range is

$$b = 4.0 \times 10^{-6} \text{ g}^{-1}\text{cm}^2$$

Table 5.1.

E (GeV)	Worker	Coll.	P.P.	Total Contin.	Brem.	Nuc.	Fluct B + N	Total
10	Rozental et al	2.28	0.03		0.022	*(K)0.0059		2.34
	George et al	2.43	0.016		0.006	(W)0.025		2.48
	Barrett et al	2.17	0.013		0.015	(W)0.007		2.21
	Ozaki	2.17	0.0075	2.18	0.010	(W)0.005	0.015	2.19
	Hayman	2.13	0.009	2.14	0.0076	(K)0.006	0.0136	2.15
	Zatsepin et al	-	-		-	-		-
	Campbell et al	2.19	-		-	(K) -		2.20
	Ramanamurthy	2.17	0.0148		0.0191	(W)0.0028		2.21
	Present work.	2.17	0.0074	2.18	0.0077	(W)0.0073	0.015	2.19
100	R	2.45	0.26		0.22	0.089		3.02
	G	2.66	0.16		0.095	0.25		3.17
	B	2.40	0.13		0.15	0.07		2.75
	O	2.40	0.075	2.48	0.105	0.05	0.155	2.63
	H	2.39	0.132	2.52	0.116	0.107	0.223	2.74
	Z	2.8	0.115		0.077	-		2.99
	C	2.38	-		-	-		2.73
	R	2.40	0.148		0.191	0.028		2.77
	P.W.	2.40	0.132	2.53	0.118	0.073	0.191	2.72
1,000	R	2.63	2.4		2.2	1.19		8.42
	G	2.89	1.6		1.3	2.5		8.29
	B	2.58	1.3		1.5	0.7		6.08
	O	2.58	0.75	3.33	1.05	0.5	1.55	4.88
	H	2.61	1.52	4.13	1.58	1.5	3.08	7.21
	Z	2.8	1.195		1.02	-		5.02
	C	2.59	-		-	-		7.08
	R	2.58	1.48		1.91	0.28		6.25
	P.W.	2.58	1.52	4.10	1.60	0.73	2.33	6.43
10,000	R	2.81	22		22	14.9		61.7
	G	3.12	16		16.4	25		60.5
	B	2.76	13		15	7		37.8
	O	2.76	7.5	10.3	10.5	5	15.5	25.8
	H	2.72	16.3	19.0	21.3	19.3	40.6	59.6
	Z	2.8	12.0		11.1	-		25.9
	C	-	-		-	-		-
	R	2.76	14.8		19.1	2.8		39.5
	P.W.	2.76	16.4	19.2	17.6	7.3	24.9	44.1

* Rozental gives results for both Williams-Weizsacker and Kessler--Kessler treatments. The figures given are those for the latter.

5.2. Range-Energy Relations, neglecting straggling.

Using the form for the rate of energy loss, it is possible to calculate the range-energy relation. The mean range of a particle of initial energy E is given in terms of E and dE/dx by

$$R(E) = R(E_o) + \int_{E_o}^{E} (dE/dx)^{-1} \, dx$$

where E_o is the lower limit of applicability of the energy loss relation. It is convenient to take $E_o = 1$ GeV where the value of $R(E_o)$ has been evaluated from the data of Sternheimer (1959) as 545 g cm^{-2}.

Using various values of the parameter b the corresponding function R(E) has been evaluated by numerical integration using the Pegasus computer at King's College, Newcastle. The results of this calculation are given in table 5.2. It will be seen that the range of muons of energy below 1,000 GeV varies only slowly with b, but at higher energies the rate of increase of range falls rapidly as the energy increases.

Table 5.2. The range-energy relation for various values of b

Energy (GeV)	Range (m.w.e. rock)				
	$b=2.3 \times 10^{-6}$	$b=3.0 \times 10^{-6}$	$b=4.0 \times 10^{-6}$	$b=5.1 \times 10^{-6}$	$b=6.0 \times 10^{-6}$
100	4.159×10^{2}	4.104×10^{2}	4.029×10^{2}	3.950×10^{2}	3.888×10^{2}
200	7.768×10^{2}	7.582×10^{2}	7.337×10^{2}	7.089×10^{2}	6.902×10^{2}
300	1.105×10^{3}	1.069×10^{3}	1.022×10^{3}	9.763×10^{2}	9.426×10^{2}
500	1.690×10^{3}	1.610×10^{3}	1.511×10^{3}	1.418×10^{3}	1.352×10^{3}
700	2.201×10^{3}	2.071×10^{3}	1.916×10^{3}	1.776×10^{3}	1.679×10^{3}
1000	2.865×10^{3}	2.659×10^{3}	2.421×10^{3}	2.213×10^{3}	2.072×10^{3}
2000	4.537×10^{3}	4.088×10^{3}	3.605×10^{3}	3.209×10^{3}	2.954×10^{3}
3000	5.735×10^{3}	5.080×10^{3}	4.402×10^{3}	3.864×10^{3}	3.526×10^{3}
5000	7.439×10^{3}	6.462×10^{3}	5.489×10^{3}	4.745×10^{3}	4.288×10^{3}
7000	8.658×10^{3}	7.434×10^{3}	6.243×10^{3}	5.350×10^{3}	4.809×10^{3}
10000	1.001×10^{4}	8.505×10^{3}	7.067×10^{3}	6.007×10^{3}	5.373×10^{3}
20000	1.279×10^{4}	1.067×10^{4}	8.717×10^{3}	7.315×10^{3}	6.491×10^{3}

Chapter 6. The Effect of Fluctuations in Range.

6.1. Approximate Cross-sections.

Over the appropriate energy range, the approximate probabilities for the four main processes of muon energy loss are as follows

(a) Ionisation $\phi_i(E,v)\,dv = \frac{A}{Ev^2}\,dv$ $g^{-1}cm^2$

(b) Pair-production $\phi_p(E,v)\,dv = \frac{B}{Ev^3}\,dv$

(c) Bremsstrahlung $\phi_b(E,v)\,dv = \frac{C}{v}\,dv$

(d) Nuclear interaction $\phi_n(E,v)\,dv = \frac{D}{v}\ln\frac{1}{v}\,dv$

where E is the muon energy, v is the fraction of energy lost per g cm^{-2} and A, B, C and D are constants or slowly varying functions of E and v. It can be seen from the above expressions that in the case of the processes of ionisation and pair-production, the probability of a fractional transfer v occurring falls much more rapidly with increasing v than for the other processes. Thus the processes of ionisation and pair-production are characterised by relatively small transfers of energy, while for bremsstrahlung and nuclear interaction there is a much higher probability of the muon losing a large fraction of its energy in traversing the same thickness of absorber. One can, therefore, attribute the straggling in range of muons almost entirely to the processes of bremsstrahlung and nuclear interaction, which can be referred to as "discontinuous" processes.

Similarly, the processes of ionisation and pair-production are categorised as "continuous" processes.

6.2. The Effect of Fluctuations on Analysis of Underground Data.

One of the main reasons for making measurements of cosmic ray intensities underground is to gain information about their rate of energy loss in passing through large thicknesses of absorbing material. The process of analysis is to assume some form for the energy loss relation and then to use the measured sea level spectrum to predict the intensity at some chosen depth underground. The predicted intensity is then compared with the measured value and the energy loss relation is varied until agreement is reached.

In order to predict the intensity at a depth d_i underground the value E_i, which is the minimum sea level energy required for a muon to penetrate to a depth d_i, is calculated. This is integrated numerically, as described in chapter 5, from the assumed energy loss relation. The intensity at the depth d_i is then

$$I_c\ (d_i) = \int_{E_i}^{\infty} N(E)\ dE$$

where N(E) is the assumed form for the differential spectrum. The assumption made in these calculations is that particles with energy greater than E_i at sea level will reach the depth d_i, and those with energy less than E_i will come to rest before reaching this depth i.e. a "survival probability" curve in the form of a step function having the value zero for $E < E_i$ and unity for $E \geqslant E_i$. If, however, straggling in range occurs due

to particles losing energy in a discontinuous manner, the survival probability curve will not be of step-function form but will take the more general form P(E). In this case the predicted intensity must be calculated from an equation of the form

$$I_f(d_i) = \int_{E_{min}}^{\infty} N(E)P(E)\,dE$$

where E_{min} is the minimum energy lost, due to continuous processes only, of a particle which just survives to the depth d_i.

In general, differing values will be obtained by the two methods. One can define R(d) as the ratio, referred to some depth d, of the intensity predicted when fluctuations in energy loss are considered to that predicted when the simple range-energy relation is used i.e. $R(d) = I_f(d)/I_c(d)$. The value of R(d) at some particular depth will depend on two parameters. These are the shape of the survival probability curve associated with that depth, and the slope of the sea level spectrum in the energy region of maximum contribution to the underground intensity. If the slope of the spectrum is increased the maximum contribution will come from particles having a lower sea level energy. Since the corresponding intensity of these particles is higher the value of R(d) will be increased. Conversely, if the slope of the spectrum is decreased the bias will be towards a higher energy and R(d) will decrease. It is thus important to calculate R(d) not only for different forms of the energy loss relation but also for spectra of differing slopes.

6.3 The Monte Carlo Calculation.

6.3.1. Energy Loss Constants used.

The rate of energy loss of muons can be represented by

(i) for continuous processes

$$-\frac{dE}{dx} = 1.88 + 0.0766 \ln \frac{E_m'}{m c^2} + b_1 E$$

(ii) for fluctuating processes

$$-\frac{dE}{dx} = (b_2 + b_3) E$$

where the term $b_1 E$ is due to pair-production, $b_2 E$ to bremsstrahlung and $b_3 E$ to nuclear interaction. The values of the constants b_1, b_2 and b_3 are not known accurately and there are some discrepancies at the moment in published values. The uncertainty in the values of these constants can be seen from table 5.1. of chapter 5 which presents the values of the energy loss due to the four processes as given by various workers.

Because of this uncertainty it was decided to carry out the Monte Carlo calculation for two widely spaced energy loss forms which approximately covered the range of variation. The values of R(d) for other energy loss relations could then be obtained to a good approximation by interpolation.

The lower energy loss taken, referred to as case I, was that due to Ozaki (1962) and the upper, case II, due to Hayman (1962). The appropriate values of b_1, b_2 and b_3 are given in table 6.1.

In fact the energy loss relation due to Hayman gives values of b varying slowly with energy. The values chosen for case II give a good fit (± 3%) in the important energy region (1,000 - 10,000 GeV) for the depths considered.

Table 6.1. Energy loss constants used.

(in units of $10^{-6} g^{-1} cm^2$)

	b_1 (pair-production)	b_2 (brem)	b_3 (nuc.)	b total
Case I (Ozaki, 1962)	0.75	1.05	0.5	2.3
Case II (Hayman, 1962)	1.6	1.8	1.7	5.1
Estimate from the present work	1.6	1.7	0.7	4.0

6.3.2. Method of Calculation.

If the survival probability curves taking into account the fluctuating losses can be obtained for a series of depths, then the ratio R(d) can be obtained as a function of depth for any chosen sea level spectrum. One method of calculating the survival probability curves is to simulate the passage of muons through absorbing material in some mathematical way, applying a random process to calculate the fluctuating losses. In this way statistical samples of particles can be taken and the required probability distributions plotted. In the past this method of

solution of this particular problem has been unsuitable due to the length of time necessary to study enough particles to reduce the statistical errors to a reasonable size, but with the aid of an electronic computer, this difficulty is removed.

The process of the calculation was to divide the absorber into a number of elements of thickness, calculating the energy loss in each element, reducing the energy of the particle by that amount and then proceeding to the next element. The energy loss in the element was calculated in two parts. The processes of collision and pair-production were treated as continuous processes, since the majority of energy lost in this way is through small fractional transfers. This was calculated from an equation of the form

$$-\frac{dE}{dx} = a + k \ln \frac{E}{m'c} + b_1 E$$

where E is the energy of the particle on entering the element and the units are arranged to refer to the elemental thickness used (in the case of this calculation this was 100 m.w.e.).

The energy lost in the element due to the discontinuous processes of bremsstrahlung and nuclear interaction was calculated from the basic cross sections. A good approximation to the form of this cross section is

$$P(v)\,dv = \frac{b_2 + b_3}{v}\,dv \qquad g^{-1}cm^2$$

where v is the fraction of energy transferred and P(v) is the

probability of a transfer between v and v+dv taking place in the equivalent thickness of 1 g cm^{-2}. In order to transfer to the unit of thickness used in the calculation (100 m.w.e.) the assumption is made that the probability distributions P(v) can be combined arithmetically with respect to depth. This assumption is discussed in the appendix. Taking the assumption to be valid

$$P'(v) = 10^4 \frac{(b_2 + b_3)}{v} \qquad (100 \text{ m.w.e.})^{-1}$$

where $P'(v)$ is the same probability referred to a thickness of 100 m.w.e. So the transfer v is given by

$$v = \exp - \frac{P'(>v)}{10\,(b_2 + b_3)}$$

where $P'(>v)$ is the probability of a transfer greater than v occuring. A random fraction is generated in the computer to correspond to $P'(>v)$ and so the discontinuous energy loss vE is found.

In this way the behaviour of a particular muon was simulated in passing through large thicknesses of absorber. The process was continued until either the particle came to rest or it reached the maximum depth considered (10,000 m.w.e.).

In the initial stages of the development of the programme, the computer was instructed to print out, at each element of depth, the main parameters of the calculation. These were the random fraction, the depth, the energy of the particle,

and the energy lost in the previous element by both the continuous and fluctuating processes. Two of the sets of data obtained are reproduced in tables 6.2 and 6.3. Table 6.2 gives an example of a 30,000 GeV muon penetrating to a depth of 3,300 m.w.e. with the case II energy loss. Table 6.3 gives similar information, but for case I energy loss. The discontinuous nature of the bremsstrahlung and nuclear interaction processes is well illustrated.

Table 6.2.

Random fraction	Depth (m.w.e.)	Energy (GeV)	Continuous loss (GeV)	Discontinuous loss (GeV)
	0	30000		
0.9942	100	29491	509	0
0.7879	200	28990	501	0
0.0309	300	16503	493	11994
0.0451	400	11659	292	4552
0.7736	500	11444	215	0
0.3129	600	11231	211	2
0.8897	700	11023	208	0
0.9104	800	10818	205	0
0.3668	900	10617	201	0
0.3664	1000	10419	198	0
0.9775	1100	10225	194	0
0.4766	1200	10034	191	0
0.1655	1300	9760	188	86
0.5432	1400	9576	184	0
0.9758	1500	9395	181	0
0.6675	1600	9217	178	0
0.8337	1700	9042	175	0
0.7447	1800	8870	172	0
0.1174	1900	8391	169	310
0.2459	2000	8222	162	7
0.1338	2100	7883	159	180
0.0131	2200	2301	154	5428
0.2828	2300	2237	63	1
0.2320	2400	2172	62	3
0.5979	2500	2111	61	0
0.7930	2600	2051	60	0
0.7700	2700	1992	59	0
0.0546	2800	1514	59	419
0.0184	2900	567	51	896
0.6629	3000	532	35	0
0.0078	3100	73	34	425
0.5801	3200	48	25	0
0.3410	3300	24	24	0

Table 6.3.

Random fraction	Depth (m.w.e.)	Energy (GeV)	Continuous loss (GeV)	Discontinuous loss (GeV)
	0	30000		
0.4688	100	29746	254	0
0.8427	200	29494	252	0
0.1053	300	29212	250	32
0.2456	400	28964	248	0
0.3392	500	28718	246	0
0.7288	600	28474	244	0
0.5402	700	28231	243	0
0.6480	800	27991	240	0
0.5277	900	27753	238	0
0.3740	1000	27517	236	0
0.4326	1100	27282	235	0
0.0544	1200	26245	233	804
0.5259	1300	26020	225	0
0.6686	1400	25797	223	0
0.5715	1500	25575	222	0
0.9241	1600	25355	220	0
0.0336	1700	22257	218	2880
0.0015	1800	1846	195	20216
0.2713	1900	1805	41	0
0.7360	2000	1765	40	0
0.1111	2100	1724	40	1
0.1749	2200	1684	40	0
0.5696	2300	1645	39	0
0.1339	2400	1606	39	0
0.9212	2500	1567	39	0
0.1712	2600	1529	38	0
0.2411	2700	1491	38	0
0.8217	2800	1453	38	0
0.8240	2900	1415	38	0

(Continued

Table 6.3. (Continued)

Random fraction	Depth (m.w.e.)	Energy (GeV)	Continuous loss (GeV)	Discontinuous loss (GeV)
0.8214	3000	1378	37	0
0.3937	3100	1342	36	0
0.5910	3200	1306	36	0
0.6567	3300	1270	36	0
0.9415	3400	1235	35	0
0.4414	3500	1200	35	0
0.8093	3600	1165	35	0
0.7279	3700	1130	35	0
0.3262	3800	1096	34	0
0.9635	3900	1062	34	0
0.4029	4000	1028	34	0
0.2963	4100	994	34	0
0.0191	4200	672	33	289
0.5317	4300	641	31	0
0.9527	4400	610	31	0
0.4216	4500	580	30	0
0.3059	4600	550	30	0
0.5908	4700	520	30	0
0.7720	4800	491	29	0
0.1987	4900	462	29	0
0.7597	5000	433	29	0
0.5891	5100	405	28	0
0.3023	5200	377	28	0
0.9716	5300	349	28	0
0.7203	5400	321	28	0
0.5359	5500	293	28	0
0.6527	5600	266	27	0
0.0738	5700	237	27	2
0.0312	5800	179	27	31
0.7703	5900	153	26	0
0.8685	6000	127	26	0

(Continued

Table 6.3. (Continued)

Random fraction	Depth (m.w.e.)	Energy (GeV)	Continuous loss (GeV)	Discontinuous loss (GeV)
0.3214	6100	102	25	0
0.2842	6200	77	25	0
0.6464	6300	53	24	0
0.0256	6400	19	24	10

The computer was programmed to store the necessary information from such a "case history" and to continue with the next particle automatically until 1,000 particles of the same initial energy had been studied. Groups of 1,000 particles of each of a series of initial energies were put through until sufficient information was obtained to draw the survival probability curves.

The calculation was carried out for both the case I and case II forms of the energy loss and the resulting survival probability curves are given in figures 6.1 and 6.2.

6.3.3. Statistical Errors on the Survival Probability Curves.

The errors shown on the survival probability curves are the calculated statistical errors. These were found from simple theory which gives a relation

$$\delta P = \sqrt{\frac{P(1-P)}{N}}$$

where P is the survival probability and N the total number of particles used in calculating that probability. A check on the analysis was afforded by taking 10 sample batches each of 100 particles all having the same initial energy. At each of the six chosen depths the mean survival probability, based on 1,000 particles, was found. The deviations of the survival probabilities as given by batches of 100 particles were plotted taking the standard deviation, as given by the above expression, as the unit. The resulting distributions were very close to Gaussian.

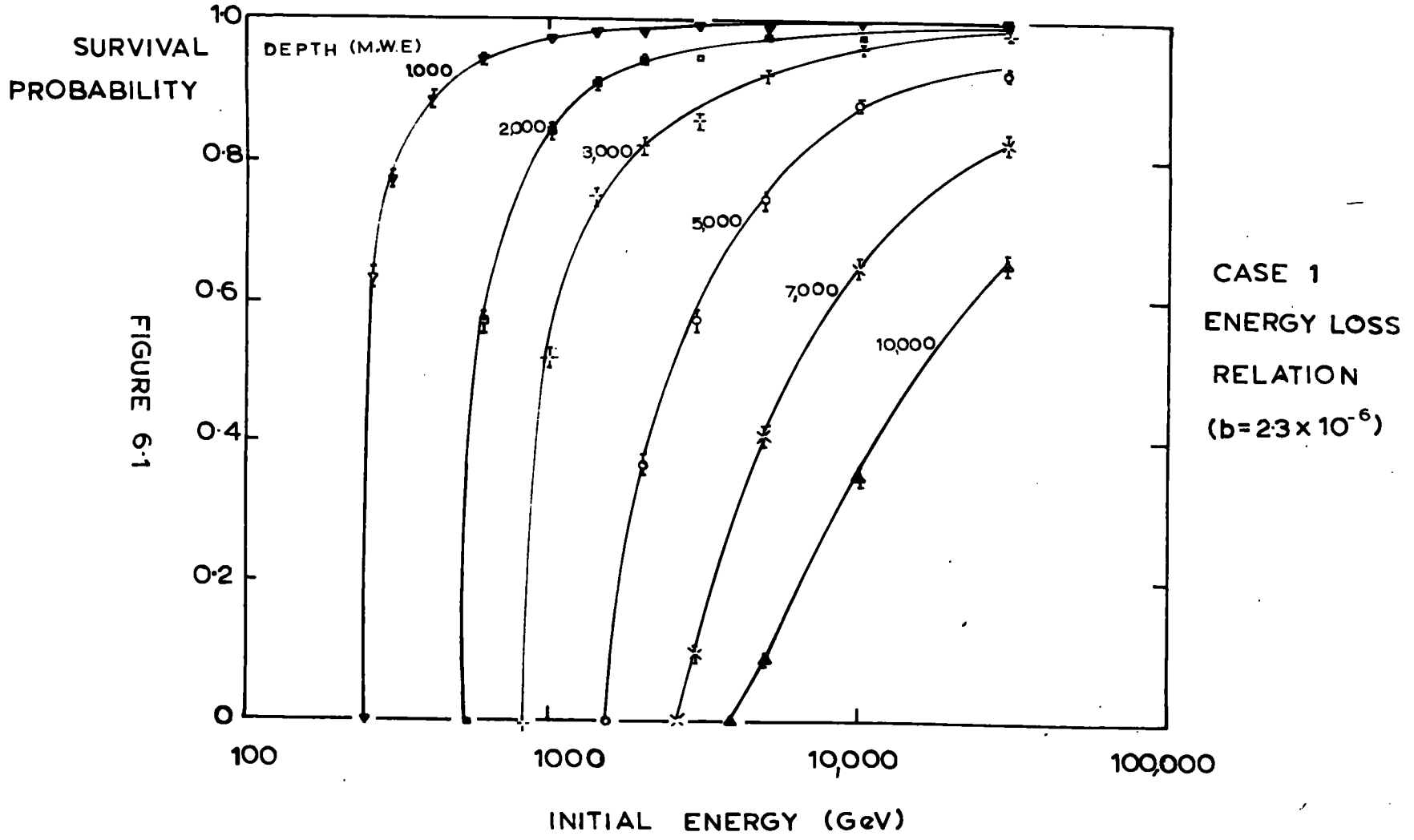
SURVIVAL PROBABILITY
1·0
0·8
0·6
0·4
0·2
0
DEPTH (M.W.E)
1000
2000
3,000
5,000
7,000
10,000
100
1000
10,000
100,000
INITIAL ENERGY (GeV)
CASE 1
ENERGY LOSS
RELATION
(b=2·3 x 10⁻⁶)

FIGURE 6·1

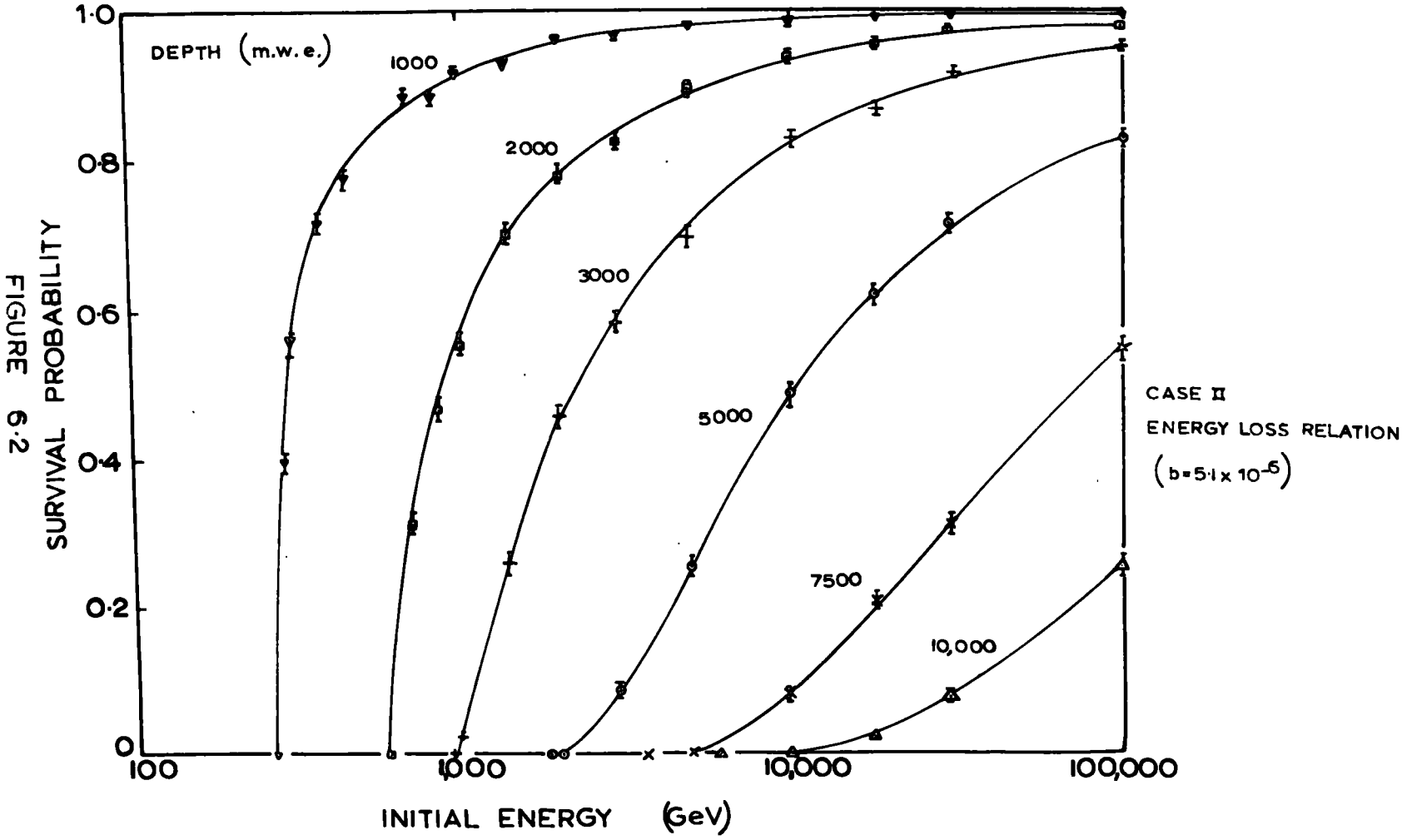
1·0
0·8
0·6
0·4
0·2
0
SURVIVAL PROBABILITY
DEPTH (m.w.e.)
1000
2000
3000
5000
7500
10,000
100
1000
10,000
100,000
INITIAL ENERGY (GeV)
CASE II
ENERGY LOSS RELATION
(b=5·1 x 10⁻⁶)

FIGURE 6·2

6.3.4. Errors due to Finite Cell Width.

In the Monte Carlo calculation the energy loss of a particle in the element of depth chosen was calculated using the energy the particle had on entering the element. This results in an over-estimate of the energy loss since the particle has in general a lower energy than this throughout the element, and thus loses energy at a lower rate. In order to obtain an estimate of the error involved due to this a number of particles were traced on the computer assuming their energy loss was due to continuous losses only. The energy necessary to reach each of the six chosen depths was thus found. These were then compared with the range-energy relations as obtained by numerical integration of the energy loss equation. The comparison is shown in table 6.4. Since the discrepancy is small and the errors involved appear both in the numerator and denominator of the quotient R(d) with the same sign it was considered to be negligible.

Table 6.4.

Depth (m.w.e.)	Energy (GeV) Numerical integration	Energy (GeV) Monte Carlo method
$b = 2.3 \times 10^{-6}$		
1000	266	275.5
2000	620	637
3000	1080	1101
5000	2430	2434
7500	5050	5280
10000	10000	10380
$b = 5.1 \times 10^{-6}$		
1000	312	328
2000	850	898
3000	1740	1865
5000	5800	6300
7500	23500	24820
10000	-	93300

6.4. Interpretation of Results.

6.4.1. Mean Range obtained from Survival Probability Curves.

An illustration of the effect of fluctuations can be obtained immediately from the survival probability curves by comparing the mean range obtained from these with the range obtained from numerical integration. Figures 6.3 and 6.4 show range straggling curves obtained from vertical sections of the survival probability curves. The mean range of a particle of given incident energy can be obtained from these quite simply and the comparison between this range and the numerically integrated range is shown in figure 6.5, where it is seen that neglecting the effect of fluctuations results in an over-estimate in the range of a muon, particularly for the higher rate of energy loss.

6.4.2. Evaluation of R(d).

Using the survival probability curves, the ratio

$$R(d) = \frac{\int_{E_{min}}^{\infty} N(E)P(E)dE}{\int_{E}^{\infty} N(E)\,dE}$$

was calculated graphically for a series of six values of d. Two forms for the sea level muon differential spectrum were taken. The first was a spectrum of the form

$$N(E) = AE^{-3}dE$$

This was used so that a comparison could be made with the results of other workers. The comparison is discussed in the next section. The second form taken was the best estimate

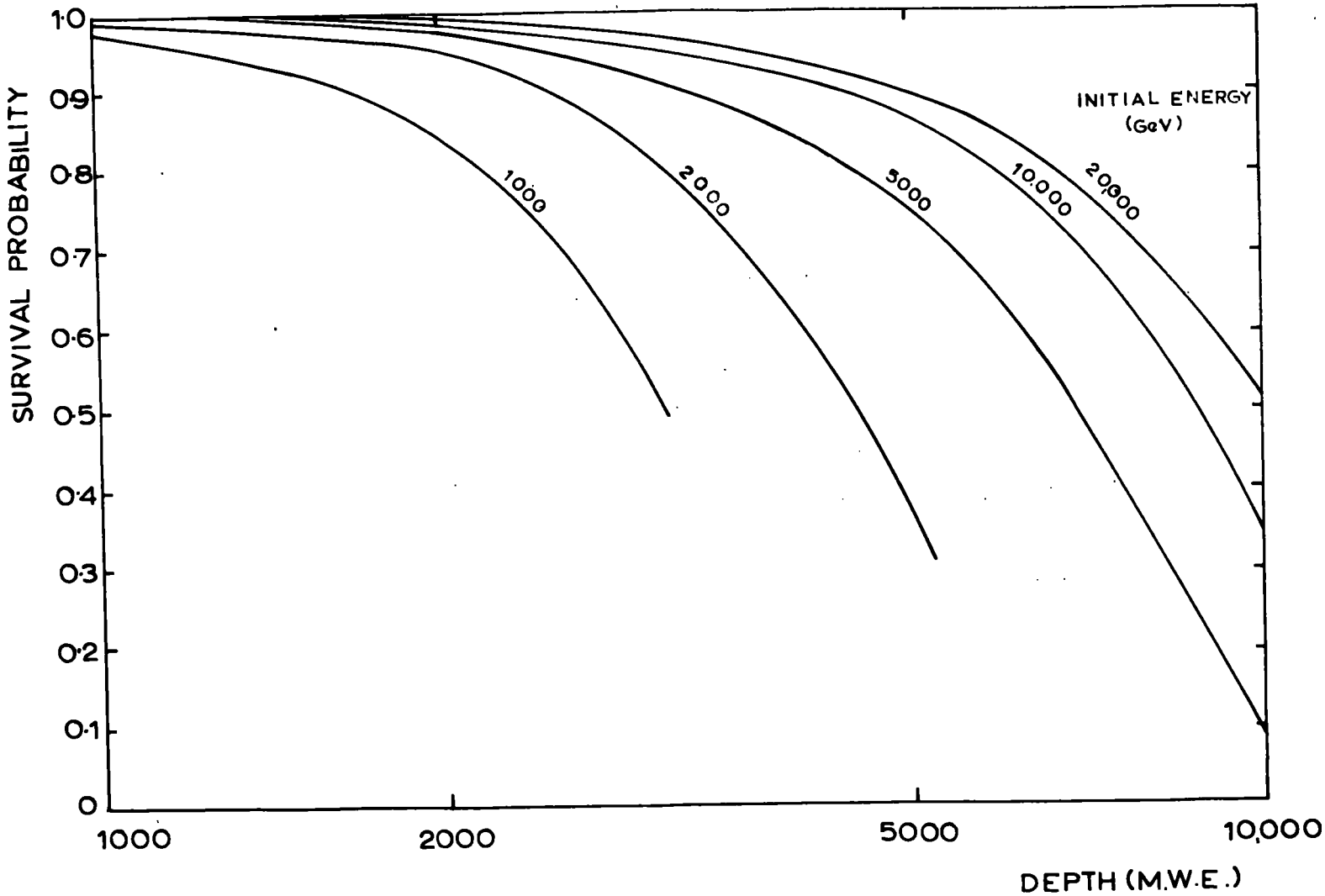
SURVIVAL PROBABILITY
1·0
0·9
0·8
0·7
0·6
0·5
0·4
0·3
0·2
0·1
0
1000
2000
5000
10,000
DEPTH (M.W.E.)
INITIAL ENERGY (GeV)
1000
2000
5000
10,000
20,000

FIGURE 6.3

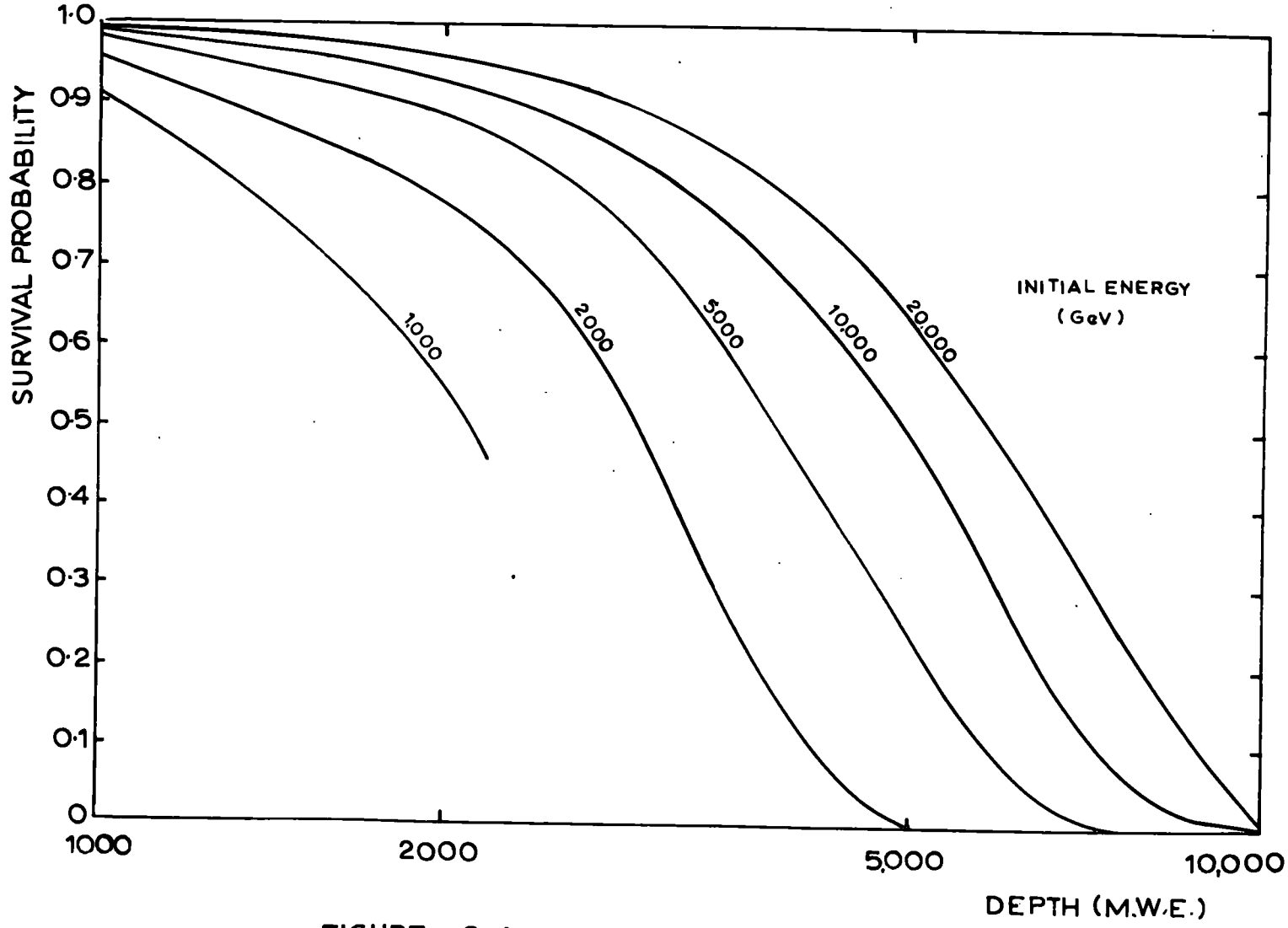
SURVIVAL PROBABILITY
1·0
0·9
0·8
0·7
0·6
0·5
0·4
0·3
0·2
0·1
0
1000
2000
5000
10,000
DEPTH (M.W.E.)
INITIAL ENERGY
(GeV)
1000
2000
5000
10,000
20,000

FIGURE 6·4

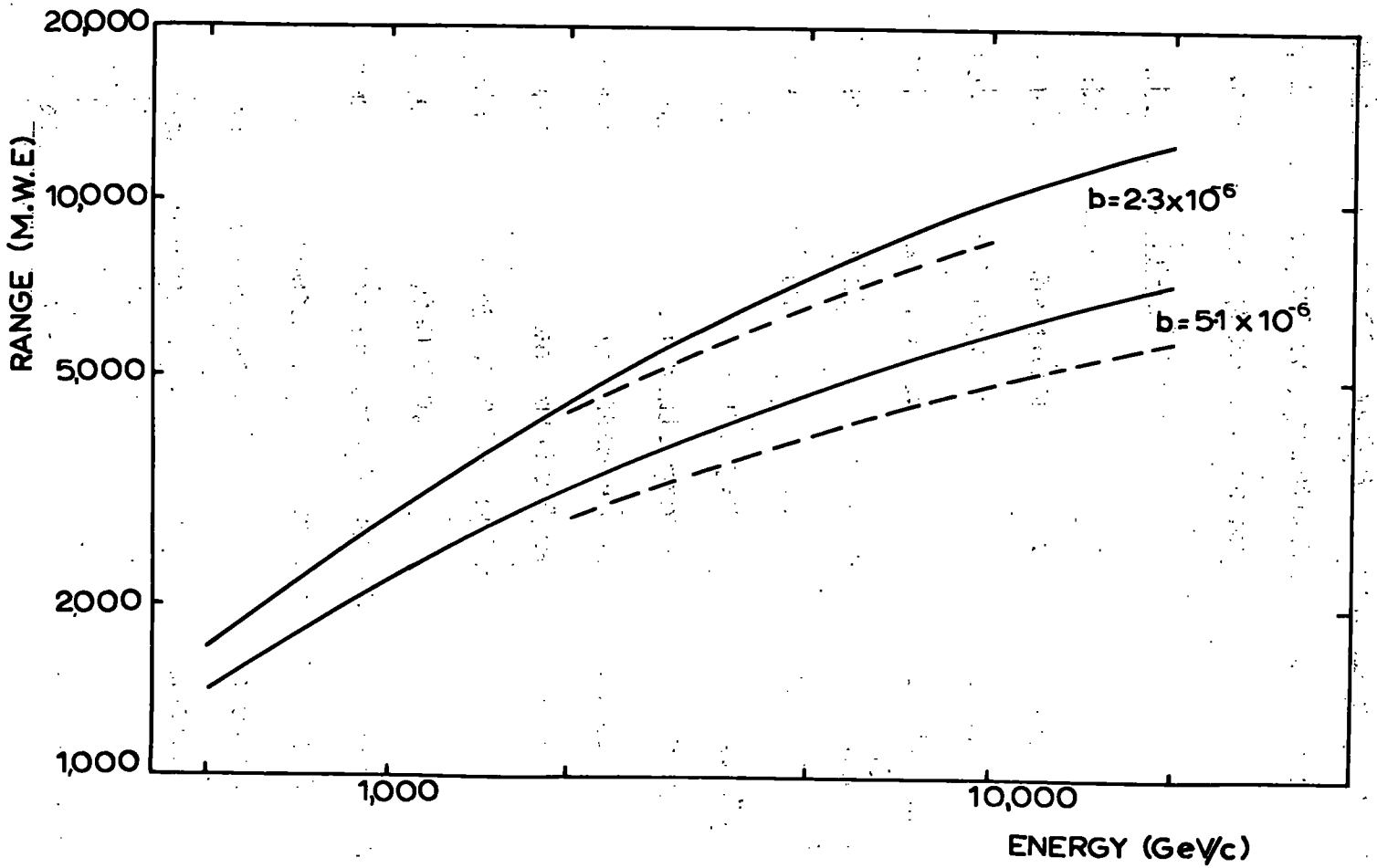
20,000
10,000
5,000
2,000
1,000
RANGE (M.W.E.)
b=2·3x10⁻⁶
b=5·1 x 10⁻⁶
1,000
10,000
ENERGY (GeV/c)

FIGURE 6·5

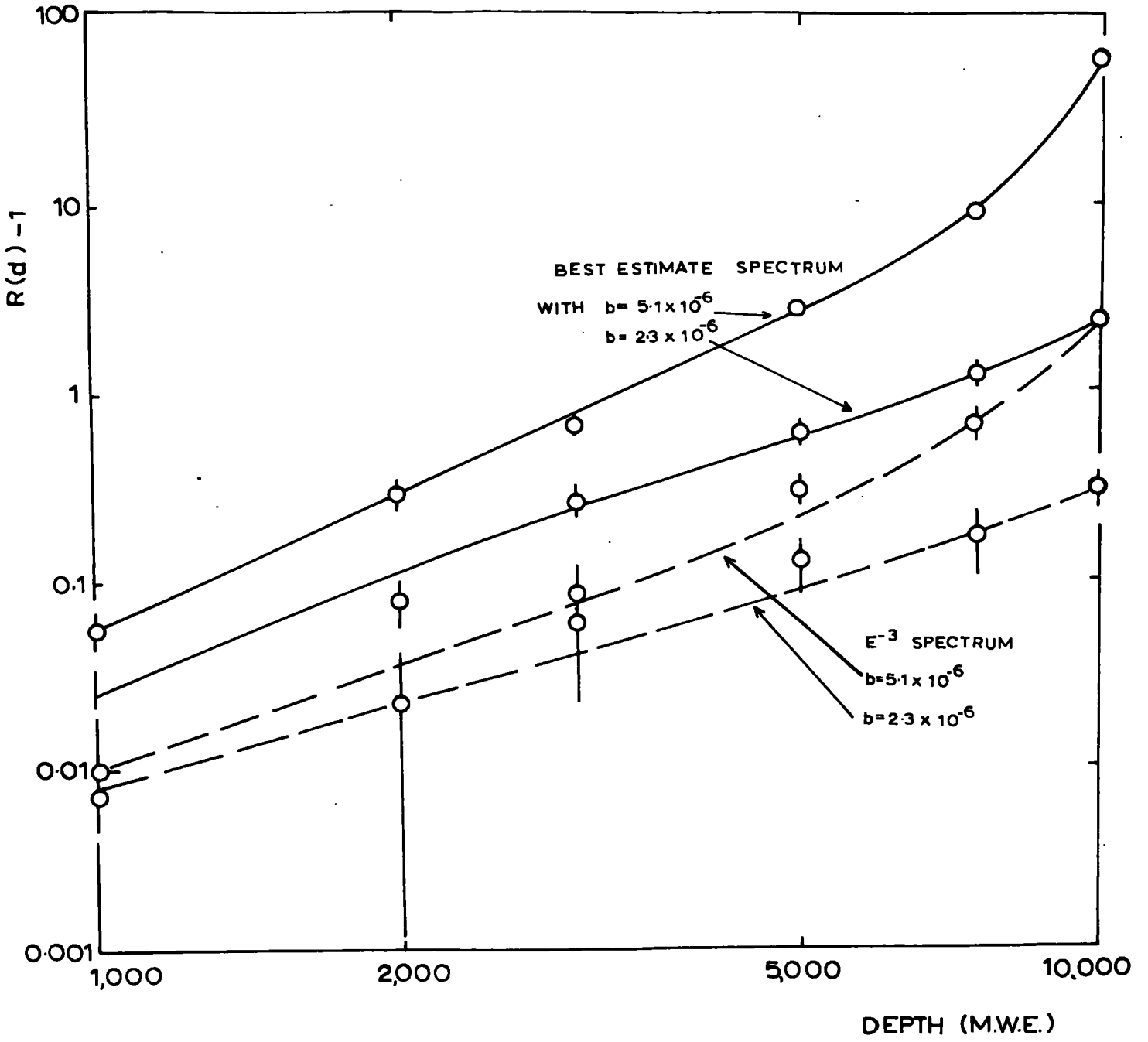
100
10
1
0·1
0·01
0·001
R(d) - 1
1,000
2,000
5,000
10,000
DEPTH (M.W.E.)
BEST ESTIMATE SPECTRUM
WITH b= 5·1 x 10⁻⁶
b= 2·3 x 10⁻⁶
E⁻³ SPECTRUM
b=5·1 x 10⁻⁶
b=2·3 x 10⁻⁶

FIGURE 6·6

and also the intensities predicted assuming all energy loss to be continuous. The resulting values of R(d) obtained were 0.91 at 3,000 m.w.e., 1.07 at 5,000 m.w.e. and 1.06 at 7,500 m.w.e.

The differences between the intensities calculated in these two ways is not considered to be significant due to the large statistical errors.

6.5.2. Analytical Treatments.

It would be very useful if analytical methods could be used to arrive at some mathematical form in which the ratio R(d) is expressed in terms of spectrum and energy loss parameters. In practice the problem is one of some complexity and all published analytical treatments to this date have used a simple power law of the form

$$N(E)dE = AE^{-\gamma} dE$$

for the sea level muon spectrum. This is obviously a very large restriction in the applicability of such methods since it is known that the sea level spectrum has a value of γ which varies with energy.

Mando and Sona (1953) used a method in which they set up the diffusion equation of muons passing through rock. They obtained an approximate solution by assuming that the discontinuous losses are due to bremsstrahlung and form only a small fraction of the collision losses. The results are given in the table, which shows the percentage correction to be made to the intensity predicted at the particular depth when using the continuous energy loss approximation.

Table 6.5. Percentage correction.			
Depth (m.w.e.)	$\gamma = 2.5$	$\gamma = 3.0$	$\gamma = 3.5$
800	-1.11	-0.33	+0.76
1200	-1.85	-0.54	+1.37
1600	-2.69	-0.79	+2.15
2000	-3.66	-1.06	+3.19

Zatsepin and Mikhalchi (1962) have used a computer to solve the relevant diffusion equation, and their results for $\gamma = 3$ are shown compared with those of the present work in figure 6.7. It is seen that the results are not inconsistent.

Rozental and Streltsov (1959) have also considered the problem but their results appear to refer not to total intensities but to integral intensities above a certain energy (~1,000 GeV) and so a comparison with other work is not possible.

6.5.3. Ramanamurthy (1962).

The problem was attempted in rather a different way by this worker. As in other treatments, he assumed continuous losses to be due to collision and pair-production, and discontinuous losses to be due to bremsstrahlung alone, for which he used the equation of Bethe and Heitler. The equation was integrated, obtaining the variation of the probability of a muon losing a certain fraction of its energy in passing through the element of depth, which was 450 m.w.e. in this case. The process of the calculation was as follows: Starting with

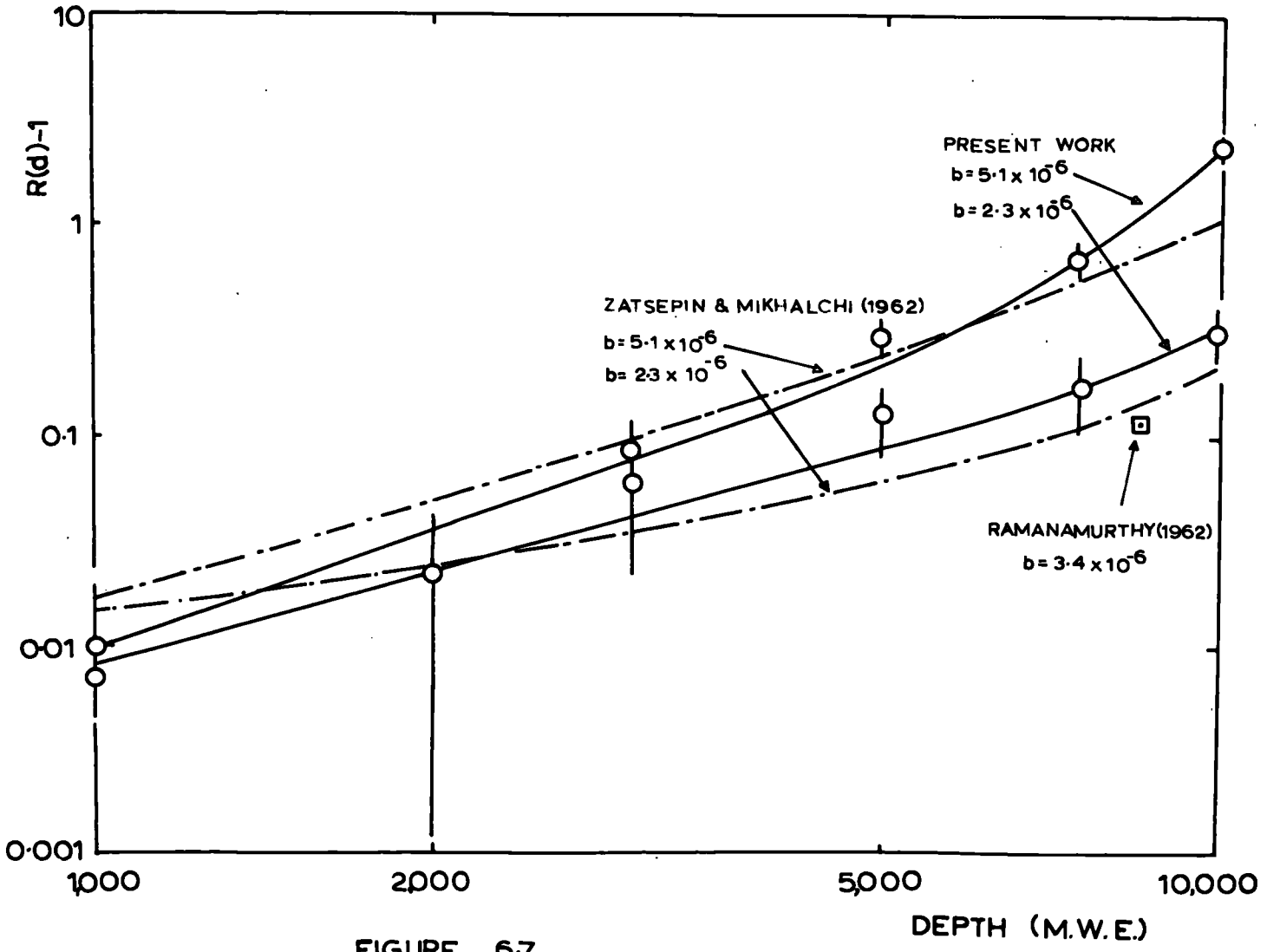
10
1
0·1
0·01
0·001
R(d)-1
1,000
2,000
5,000
10,000
DEPTH (M.W.E.)
PRESENT WORK
b = 5·1 x 10⁻⁶
b = 2·3 x 10⁻⁶
ZATSEPIN & MIKHALCHI (1962)
b = 5·1 x 10⁻⁶
b = 2·3 x 10⁻⁶
RAMANAMURTHY(1962)
b = 3·4 x 10⁻⁶

FIGURE 6·7

a muon of energy E , the probability distribution was evaluated at intervals of E/20. Subtraction of bremsstrahlung and continuous losses gave the "spectrum" after one unit. The spectrum was divided into intervals and the process repeated for the second element. In this way a series of range distributions for muons of unique incident energies was obtained, and the survival probability curves derived from them.

The values of R(d) obtained are shown in figure 6.8 in which the reciprocal of R(d) is plotted against the slope of the integral sea level muon spectrum.

Unfortunately, only one point on this graph is available for direct comparison with other results; this is shown as the single point in figure 6.7. Ramanamurthy's effective value of b was 3.4 (this is corrected for Z^2/A as described in chapter 2) and it can be seen from figure 6.7 that the resulting value of R(d) is much lower than the value expected from the present work. The main reason for this is thought to be the fact that the ratio of the fluctuating component of b (b (fluc)) to the continuous component (b(cont)) is much lower in Ramanamurthy's case. The figures are

Table 6.6.

Energy loss	b(fluc)	b(cont)	Ratio b(fluc)/b(cont)
Ramanamurthy	1.91	1.48	1.29
Present work:			
Case I	1.55	0.75	2.07
Case II	3.5	1.6	2.19

This point is duscussed further in chapter 7.

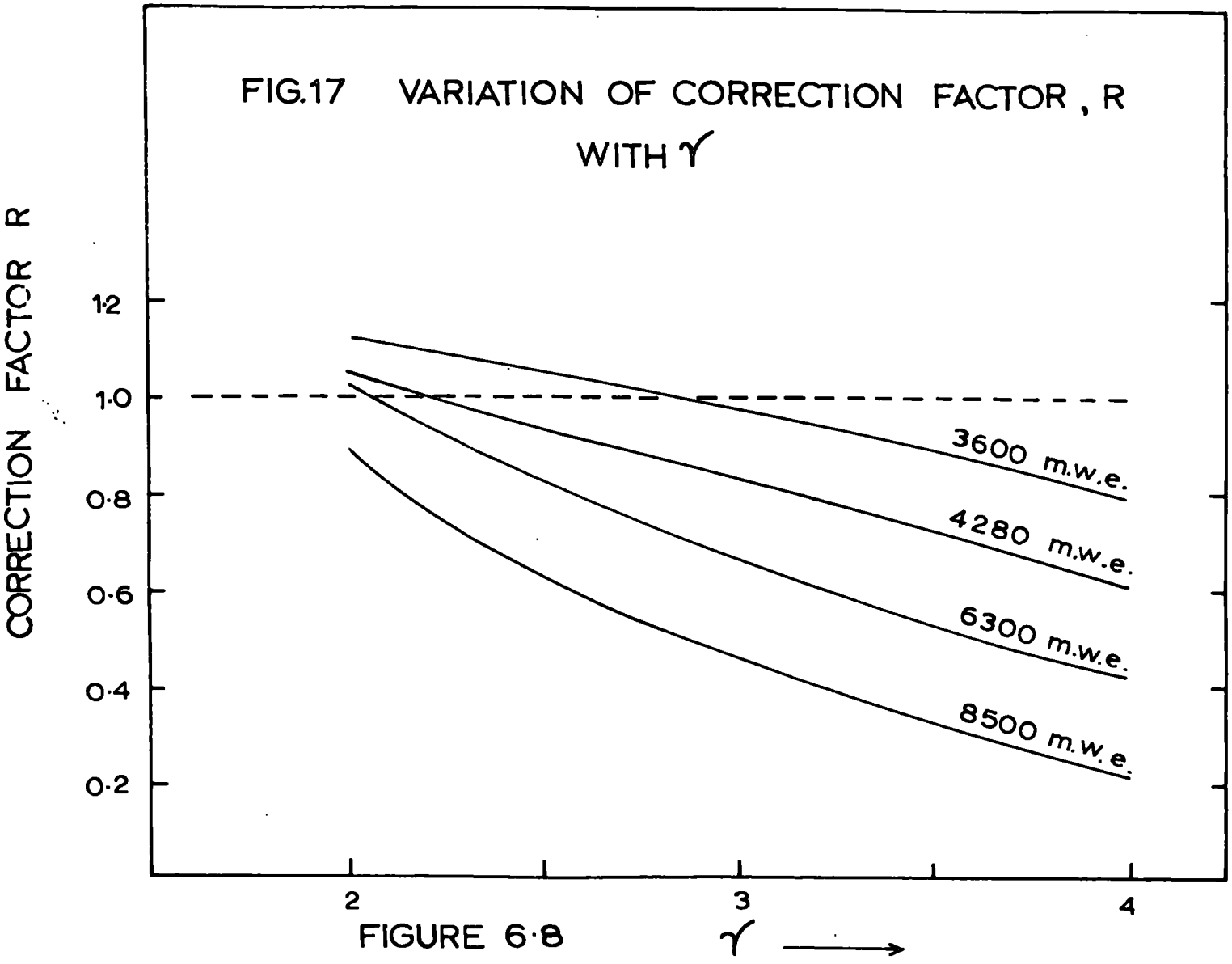
FIG.17 VARIATION OF CORRECTION FACTOR, R WITH γ
CORRECTION FACTOR R
1·2
1·0
0·8
0·6
0·4
0·2
3600 m.w.e.
4280 m.w.e.
6300 m.w.e.
8500 m.w.e.
2
3
4
γ

FIGURE 6·8

Chapter 7. Derivation of Experimental Energy Loss Relation.

7.1. Comparison of Predicted and Observed Depth-Intensity Relations.

The range-energy relations for the two cases of energy loss have been derived in chapter 4. Using the spectrum described in chapters 3 and 4 the predicted depth-intensity curves have been calculated and compared with the best estimate of the experimental depth-intensity curve described in chapter 2. The results are shown in figure 7.1 where the ordinate I_p/I_o is the ratio of predicted and observed intensities. The chain lines represent the results obtained when the correction for fluctuations is applied. Also shown in the figure are the ratios corresponding to the confidence limits on the observed depth-intensity relation.

7.2. Derivation of the Energy Loss Parameter b.

Derivation of the energy loss parameter b by direct comparison of the measured sea level spectrum and underground intensity is not useful in that the result can not be compared with the theoretical value, A value of b has been calculated from the experimental results such that the effect of fluctuations is included. This has been accomplished by an iterative method, in which the value of b is progressively corrected until acceptable agreement is obtained between observed and corrected predicted underground intensity. This has been carried out at a series of depths and the results for b are shown in figure 7.2. The abscissa has been converted from units of depth to units of energy, the values being plotted at the energy given by the

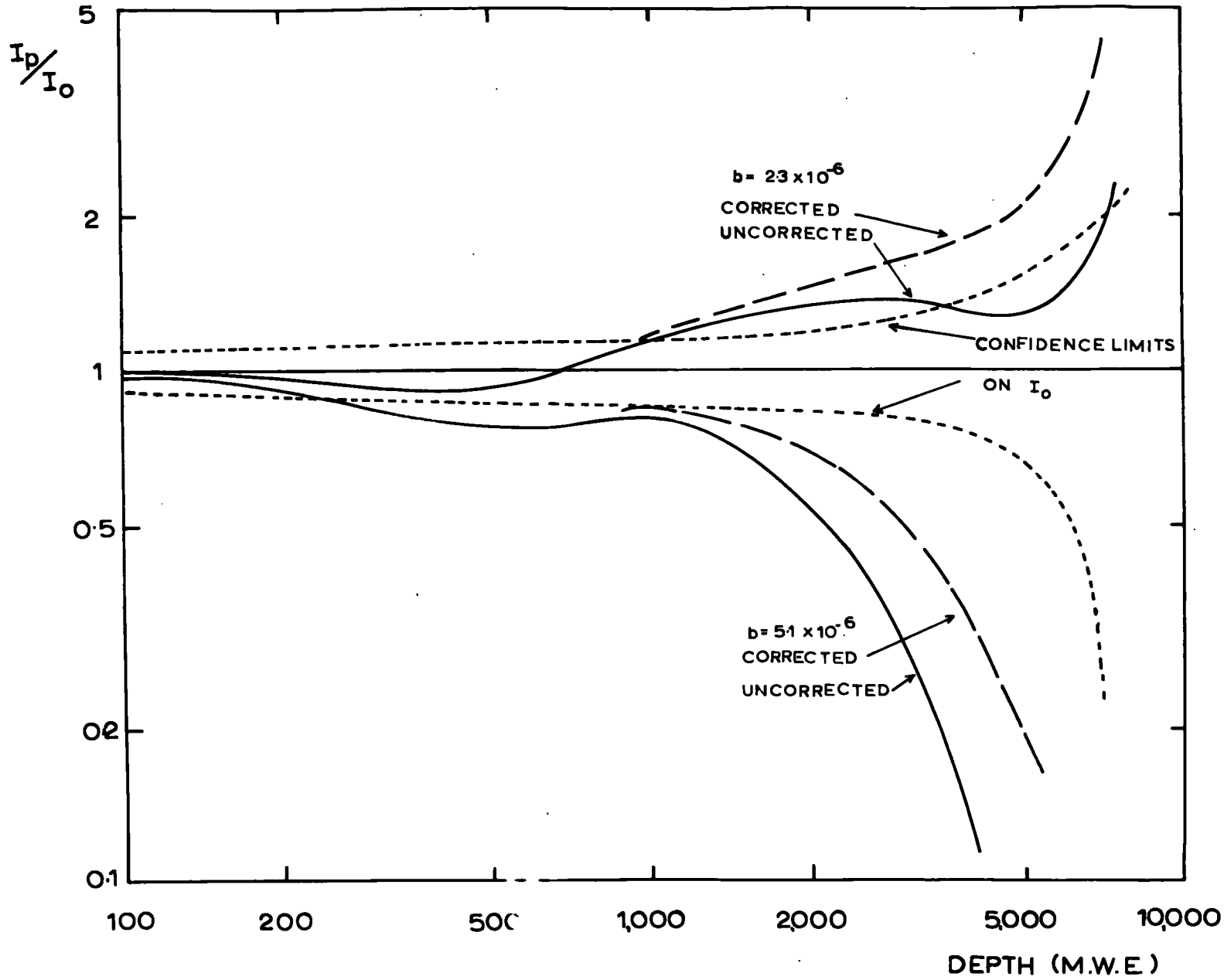
I_p/I_o
5
2
1
0·5
0·2
0·1
100
200
500
1,000
2,000
5,000
10,000
DEPTH (M.W.E.)
b= 2·3 x10⁻⁶
CORRECTED
UNCORRECTED
CONFIDENCE LIMITS
ON I_o
b= 5·1 x10⁻⁶
CORRECTED
UNCORRECTED

FIGURE 7 1

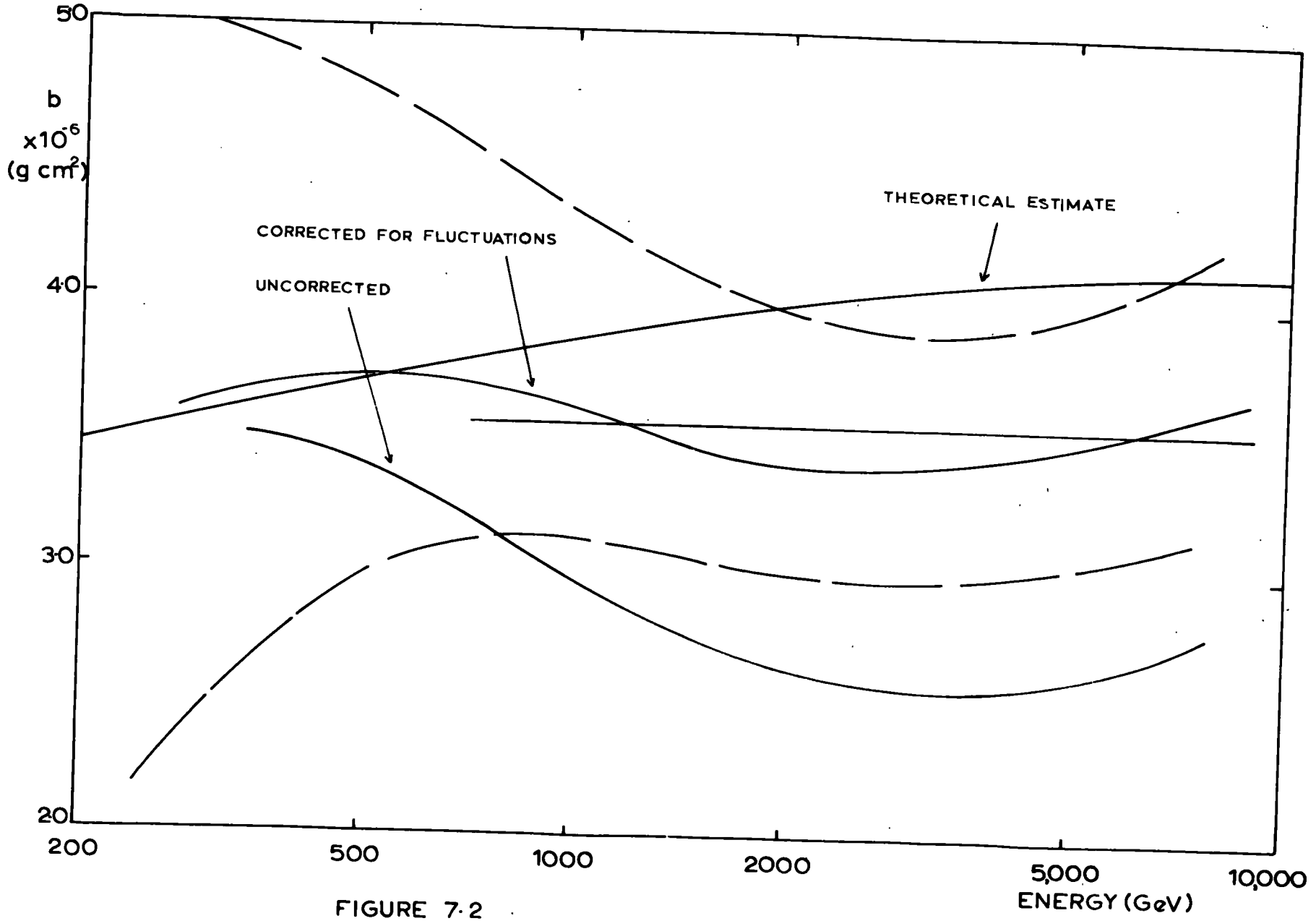
50
b
x10⁻⁶
(g cm²)
40
30
20
200
500
1000
2000
5,000
10,000
ENERGY (GeV)
THEORETICAL ESTIMATE
CORRECTED FOR FLUCTUATIONS
UNCORRECTED

FIGURE 7·2

range energy relation for the appropriate value of b. The confidence limits (shown dashed) correspond to the confidence limits on the best estimate of the depth intensity curve. Also included in the diagram is the resulting variation of b when the effect of fluctuations is neglected, and lastly the best theoretical estimate of b. The value of b obtained is $(3.55 \pm 0.25) \times 10^{-6} g^{-1} cm^2$.

This can not be directly compared with the theoretical value since the division between the fluctuating and continuous components is different in each case, and it is known that R(d), and thus the derived experimental value of b, is dependent on the ratio b(fluc)/b(cont. This ratio, as can be seen from table 6.6, has an average value of 2.13 for the two trial values of b, and so also for the derived value of b = 3.55. For the theoretical value, however, the ratio has a value 1.5. Figure 7.3 shows the approximate variation of the derived value of b with b(fluc)/b(cont). The circled points have been obtained from figure 7.2; the adopted value is the squared point. The result is $b = (3.15 \pm 0.3) \times 10^{-6} g^{-1} cm^2$.

7.3. Conclusions.

7.3.1. The Effect of Fluctuations.

It can be seen from figures 6.7, 7.1 and 7.2 that the effect of fluctuations is a factor which must be taken into account in the analysis of underground data. The effect becomes noticable at about 1500 m.w.e. and becomes correspondingly larger with

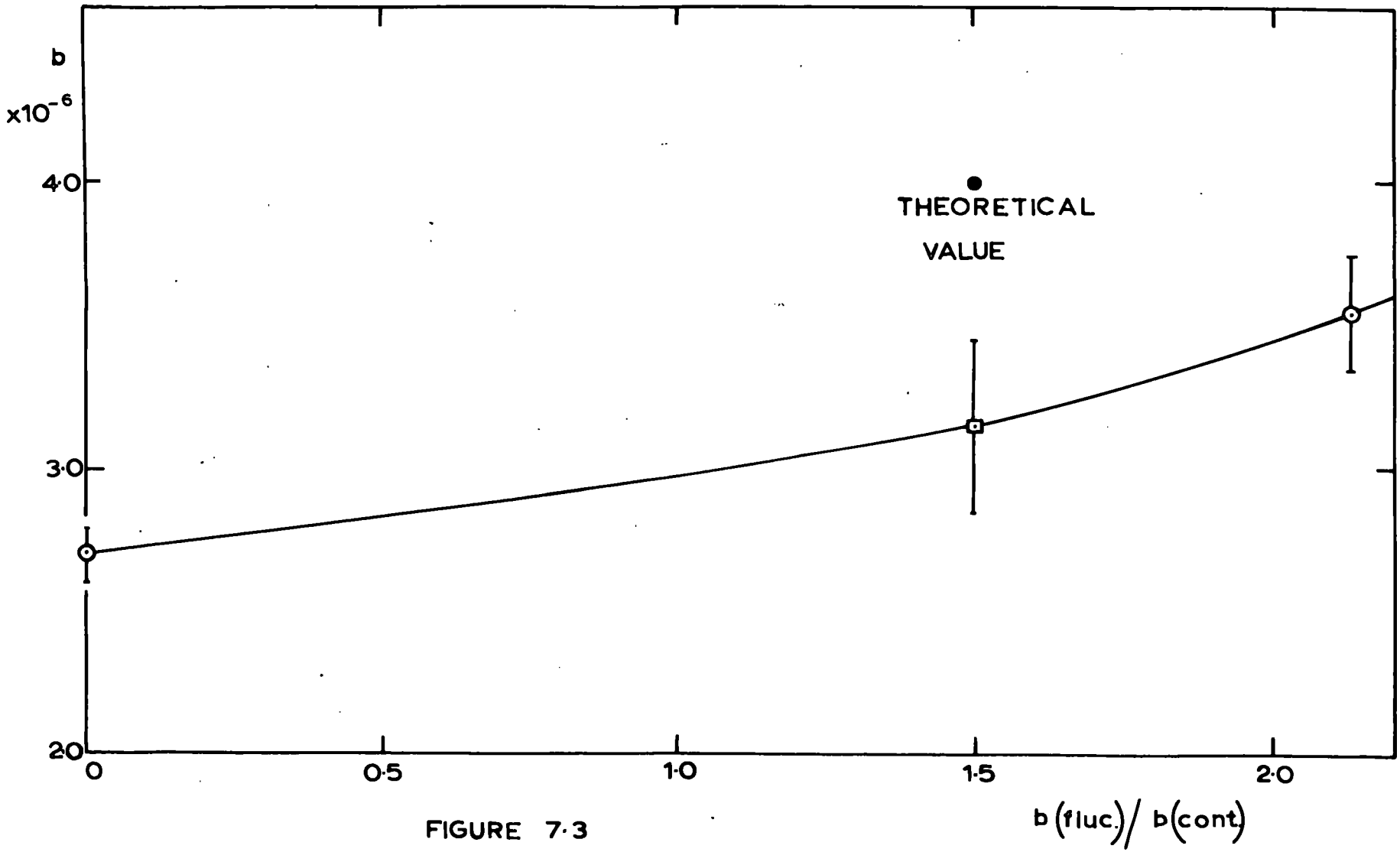

FIGURE 7·3

increasing depth. Of the attempts which have been made to determine the magnitude of the effect, it is thought that the present calculations have provided the most reliable results to date. However, due to the limiting assumptions which have been made, it is felt that further work on the subject would not be misplaced.

One of the approximations made is to represent the cross sections for the processes of bremsstrahlung and nuclear interaction by the simplified forms. The result is to overestimate the amount of energy lost in fractional transfers of the order of unity i.e. to increase the effect of fluctuations. However, since the amount of energy lost in this way does not represent a large fraction of the total (the majority being lost in fractional transfers of about 0.2) it is considered that the resulting overestimate in the effect is only a few per cent.

A rather more important assumption is the one concerning the ratio b(fluc)/b(cont). In the case of the present calculation this ratio was approximately two in both the cases of energy loss considered, whereas theory predicts a rather lower value. While it is possible to made approximate corrections for this discrepancy, it is considered that further work on the variation of R(d) with b(fluc)/b(cont) is required.

7.3.2. The Energy Loss Parameter.

It appears from figure 7.2 that at high energies there is poor agreement between the experimental and theoretical results. While some uncertainty does exist, both in the theoretical value of the energy loss and in the depth-intensity curve, it is considered most likely that the discrepancy originates in the sea level spectrum. The high energy region of the composite spectrum derived in chapter 4 uses the results of Duthie et al. which are of indirect derivation and assume that pions are the sole source of sea level muons. It is therefore concluded that a contribution from kaons may be effective at these energies.

If it is assumed that the discrepancy lies solely in the sea level spectrum, the spectrum necessary to give agreement with the theoretical variation of b, the derived depth-intensity curve and the effect of fluctuations, can be calculated. The results are given in table 7.1. The increase over the derived spectrum of chapter 4 varies from zero at 500 GeV up to 200% at 10,000 GeV. The k/π ratio necessary to account for the figures of table 7.1 has been calculated by Osborne and Wolfendale (1963), and found to be of the order of 20%. Such a result is in agreement with other determinations of the k/π ratio from measurements on high energy jets in emulsions.

Table 7.1.

Energy (GeV)	Intensity ($cm^{-2}\ sec^{-1}\ st^{-1}$)
10	7.13×10^{-4}
15	3.91×10^{-4}
20	2.45×10^{-4}
30	1.21×10^{-4}
50	4.54×10^{-5}
70	2.31×10^{-5}
100	1.08×10^{-5}
150	4.50×10^{-6}
200	2.40×10^{-6}
300	9.50×10^{-7}
500	2.70×10^{-7}
700	1.16×10^{-7}
1000	4.60×10^{-8}
1500	1.57×10^{-8}
2000	7.20×10^{-9}
3000	2.41×10^{-9}
5000	5.10×10^{-10}
7000	1.58×10^{-10}
10000	4.35×10^{-11}

Acknowledgements.

The author wishes to thank Professor G. D. Rochester for the facilities made available, Dr. A. W. Wolfendale for his advice and encouragement during the work, and Professor L. F. Bates and Dr. W. F. Nash of the University of Nottingham, where the thesis was completed.

The staff of the University Computing Laboratory, Newcastle upon Tyne, are thanked for their advice and for the computing facilities.

The author acknowledges his debt to his colleagues at Durham, in particular Mr. K. Tindale, Mr. K. J. Gijsbers and Dr. P. J. Hayman for their help with the spectrograph, and Dr. Y. Kamiya for her assistance with the experimental data.

Financial support from the Department of Scientific and Industrial Research made the work possible.

Appendix.

The theoretical probabilities for energy transfer for the various energy loss processes refer to an absorber thickness of 1 g cm^{-2}. The Monte Carlo calculation used an element thickness of 100 m.w.e. (i.e. 10^4 g cm^{-2}), and assumed that the individual probability distributions for the sub-element thickness of 1 g cm^{-2} could be simply summed to give the probability distribution of energy loss for an element of 100 m.w.e.

In order to obtain an estimate of the error due to this assumption, let v_m be the mean fractional energy loss in each sub-element. On the assumption, the fraction lost in each sub-element is referred to the energy on entering the element, so the fractional loss in each sub-element will be v_m and thus the fraction lost after n sub-elements will be nv_m.

The correct method would be to calculate the energy loss from the energy of the particle on entering the sub-element. In this case the fraction lost after n sub-elements will be $1-(1-v_m)^n$. If the assumption is accurate,

$$R = \frac{nv_m}{1-(1-v_m)^n} \rightarrow 1$$

A probability distribution of the form

$$P(v)dv = \frac{b}{v}\,dv \qquad g^{-1}cm^2$$

has been assumed. If the lower limit to v is taken to be some

very small fraction ε, then the mean fractional transfer is

$$V = \frac{\int_{\varepsilon}^{1} \underline{v}.\frac{\underline{b}}{\underline{v}}\, dv}{\int_{\varepsilon}^{1} \frac{\underline{b}}{\underline{v}}\, dv} = b(1 - \varepsilon) \simeq b$$

since ε is small. The quantity of interest, R, is then given to a good approximation by

$$R = 1/\left[1+\tfrac{1}{2}(n-1)b\right]$$

The largest error which can occur is in the case of the larger (case II) energy loss, where $b = 3.5 \times 10^{-6}$ $g^{-1}cm^2$. With $n = 10^4$ this gives

$$R = 1/1.018$$

i.e. a maximum error of 1.8% in the calculation of the energy loss in the element of 100 m.w.e.

It is interesting to note that the calculation of Ramanamurthy, with $b = 2.2 \times 10^{-6}$ and $n = 4.5 \times 10^4$, gives a corresponding error of 5%.

References.

Ashton, F., 1961, Proc. Phys. Soc., 77, 587.

Avan, L., and Avan, M., 1955, Compt. Rend., 241, 1122.

Barrett, P. H., Bollinger, L. M., Cocconi, G., Eisenberg, Y., and Greisen, K., 1952, Rev. Mod. Phys., 24, 133.

Barton, J. C., 1961, Phil. Mag., 6, 1271.

Bennett, H. W., and Nash, W. F., 1960, Nuovo Cim. Suppl., 15, 193.

Bethe, H. A., and Heitler, W., 1934, Proc. Roy. Soc., A146, 83.

Bethe, H. A., 1930, Ann. Phys. Lpz., 5, 325.

Bethe, H. A., 1932, Z. Phys., 76, 293.

Bhabha, H. J., 1935, Proc. Roy. Soc., A152, 559.

Bhabha, H. J., 1938, Proc. Roy. Soc., A164, 257.

Block, M. M., King, D. T., and Wada, W. W., 1954, Phys. Rev., 96, 1627.

Bollinger, L. M., 1951, Ph. D. Thesis, Cornell University.

Brooke, G., Gardener, M., Lloyd, J. L., Kisdnasamy, S., and Wolfendale, A. W., 1962, Proc. Phys. Soc., 80, 674.

Campbell, M. J., Jauncey, D. L., Murdoch, H. S., Rathgeber, H. D., and Ogilvie, K. W., 1962, Proc. Int. Conf. Cosmic Rays and the Earth Storm, Kyoto, Japan: J. Phys. Soc. Japan, (Suppl. AIII), 17, 318.

Christy, R. F., and Kusaka, S., 1941, Phys. Rev., 59, 414.

Clay, P. H., Van Gemert, A., and Clay, J., 1939, Physica, 6, 184.

Clay, J., and van Gemert, A., 1939, Physica, 6, 497.

Clay, J., 1939, Rev. Mod. Phys., 11, 128.

Cousins, J. E., 1960, Ph. D. Thesis, Nottingham University.

Cousins, J. E., and Nash, W. F., 1962, Phil. Mag. Suppl., 11, 349.

Dalitz, R. H., and Yennie, D. R., 1957, Phys. Rev., 105, 1598.

Duthie, J., Fowler, P. H., Kaddoura, A., Perkins, D. H., and Pinkau, K., 1962, Nuovo Cim., 24, 122.

Ehmert, A., 1937, Zeit. f. Phys., 106, 751.

Fermi, E., 1939, Phys. Rev., 56, 1242.

Fermi. E., 1940, Phys. Rev., 57, 485.

Gaebler, J. F., Hazen, W. E., and Hendel, A. Z., 1961, Nuovo Cim., 10, 265.

George, E. P., and Evans, J., 1950, Proc. Phys. Soc., A63, 1248.

George, E. P., 1952, Progress in Cosmic Ray Physics (North Holland Pub. Co.), I, 395.

Greisen, K., 1942, Phys. Rev., 61, 212.

Greisen, K., and Nereson, N. G., 1942, Phys. Rev., 62, 316.

Greisen, K., 1943, Phys. Rev., 63, 323.

Hayakawa, S., and Tomonaga, S., 1949, Prog. Theor. Phys., 4, 496.

Halpern, O., and Hall, H., 1940, Phys. Rev., 57, 459.

Halpern, O., and Hall, H., 1948, Phys. Rev., 73, 477.

Hayman, P. J., Palmer, N. S., and Wolfendale, A. W., 1962, Proc. Phys. Soc., 80, 800.

Hayman, P. J., Palmer, N. S., and Wolfendale, A. W., 1963, Proc. Roy. Soc., 275, 391.

Hayman, P. J., and Wolfendale, A. W., 1962, Proc. Phys. Soc., 80, 710.

Hayman, P. J., 1962, Ph. D., Thesis, Durham University.

Higashi, S., Kitamura, T., Mishima, Y., Mitani, S., Miyamoto, S., Oshio, T., Shibata, H., Watanabe, K., and Watase, Y., 1962, Proc. Int. Conf. Cosmic Rays and the Earth Storm, Kyoto, Japan: J. Phys. Soc. Japan (Suppl. AIII), 17, 362.

Jones, D. G., Taylor, F. E., and Wolfendale, A. W., 1962, Proc. Phys. Soc., 80, 686.

Kessler, D., and Kessler, P., 1957, Compt. Rend., 244, 1896.

Krasilnikov, D. D., 1962, Proc. Int. Conf. Cosmic Rays and the Earth Storm, Kyoto, Japan: J. Phys. Soc. Japan (Suppl. AIII) 17, 335.

Mando, M., and Ronchi, L., 1952, Nuovo Cim., 9, 105.

Mando, M., and Ronchi, L., 1952, Nuovo Cim., 9, 517.

Mando, M., and Sona, P. G., 1953, Nuovo Cim., 9, 1275.

Marshak, R. E., 1952, Meson Physics (New York: Dover Pub. 1958).

Massey, H. S. W., and Corben, H. C., 1939, Camb. Phil. Soc., 35, 463.

Miyake, S., Narasimham, V. S., and Ramanamurthy, P. V., 1962, Proc. Int. Conf. Cosmic Rays and the Earth Storm, Kyoto, Japan: Phys. Soc. Japan (Suppl. AIII), 17, 318.

Murota, Ueda, and Tanaka, 1956, Prog. Theor. Phys., 16, 482.

O'Connor, P. V., and Wolfendale, A. W., 1960, Nuovo Cim. Suppl., 15, 202.

Osborne, J. L., and Wolfendale, A. W., 1963, Proc. Jaipur Conf. (to be published)

Ozaki, S., 1962, Proc. Int. Conf. Cosmic Rays and the Earth Storm, Kyoto, Japan: J. Phys. Soc. Japan (Suppl. AIII), 17, 330.

Pine, J., Davisson, R. J., and Greisen, K., 1959, Nuovo Cim., 14, 1181.

Racah, G., 1937, Nuovo Cim, 14, 93.

Ramanamurthy, P. V., 1962, Ph. D. Thesis, Bombay University.

Randall, C. A., and Hazen, W. E., 1951, Phys. Rev., 81, 144.

Randall, C. A., and Hazen, W. E., 1958, Nuovo Cim., 8, 878.

Roe, B. P., and Ozaki, S., 1959, Phys. Rev., 116, 1022.

Rossi, B., 1948, Rev. Mod. Phys., 20, 537.

Rossi, B., 1952, High Energy Particles, (New York: Prentice-Hall).

Rozental, I. L., and Streltsov, V. N., 1959, J.E.T.P., 8, 1007.

Schönberg, M., 1951, Nuovo Cim., 8, 159.

Sreekantan, B. V., and Naranan, S., 1952, Proc. Ind. Acad. Sc., 36, 97.

Sreekantan, B. V., Naranan, S., and Ramanamurthy, P. V., 1956, Proc. Ind. Acad. Sc., 43, 113.

Sternheimer, R. M., 1952, Phys. Rev., 88, 851.

Sternheimer, R. M., 1953, Phys. Rev., 89, 1148.

Sternheimer, R. M., 1956, Phys. Rev., 103, 511.

Stoker, P. H., Hofmeyr, C., and Bornmann, C. H., 1961, Proc. Phys. Soc., 78, 650.

Wick, G. C., 1941, Ric. Scient., 12, 858.

Wick, G. C., 1943, Nuovo Cim., 1, 302.

Zatsepin, G. T., and Kuzmin, V. A., 1961, J.E.T.P., 12, 1171.

Zatsepin, G. T., and Mikhalchi, E. D., 1962, Proc. Int. Conf. Cosmic Rays and the Earth Storm, Kyoto, Japan: J. Phys. Soc. Japan, (Suppl. AIII), 17, 356.